Technical Report

TR-14-15

Possible influence from stray currents from high voltage DC power transmission on copper canisters

Claes Taxén, Bertil Sandberg
Swerea KIMAB AB

Christina Lilja, Svensk Kärnbränslehantering AB

October 2014

Svensk Kärnbränslehantering AB
Swedish Nuclear Fuel
and Waste Management Co

Box 250, SE-101 24 Stockholm
Phone +46 8 459 84 00

ISSN 1404-0344
SKB TR-14-15
ID 1422410

Possible influence from stray currents from high voltage DC power transmission on copper canisters

Claes Taxén, Bertil Sandberg
Swerea KIMAB AB

Christina Lilja, Svensk Kärnbränslehantering AB

October 2014

Summary

The possible influence of High Voltage Direct Current (HVDC) electrodes on a KBS-3 repository for spent nuclear fuel at Forsmark is analysed in this study. Corrosion of copper canisters is an electrochemical process that is accelerated by currents that pass through the canister. Present HVDC technology is first examined and the anticipated future development in the field is discussed. The influence from the existing sea-based HVDC transmission, the Fenno-Skan cable, is reviewed. Possible locations of new HVDC transmissions in the Forsmark region are found to be limited by the high resistivity bedrock so that a land based electrode will never be economical in the region. However, major changes in the location of the shoreline due to combinations of sea level change and isostatic change may, during some periods, cause the shoreline to be located several kilometers inland from the present position.

A sea-based electrode for HVDC transmission could then possibly be located in the vicinity of the repository during such periods. Most of the current from a sea-based electrode is conveyed by the water but large gradient fields arise nearby the electrode. These gradient fields are so large that danger to humans forces the electrodes to be located a few kilometers from the shoreline.

The possible influence of currents from HVDC electrodes on corrosion of the copper canisters is estimated from Finite Element Models (FEM) representing the tunnel system in the repository and the potentials that arise at the most affected positions when the tunnels are located in various electrical fields. Four model types of electrical fields are studied: 1) a uniform horizontal field with a field strength of 50 V/km, 2) Forsmark power station behaving as a secondary electrode, through the groundings and earth lines in overhead power lines, with an output of 20 A through the ground, 3) direct influence from a hypothetical future HVDC sea-based electrode operating at 2,500 A in monopolar mode when the electrode is located directly on top the repository, 4) influence from a hypothetical future HVDC sea-based electrode operating at 2,500 A in monopolar mode at various distances from the repository. In all cases calculations include conditions where the tunnels are oriented to represent the maximum influence at the site of the deposition holes.

For short distances between the repository and the electrode, where electrode design may be of importance, a representation consisting of 8 sub electrodes in a ring with 100 m radius is used. An equal current is fed to all sub electrodes.

The type of corrosion that a canister can suffer by currents from HVDC transmissions and stray currents is primarily determined by the voltages that arise along the height of a canister when it is surrounded by bentonite in a deposition hole. For the chemical environment expected in the repository, there is no process identified that could cause pitting, and thus only general corrosion is analyzed.

The highest value of the potential that will develop along the height of a canister surrounded by bentonite is about 0.46V, at reducing conditions with sulfide available. The maximum additional corrosion rate is lower than 0.20 μm/year for a monopolar operation. During the initial oxidizing conditions, where the cathodic reaction is reduction of oxygen gas or earlier formed corrosion products, corrosion would consume these oxidants so that the presence of an electrical field under these conditions would not cause any additional corrosion.

With the electrical fields from the present Fenno-Skan installation, the voltages that arise along the height of a canister will be low also for conditions with ‘as-deposited’ bentonite. Estimated from the highest local field strength observed (1.5 V/km) the voltage may be about 0.008 V, corresponding to a corrosion rate of about 0.003 μm/year. These values are expected to decrease as the conductivity of the surrounding bentonite increases when its water content increases.

It is concluded that for the current situation of potential gradients over the canister at the Forsmark site, the estimates in the present report are in line with those estimated in the safety assessment SR-Site. The present study additionally addresses influences of possible future HVDC electrodes. The results show that, with pessimistic assumptions on future HVDC locations, the influences may be larger than today. However, also with the very pessimistic assumptions of a location directly on top of the shaft that connects the repository level and ground level, only moderate additional corrosion is predicted from an HVDC installation.

Contents

1 Background

The presence of earth currents and their influence on copper corrosion in a repository for spent nuclear fuel was analyzed in the Process report for fuel and canister for the safety assessment SR-Site (SKB 2010b). Both natural and anthropogenic sources to earth currents were described, and the effects on corrosion discussed. Measured self-potentials and self-potential gradients at the Forsmark site were used to estimate possible potential gradients due to a High Voltage Direct Current (HVDC) installation over a canister in the planned repository. It was concluded that earth currents from natural sources were anticipated to be small, and that stray currents from an HVDC electrode station would not increase the extent of corrosion. The corrosion would still be limited by the availability of oxygen and sulfide.

As part of the review of the SKB license application for a repository for spent nuclear fuel, SSM has asked for complementing information regarding the effect of stray currents from high voltage cables on copper corrosion (SSM 2012). SKB therefore has performed an extended study of the effects of high voltage DC power transmission as support for answering SSM. SSM especially asked for the influence of different degrees of saturation of the buffer on the corrosion effect. With a Best Available Technique (BAT) perspective SSM also asked for an assessment of the influence of repository depth on copper corrosion caused by stray currents from high voltage cables.

2 Purpose and scope of analysis

2.1 Purpose

The aim of this investigation is to evaluate the effect of stray currents from an HVDC power transmission installation on canister corrosion in a repository for spent nuclear fuel.

2.2 Scope and methodology

An analysis of the effects of HVDC electrodes on the corrosion of copper canisters requires that the extent of the electrical field is calculated over distances of several kilometers and that the local electrical field around a canister in a deposition hole is calculated with high resolution. To achieve this, the analysis is performed in steps. A quite detailed description is given below, to facilitate the understanding of the analyses and discussions leading up to the actual modeling in Chapter 5.

The analysis is started with large-scale models, where only a part of the tunnel system, without deposition holes, is represented. This allows the potentials at the levels of the deposition holes and the canisters to be calculated for the case where the resistivity in the deposition holes is the same as in the surrounding rock.

Further on, with models that do not require calculations over large distances one deposition hole is represented, and the resistivity of the medium in the deposition hole is varied. It is shown that the voltage along the height of a deposition hole is a linear function of the current through the deposition hole. Also with very low resistivity in the deposition hole, the current is limited. The current through a deposition hole has to pass through rock and parts of the tunnel system. This resistance in the current's path through the rock limits the current through a deposition hole when the resistance in the deposition hole is set very low. Conversely, a maximum voltage along the height of a deposition hole is found when the resistance in the hole is set very high.

The resistance in the current's path, outside of the deposition hole, is here referred to as the internal resistance of the field and the maximum voltage is here referred to as an electro-motive force, given in V. It is shown that the value of the internal resistance is determined almost exclusively by the resistivity of the rock at repository depth. The value is practically independent of the location of the hole along a tunnel and of the source of the external field.

Thus, one value of the voltage along the height of a deposition hole for the case where it has the same resistivity as the surrounding rock, allows the voltage to be recalculated to other cases when there is a canister surrounded by bentonite in the deposition hole.

The current that passes through a deposition hole, with canister and bentonite, branches so that a part of the current stays in the bentonite and passes parallel to the canister without interfering. Another branch of the current passes into the canister and exits at the other end where it results in corrosion of the canister. It is found that the total current through a deposition hole is close to the maximum value as found by the electro-motive force divided by the internal resistance.

The resistance parallel to the canister is predicted to be low also before water saturation of the bentonite. However, there is a finite resistance in the deposition hole parallel to the canister and the voltage across this parallel resistance is also the voltage along the height of the canister.

The voltage over the canister is then compared to potentials derived from electrochemical scanning to assess the applicability of a linear relationship between the corrosion and the voltage over the canister. This is dicussed for the initial oxidizing conditions as well as for a long-term reducing (sulfide) environment.

The methodology is used for different cases. The first case treats a uniform electrical field resulting from a remote electrode. The second case treats the effect of a secondary field caused by current being picked up by a grounding system installed in the vicinity of the repository. Finally calculations

are being done for the cases that a future electrode is being installed on top of, or close to, the repository. For these cases the sensitivity to e.g. rock resistivity, the degree of saturation of the bentonite buffer as well as some aspect of the tunnel layout and the depth of the repository are considered.

2.3 Report structure

The report is structured such that Chapter 3 gives the basics of the HVDC technology. Chapter 4 describes the interference situation at Forsmark today with the installed Fenno-Skan cable (Section 4.1), followed by possible set-ups for a future installation at Forsmark. The prerequisites for an installation are given in Section 4.2, while Section 4.3 elaborates on the modeling of such a construction. In Chapter 5 the large-scale models for the different cases are set up, with some sensitivity analyses included, and the potentials over the deposition hole are calculated. Chapter 6 gives the analysis procedure for deriving the voltage over the canister, as a function of degree of saturation of the bentonite. In Chapter 7 the voltages over the canisters are calculated for the different cases. The type and extent of the corrosion is evaluated in Chapter 8. Some uncertainties are discussed in Chapter 9 and conclusions are presented in Chapter 10.

3 The HVDC technology

3.1 Different systems

The High Voltage Direct Current (HVDC) technology is used to transmit electricity over long distances by overhead transmission lines or cables. It is also used to interconnect separate power systems, where traditional alternating current (AC) connections cannot be used.

In an HVDC system, electric power is taken from one point in a three-phase AC network, converted to DC in a converter station, transmitted to the receiving point by an overhead line or cable and then converted back to AC in another converter station and injected into the receiving AC network.

The vast majority of electric power transmissions use three-phase alternating current. The reasons justifying the choice of HVDC are:

1. Lower losses.
2. Long distance water crossing.
3. Asynchronous interconnections.
4. Controllability.
5. Limit short circuit currents.
6. Environment.

An HVDC system can be monopolar or bipolar. In a monopolar system the return current is transmitted by seawater and ground using buried or immersed electrodes, see Figure 3-1.

In a bipolar system overhead lines or cables transmit all current. No electrodes are therefore needed. Most bipolar systems are however in reality two combined monopolar systems, see Figure 3-2.

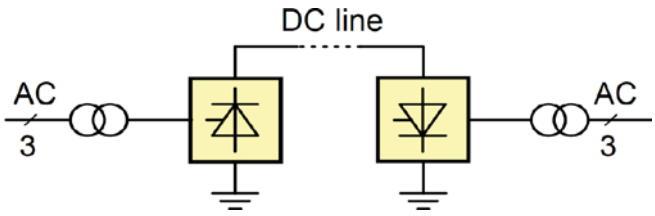

Figure 3-1. *Monopolar HVDC system.*

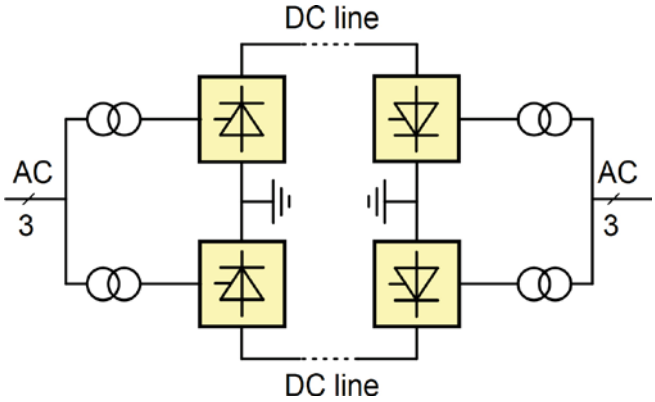

Figure 3-2. *"Bipolar" HVDC system consisting of two combined monopolar systems.*

The two systems operate separately why the electrodes transmit unbalance currents. If one cable is damaged the system can continue to function as a monopolar system.

There are two types of HVDC, the classic technology using thyristors for conversion and HVDC Light, which uses transistors for conversion. HVDC Light is used to transmit electricity in lower power ranges over short and medium long distances.

The increased interest in recent years for transporting clean and renewable energy from remote hydro generation plants has also increased the interest in higher DC transmission voltage than presently used (i.e. 600 kV DC). This has led to development of Ultra High Voltage Direct Current (UHVDC) at 800 kV DC.

Ultra High Voltage Direct Current (UHVDC) transmissions are economically attractive for bulk power transmissions of 5,000–8,000 MW over 1,000–1,500 km or above. UHVDC transmission projects are already in execution phase, and 800 kV is now an established voltage level for bulk power transmission over long distances. These systems transmit current through ground only during short periods, minutes per occasion.

Copper is one of the metals that is sensitive to stray currents and HVDC transmissions have long been identified as a factor contributing to underground copper corrosion (Myers and Cohen 1984).

The total unbalance current, time and magnitude, is higher with a monopolar system and the place for corrosion attack does not shift. A classic system transmits higher power than an HVDC Light system why this evaluation will be based on interference from a classic monopolar system.

3.2 Anticipated future development of the HVDC technique

For a sea cable connection it is the HVDC cable, which limits the capacity of the transmission. The first HVDC subsea cable was delivered to the transmission system supplying Gotland with electricity in 1954 having the capacity of 20 MW at 100 kV. In 1994 The Baltic Cable was installed designed for 600 MW/ 450 kV. Today it is possible to produce cables with a capacity of 1,000 MW at 550 kV corresponding to a current of 1,820 A. It is foreseen that in the future cables can be produced capable of transmission of 1,500 MW at 600 kV, which would mean a current of 2,500 A.

Due to high risk for interference with the infrastructure, monopolar systems are, in principle not installed any more. Bipolar systems with the possibility to operate as monopolar are however common. Periods of maintenance/repair can be as long as one year why we have to consider the possibility of monopolar operation even in the future, at least for limited periods.

3.3 Interference from HVDC

In HVDC transmission with monopolar operation or with bipolar operation with high unbalance current, the electric field around the electrode can cause stray current influence on buried or immersed metallic structures. The main concern is the risk of increased corrosion but also other forms of interference have to be considered such as transformer saturation (overheating) and disturbances in the telephone network (noise). The electrical field in the vicinity of the electrode may also have an impact on humans and animals.

Corrosion normally takes place where the current leaves the object, see Figure 3-3, where the arrows represent the current.

The most sensitive constructions, for stray current corrosion, are those with a long extension in combination with low resistance and having a good external coating. This combination results in high current densities (corrosion rates) in small coating damages. Well-coated steel pipeline is such a construction.

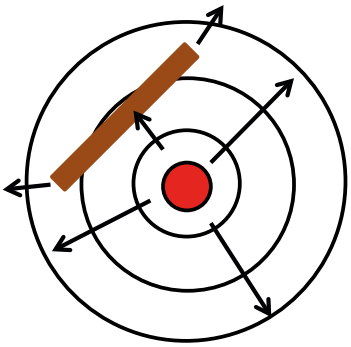

Figure 3-3. *Stray current corrosion caused by an electrical field in the ground.*

The primary method to avoid interference is to provide sufficient distance between the location of the earth electrode and critical structures. The influence area shall not reach densely populated areas.

The design of the electrode is important both to achieve the lowest possible earth resistance (ohmic losses) and to avoid steep electrical gradients in the nearby area (impact on humans and animals as well as stray current corrosion). It is only in the close vicinity of the electrode that the design of the electrode influences the magnitude of the electric field. At a distance of a few km the electrode design has no influence at all; the geological parameters determine the field strength.

The highest field strength and therefore the greatest risk for humans and animals are in the direct vicinity of the electrode. Tests at different water salinities (Nyman et al. 1988) revealed that fish do not appear to react to electric field strength of 2 V/m or below. Current entering a human body must not exceed 5 mA in order not to be harmful (Magg et al. 2010). The body resistance can be set to 1,000 Ω, for wet or broken skin (NIOSH 2014). Maximum acceptable step voltage (voltage between the feet of a person or animal standing in an electrical field) is influenced by the soil resistivity. For example, in ABB's requirements the resistivity is assumed to be very low and the step voltage must not exceed a value corresponding to 5 V/m. These criteria are based on impact on humans and this risk will also be valid in the future. Even if new systems with higher capacity are developed in the future, the electrodes will most probably be designed not to exceed 2 V/m in sea and 5 V/m on land.

4 Interference situation at Forsmark

4.1 Interference situation of today

In 1989 the monopolar HVDC system Fenno-Skan 1 was started. The capacity was 500 MW at 400 kV, with a maximum current of 1,250 A. The electrode on the Swedish side is located in the sea, 2.3 km from the shoreline north of the village Fågelsundet, see Figure 4-1. The distance from the electrode to Forsmark is approximately 25 km.

After 10 years operation the system was upgraded to 550 MW giving a maximum current of 1,360 A. In December 2011 Fenno-Skan 2 was started. Also this is a monopolar system, 800 MW, 500 kV with maximum current 1,670 A. The two systems use the same electrodes but have reverse current directions, see Figure 4-2. If the current in the Fenno-Skan 1 system is higher than the current in Fenno-Skan 2 system, the electrode acts as anode and vice versa.

Figure 4-1. *Location of electrode 25 km north of Forsmark.*

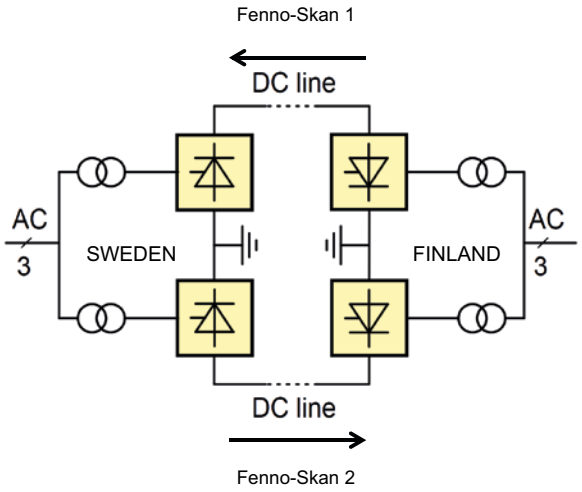

Figure 4-2. *Direction of current in Fenno-Skan 1 and 2.*

Due to the high resistivity of the bedrock the gradient field around the Fenno-Skan electrode is extensive. The potentials around some of the Scandinavian electrodes are presented in Figure 4-3 (Tykeson et al. 1996). The curves represent the voltage in a direction from the electrode out towards the sea.

The geological impact on the electrical fields is clearly shown by Figure 4-3. In Denmark where the Konti-Skan anode (C) is situated and in Skåne and northern Germany where the Baltic Cable electrodes are installed (E and F) the field strengths are very low. This is due to the crystalline bedrock being more than 2 km below the ground level. The remaining electrodes are located where the crystalline bedrock goes all the way up to the surface Västervik (A), Göteborg (B) and Uppland (D). The curve for Fenno-Skan (D), represents a current output of 1,250 A for Fennoskan 1 and 0 A for Fenno-Skan 2. At a distance of 5 km from the electrode the potential is still above 20 V.

Measurements recently performed by Swerea-Kimab, close to the electrode but onshore, show that from the shoreline (2.3 km from the electrode) and to a point 2.7 km further on shore the voltage drop is over 200 V when Fenno-Skan 2 is at maximum and Fenno-Skan 1 is out of operation. The highest field strength was registered at the shoreline, 0.2 V/m. The measurements were made at ground level.

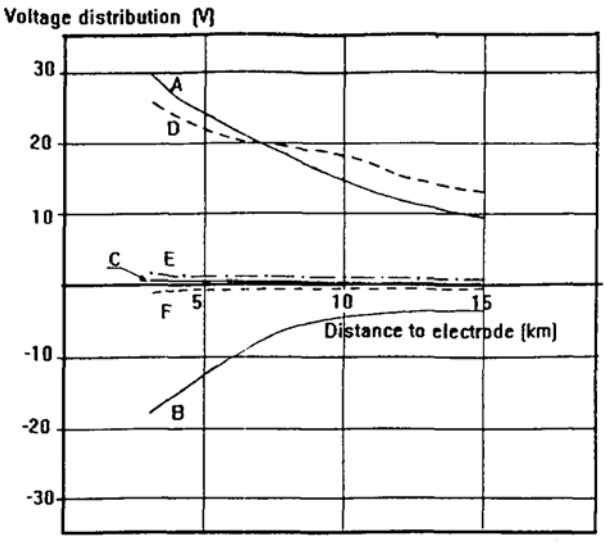

Figure 4-3. *Voltage distribution at different Scandinavian electrodes (Tykeson et al. 1996).*

The observation of a voltage of 200 V between a point located 5 km (2.3 km + 2.7 km) from the electrode and a point located 2.3 km from the electrode seems to be in conflict with the data shown in Figure 4-3. One reason for the apparent disagreement is that Fenno-Skan 2 operates at a higher current output than Fenno-Skan 1. Data in Figure 4-3 is obviously from Fenno-Skan 1 since the results were published before Fenno-Skan 2 was in operation. Another reason for the apparent disagreement is that the electrical field is not symmetric. The measurement of 200 V over a distance of 2.7 km was made on land whereas the measurements for Figure 4-3 were made in the sea and in the opposite direction. A contributing factor may be temperature differences. The water is quite shallow close to the coast and the water temperature may show some seasonal variations. Slightly lower voltages are expected in warm water (18°C) than in cold water (0°C).

At the location of Forsmark, a distance of 25 km from the electrode, the gradient is anticipated to be below 0.5 V/km and having equipotential curves as shown in Figure 4-4.

However, measurements have shown that a local gradient field exists around the groundings installed in the area of the nuclear plants (Sandberg et al. 2010), see Figure 4-5. These measurements were performed before Fenno-Skan 2 was taken into operation. The groundings pick up stray current from the electrical field created by Fenno-Skan and transport this current to remote groundings through the top wires installed on the overhead power lines. The groundings with overhead power lines act as a secondary electrode. The resulting electrical field is composed of the local electrical field superimposed on the large-scale field of the Fenno-Skan transmission.

The local field alters the direction of the current and increases locally the field strength from below 0.5 to 1.5 V/km, which is reflected in the dip shown in the principal diagram in Figure 4-6.

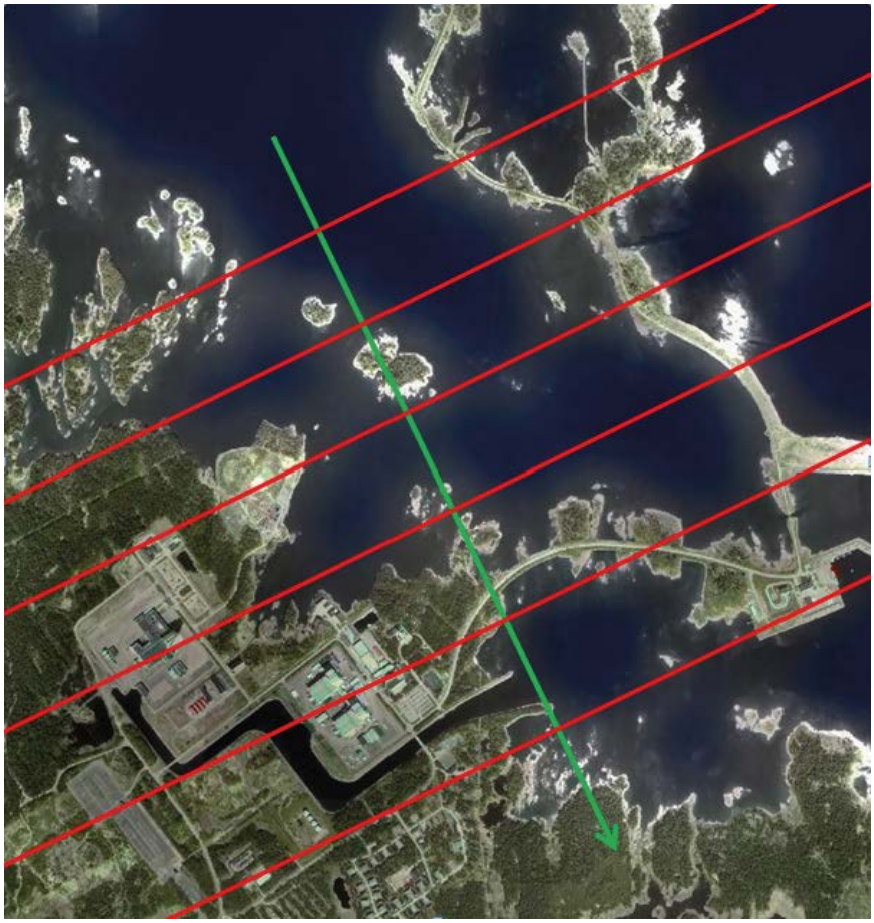

Figure 4-4. *Anticipated equipotential curves in the area of Forsmark. (Green arrow represents the current direction when Fenno-Skan 1 dominates over Fenno-Skan 2 and the red lines approximate equipotential curves).*

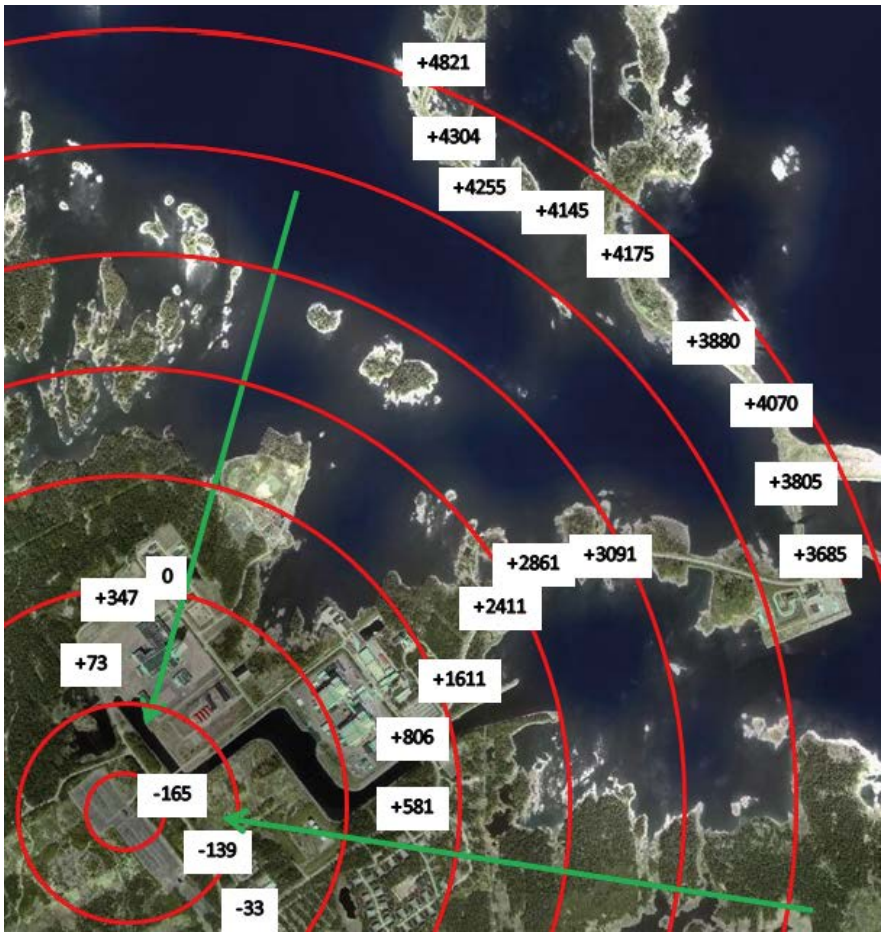

Figure 4-5. *Measured ground potentials vs. a point close to Forsmark 3. Figures in mV. (Green arrows represent the current direction and the red circles the equipotential curves.)*

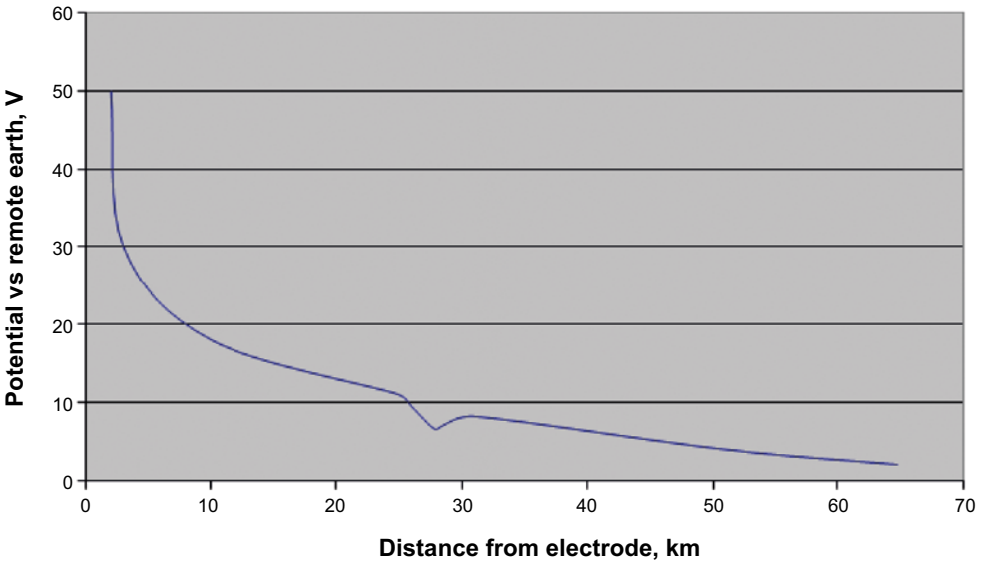

Figure 4-6. *Principal voltage distribution, at ground level, around the electrode in a direction passing Forsmark.*

4.2 Possible future influence situations at Forsmark

4.2.1 Defining the cases and system to be analysed

The highest degree of influence will take place if the electrode of a monopolar system is located in the sea in the vicinity of Forsmark. The following cases of interference must be considered:

- A close to horizontal gradient field if the electrode is several km from the repository (case 1).
- A close to vertical gradient field if a foreign grounding system is located directly on top of the repository and interacts with the HVDC system, resulting in a local secondary gradient field (case 2).
- A close to vertical gradient field if the HVDC system is located directly on top of the repository (case 3).
- A gradient field with an angle if the electrode is closer than a few km (case 4).

Cases 1, 2 and 4 are illustrated in Figures 4-7 to 4-9. They schematically show the interference on a single canister (orange rectangle) located in an electrical gradient field (brown curves) created by current (black arrow) from an electrode (red rectangle). In these principal figures the electric field is assumed to be undisturbed in the vicinity of the canister and not influenced by deposition tunnels. Case 3 where the HVDC electrode is located directly on top of the repository is special. Current from the electrode can then be directly fed into the ramp and the various shafts that connect the repository with ground level. In the treatment of the various cases, the principal difference between cases 3 and 4 is not sharp because also small distances between the electrode and the shafts are included in case 4.

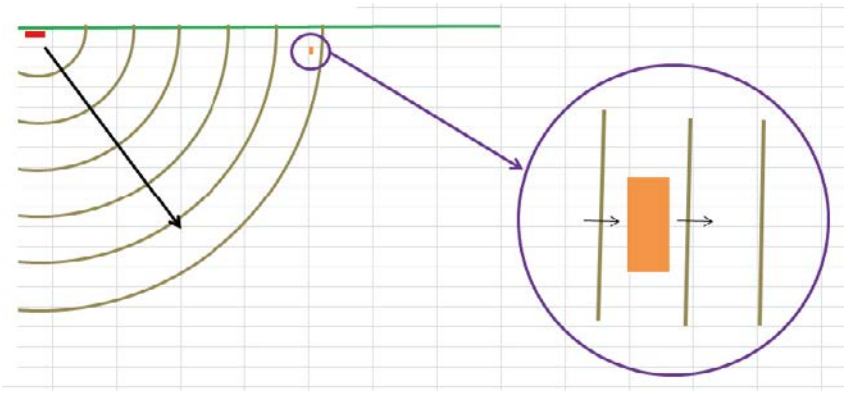

Figure 4-7. *Stray current influence if the electrode is several km away from the repository and causing a horizontal electrical field at the repository (case 1).*

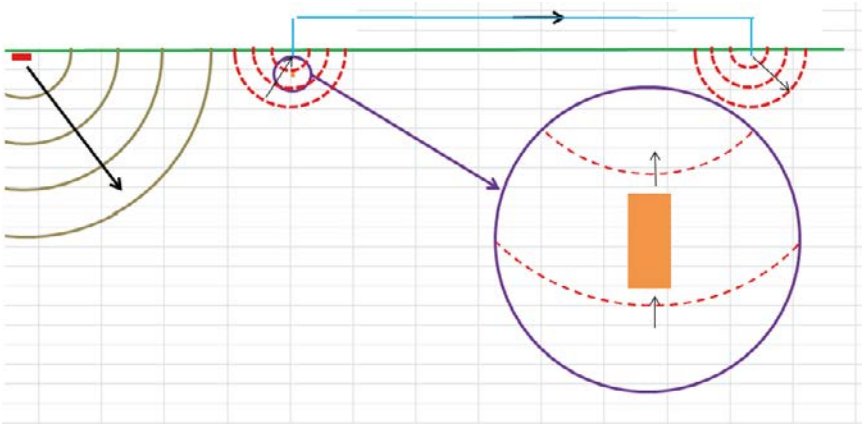

Figure 4-8. *Stray current influence if a local vertical electric field is created by a secondary construction picking up current from the HVDC electric field (case 2).*

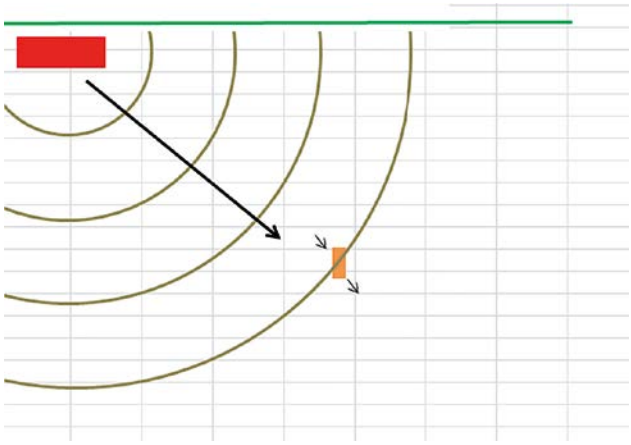

Figure 4-9. *Stray current influence if the electrode is located close to the repository (case 4).*

A monopolar HVDC system in the surroundings of Forsmark or any other part of northern Uppland will most probably never use a land-based electrode. The bedrock has a very high resistivity and the soil layer is thin which would result in unacceptable power losses in combination with massive interference and hazards to human lives. Any system installed in this area in the future will most likely be used for transmission of energy across the Baltic Sea using a sea-based electrode.

Future subsea cables are anticipated to be capable of transmitting 1,500 MW at 600 kV, see Section 3.2. Two or more cables can, however, be installed in parallel. If two cables are installed it is most likely that they are operated as a bipolar system. With 3 cables there will be one bipolar and one monopolar system. In the most pessimistic case we would therefore have an electrode in the sea outside Forsmark transmitting 2,500 A in to the sea.

In the future, installations with a grounding system could be located close to the repository, like the situation for the current power plants, see Figure 4-10.

When designing the HVDC system, efforts are made to limit the losses in the system. A 200 km long cable to Finland has a resistance just below 2 Ω. The grounding resistance of each electrode should not exceed 0.3 Ω. According to Section 3.3 the design must also fulfill the requirements concerning maximum field strength, 2 V/m in sea and 5 V/m on land.

The gradient field around an electrode, located near shore, can be calculated using the formula (Rusck 1962):

$$V = \frac{1}{\frac{\alpha \cdot \rho_e}{\pi \cdot \rho_w} + \frac{\pi - \alpha}{\pi}} \cdot \frac{\rho_e \cdot I}{2 \cdot \pi \cdot x} \qquad (4\text{-}1)$$

where I is the current, x is the distance from the electrode, ρ_e and ρ_w are the resistivity of the bedrock and the water, respectively. The parameter α is the slope angle of the sea bottom in radians, see Figure 4-11.

The resistivity of the bedrock, in the area of the repository, has been reported by SKB to be in the order of 10^4 Ωm (Löfgren 2007). The water resistivity is set to 1.6 Ωm (Tykesson et al. 1996). The slope angle of the sea bottom outside Forsmark is approximately 1 m/km (Nyman et al. 1988). With a current output of 2,500 A we get the potential distribution shown in Figure 4-12.

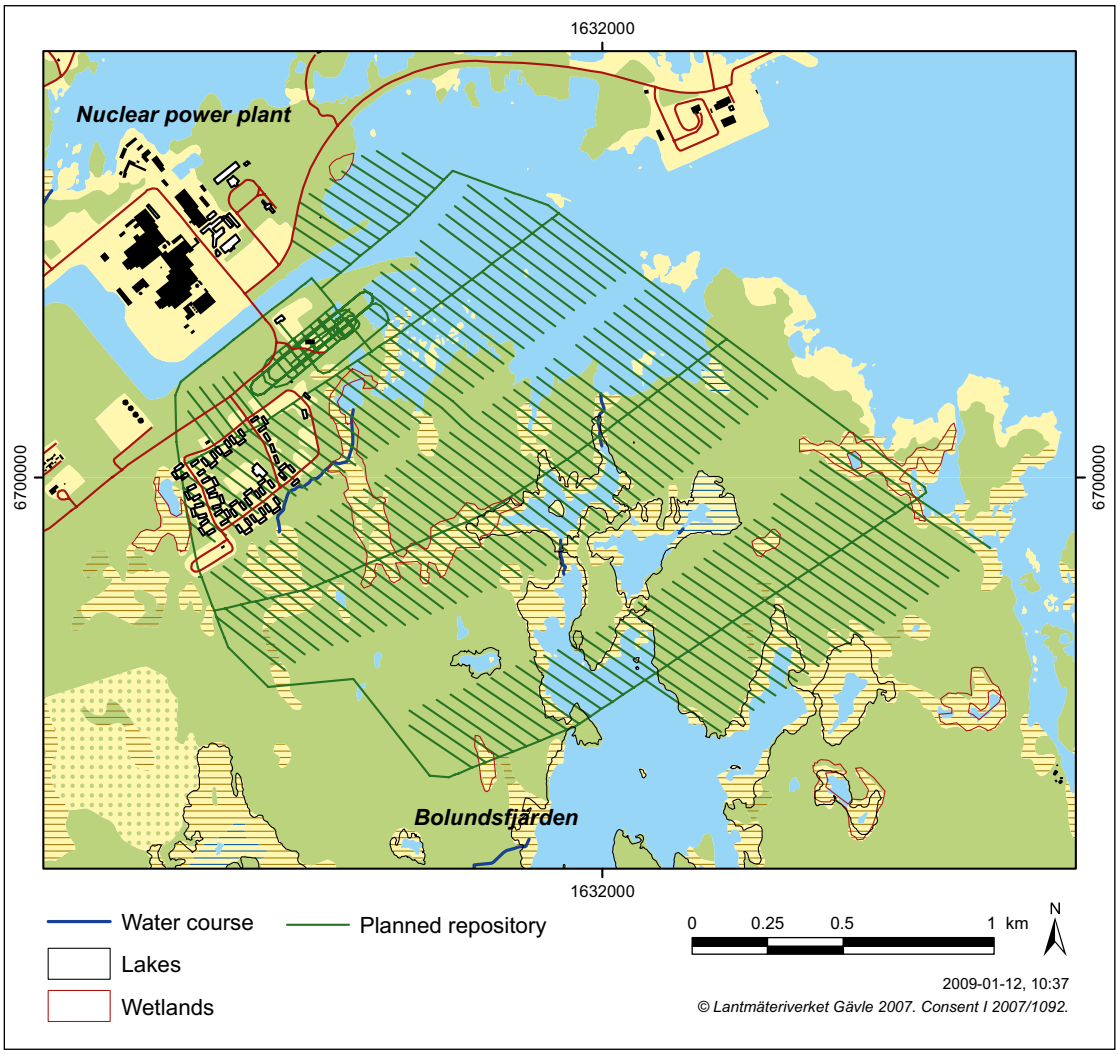

Figure 4-10. *Location of the planned repository, close to the current power plants.*

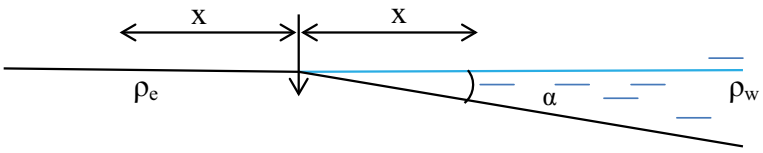

Figure 4-11. *Model for electrode potential calculations.*

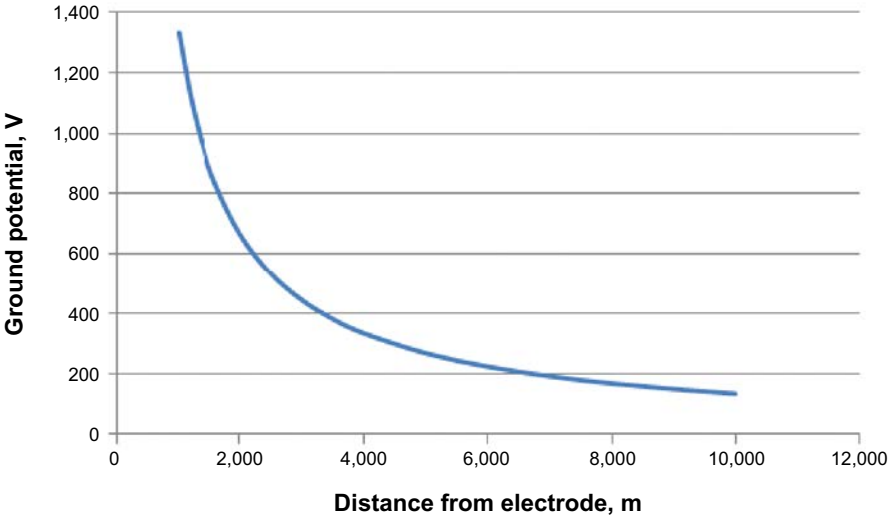

Figure 4-12. *Calculated ground potentials around a hypothetical shoreline electrode located outside Forsmark.*

The ground potential is directly proportional to the current. With a current of 1,250 A instead of 2,500 A the potentials would be half of those presented if Figure 4-12. Compared to the measured potentials in Figure 4-3, the calculated values are much higher. This indicates that Equation 4-1, with a constant resistivity of the bedrock gives too high values of the potential. Further calculations for conditions representing the case for Figure 4-3 are reported in Section 4.3.6, where the resistivity of the bedrock is allowed to vary with the depth below ground.

The grounding resistance (maximum 0.3 Ω) and the maximum field strength in the water (2 V/m) will depend on the size of the electrode. Normally the electrode consists of many sub-electrodes. To avoid causing harm to larger organisms by the high local field strength in the direct vicinity of the electrode surface, rocks are placed on top of the electrode. The field strength as well as the grounding resistance can also be lowered by increasing the number of sub-electrodes and the distance between them.

The Fenno-Skan electrode outside Fågelsundet is influencing electrically grounded objects in the area, even though the maximum field strength on shore is only a fraction of the limit for maximum step voltages, 5 V/m. In practice it is the influence on the low voltage network that decides how close to shore an electrode can be installed. For safety reasons it is not recommended to have higher differences in ground potentials within a low voltage network than 50 V. In the area of Fågelsundet each low voltage network is connected to each other by a medium voltage network (24 kV) carrying no grounding wire, thus avoiding high potential differences in the total electrical network due to the stray currents from the HVDC. Each low voltage network is separately grounded. The low voltage networks have normally an extension of up to 1 km, leading to an allowed field strength of 50 V/km. These deliberations are the basis for one of the type cases of electrical fields that will be studied in this report: Case 1, uniform field strength of 50 V/km. Thus this case treats an electrical field 100 times stronger than today's field at the site of the repository, 0.5 V/km although the effect of Forsmark power station locally rises the value to 1.5 V/km, see Section 4.1.

4.2.2 Possible location of the electrode

The location of the shoreline varies on short timescales (hours to days), e.g., due to variations in the atmospheric pressure distribution and wind speed and wind direction. These short-timescale variations are, however, not of primary importance in the decision process for locating an HVDC electrode. Therefore, only long-term (inter-annual) contributions to the shoreline evolution are considered here.

The water is shallow outside Forsmark why the closest location for an HVDC electrode is presumed to be at least a few km from the repository, see Figure 4-13.

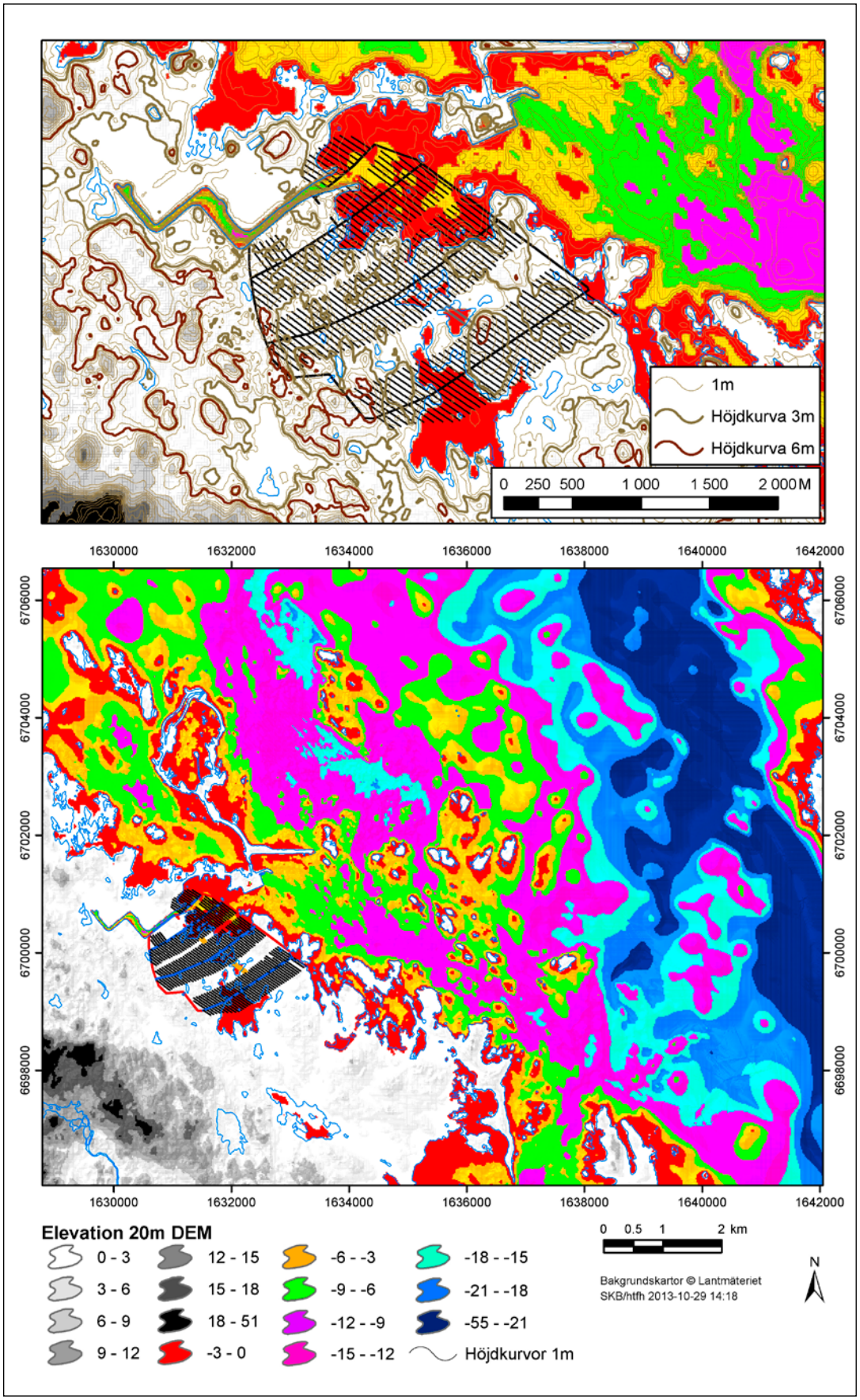

Figure 4-13. *Present elevation distribution in the Forsmark region relative to mean sea-level. Elevations above mean sea-level appear in white and grey tones, whereas elevations below mean sea-level range from red to dark blue.*

The shoreline evolution in Forsmark is determined by the net effect of *eustatic* changes (i.e. sea-level change due to, e.g., changes in the volume and spatial distribution of ocean water) and *isostatic* changes (at the Forsmark site manifested through glacial isostatic rebound with an uplift rate of about 8.4 mm/y). The present day net effect of the two processes at the Forsmark site is a slow lowering of the shoreline.

The current scientific understanding on future shoreline evolution at Forsmark is evaluated in the safety assessment for the final repository for low- and intermediate short-lived radioactive waste, SFR (SKB 2014). The main conclusions reported for the next few thousand years, i.e. in the time perspective for saturation of the buffer are:

- The shoreline at Forsmark may migrate inland during the current century. The worst-case scenarios for sea-level rise until 2100 AD result in submerged conditions for part of the land at the KBS-3 repository with a maximum water depth of cirka 1 m. In a worst-case scenario, a maximum total sea-level rise of 10 m at Forsmark may be realized until 5,000 years after present.
- Shoreline changes at Forsmark due to isostatic rebound amount to 8.4 mm per year at present. The rate of change can be assumed to be constant until 10,000 years after present.
- The longest possible time that the shoreline may remain in the vicinity of the present shoreline location, and thus in the vicinity of the planned repository, was estimated to 1,200 years, under the assumption that the maximum total sea-level rise to occur within the next millennium.

One of the purposes with the present report is to determine whether a future HVDC electrode may cause corrosion problems in the repository and if so, to estimate the minimum distance between an HVDC electrode and the repository where the operation of the HVDC electrode does not cause corrosion problems in the repository. In a one million year time perspective the global climate is likely to experience a number of glacial-interglacial cycles, such as the Weichselian-Holocene glacial-interglacial cycle, which started about 120,000 years ago (SKB 2010c). In SR-Site a reconstruction of the last glacial cycle climate at Forsmark was used as a reference evolution for climate and climate related issues (SKB 2010c, Section 4.5). During the 120,000-year evolution, the Forsmark site is situated below the sea for 16% of the time.

Depending on the relative rates of sea-level change and isostatic change there may be a limited time span during which a future HVDC electrode may be installed closer to the repository than the present shoreline permits.

4.3 Modeling a future HVDC electrode close to the repository

The mathematical (analytical) or numerical description of the electrical field arising around an HVDC electrode is sometimes approximated by exact mathematical solutions such as Equation 4-1. Cases that allow mathematical descriptions of the electrical field include shoreline electrodes where the electrode is located at the shoreline and the sea can be described as slope with a constant angle.

However most HVDC electrodes are located some distance away from the shoreline out in the sea. The reasons may be personal safety and economical.

4.3.1 Modeling the potential field around an HVDC electrode

There are no mathematical solutions to the description of the electrical field around an electrode located one or a few kilometers away from the shoreline. Alternatives are to use the mathematical solution for a shoreline electrode as an approximation or to use numerical methods. However, rather large model volumes may have to be included in a numerical model to give accurate values of the potential relative to distant earth. The only reliable boundary condition is that the effect of the HVDC electrode on the local potential tends towards zero at very long distances. For the present problem we use numerical methods and try to find a compromise between model volume and detailed resolution of conditions at the site of the repository. The potentials relative to distant earth are of little importance for the conditions at the repository provided that differences in potential between different locations within the scale of the repository can be resolved.

The electrical fields that arise around an HVDC electrode will first be studied for locations 2 km from the shoreline, 1 km from the shoreline and at the shoreline. The local field strengths will be compared to today's permissible values as discussed in Section 3.3. Power losses will be compared between the alternative locations of the electrode relative to the shoreline. It will be shown that a location at the shoreline and a location 1 km from the shoreline are not suitable. Resistive power loss and step voltage become acceptable, although still unfavorable, only for the location 2 km from the shoreline. The distance 2 km from the shoreline will thus be selected for study as a location giving conditions corresponding to a 'worst case' in terms of possible corrosion effects on a copper canister in a repository. Finally, the examples generated will be used to connect the FEM-calculations to the theoretical electrical field by applying both procedures to the case of a shoreline electrode where both approaches are possible.

First, however, approximations of the resistivity of the rock in the Forsmark region and the representation of the seabed in the models, are discussed.

4.3.2 Rock resistivity

There seems to be some uncertainty in the determination of the resistivity in the rock surrounding the repository. The values of resistivity that are of importance for the extent of the electrical field from an HVDC are average values including conducting small cracks. Local deviations from the average over distances smaller than the width of a repository tunnel would have little effect on the currents conveyed, by the rock, to or from the repository tunnel.

A total of six different functions for the resistivity of the rock are studied. The resistivity is assumed to be layered and there is no variation in the x-y plane but only vertically. Figure 4-14 illustrates the resistivity as a function of depth below ground, for the different cases. The function *f1* uses a constant resistivity of 10,000 Ωm for all depths. Function *f2* shows a decrease in resistivity in two steps, from 1,000 m to 1,200 m and from 2,000 m to 2,200 m depth. Function *f3* decreases from 10,000 Ωm to 1,000 Ωm in one step from 1,000 m to 1,400 m depth. Function *f4* decreases from 10,000 Ωm to 1,000 Ωm between 800 m and 1,200 m depth and from 1,000 Ωm to 500 Ωm between 1,800 m and 2,000 m depth. Function *f5* uses a low resistivity of 5,000 Ωm from ground level to 800 m depth and function *f6* uses a high resistivity of 20,000 Ωm from ground level to 800 m depth. Both function *f5* and *f6* follow the same curve as function *f4* below 1,000 m depth.

The resistivity functions were selected to cover measured and estimated values of the resistivity in the bedrock in the Forsmark region (Thunehed and Pitkänen 2007).

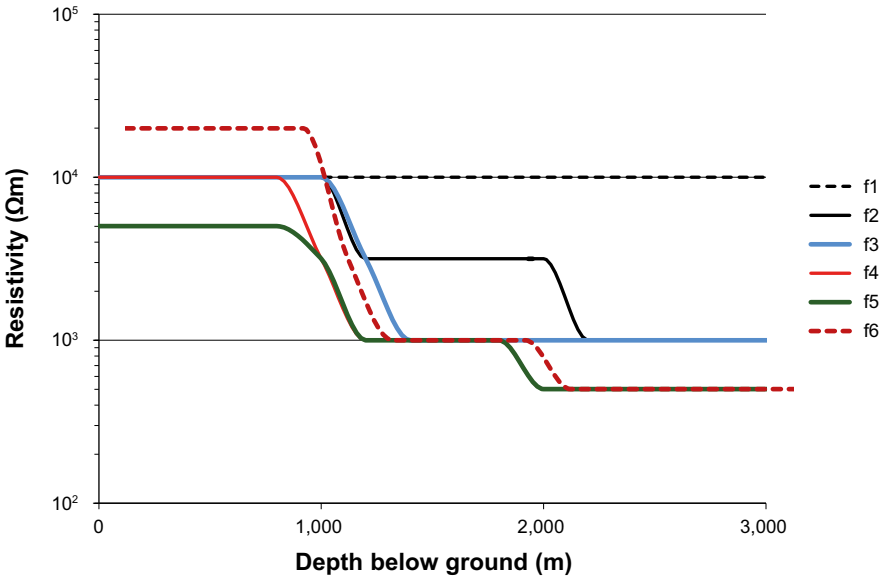

Figure 4-14. *Rock resistivities as a function of depth below ground. Different alternative dependencies (f1 through f6) are illustrated.*

4.3.3 Approximation of a small angle of the seabed as a larger angle with a modified conductivity

For the present numerical case it is found impractical to represent so small angles as 1 m/1,000 m. This angle is approximately 0.0573°. In this study the seabed is instead represented as having a slope of 2°. Estimates of the resistivity of the seabed and the bedrock are 1.6 Ωm and 10,000 Ωm, respectively. The resistance in the sea and in the rock will mainly behave as parallel conductors. The conductance over the 2° angle consists of 0.0573° seawater and (2–0.0573)° rock. The average conductivity becomes (0.0573/1.6+(2–0.0573)/10,000)/2=0.018 S/m. Thus a conductivity of 0.018 S/m over an angle of 2° is used to represent the aqueous volume. Rock resistivity functions *f5* and *f6* have resistivities that differ from 10,000 Ωm but the difference in the average conductivity is so small that the same value is used for all resistivity functions.

With the increased angle of the seabed to 2°, the water depth at the site of an electrode located 2 km from shoreline is 2/0.0573×2 m = 69.8 m, which is still small compared to the repository depth.

4.3.4 Electrical field strength

The model geometry used is depicted in Figure 4-15. A hemisphere with a radius of 8 km around the electrode is considered. The slope angle of the seabed is assumed to be 1m/1,000m but recalculated to the larger slope angle of 2° as described in Section 4.3.3.

Figure 4-16 shows the field strength that arises at ground level in the direction towards land and inland from the shoreline. Rock resistivity function *f2* is used. The green curve corresponds to a location of the electrode 2 km from the shoreline. As Figure 4-16 shows there is a peak in the electrical field strength where the conductive medium changes from water to rock, at 2 km distance from the electrode. For this location the maximum field strength is about 3 V/m on shore. This value is lower than the value discussed as a likely maximum in Section 3.3, which is 5 V/m on land. The field strength in the sea is much higher, close to the electrode. However, engineering of the electrode itself in terms of shape and effective radius can mitigate the field strength close to the electrode. Local fencing around the electrode can also be applied to prevent damage to fish. The maximum value for the field strength in the sea discussed in Section 3.3 is 2 V/m. For the location of the electrode 2 km from the shoreline, this value is exceeded only within 200 m from the electrode center and the mitigating procedures seem reasonable. Figure 4-16 also shows a curve for the location of the electrode 1 km from the shoreline. The maximum field strength for this case is higher than 10 V/m on land, which exceeds the 5 V/m discussed as a likely maximum value. Such a location of the electrode would require fencing of parts of the shoreline, in order to protect mammals, as well as fencing of a larger radius around the electrode, in order to protect fish. The third curve, blue, in Figure 4-16 represents the field strength around a shoreline electrode. Today's allowed values of the electrical field strength are exceeded within a distance of about 500 m inland and within a large distance from the electrode, in the sea.

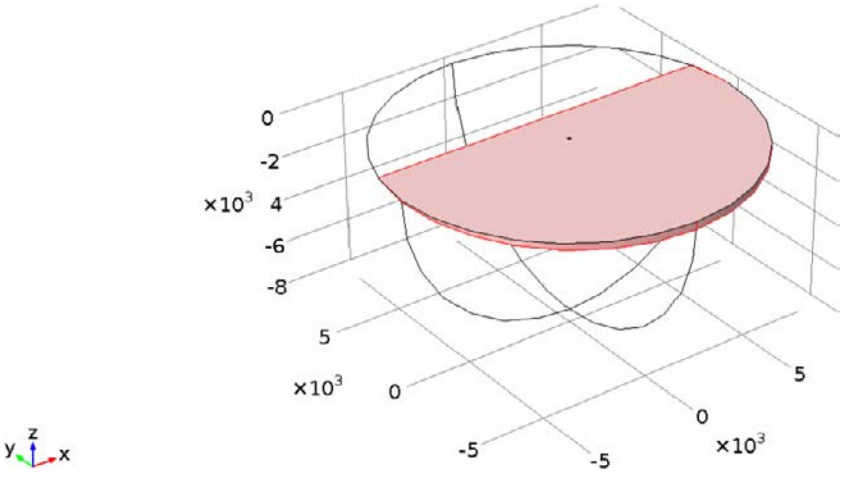

Figure 4-15. *The geometry used for studying the effects on land of an HVDC electrode located 2 km from the shoreline. The colored disc shows the extent of the sea, in the model. The black dot at the center of the hemisphere indicates the location of the electrode. The radius of the model hemisphere is 8 km.*

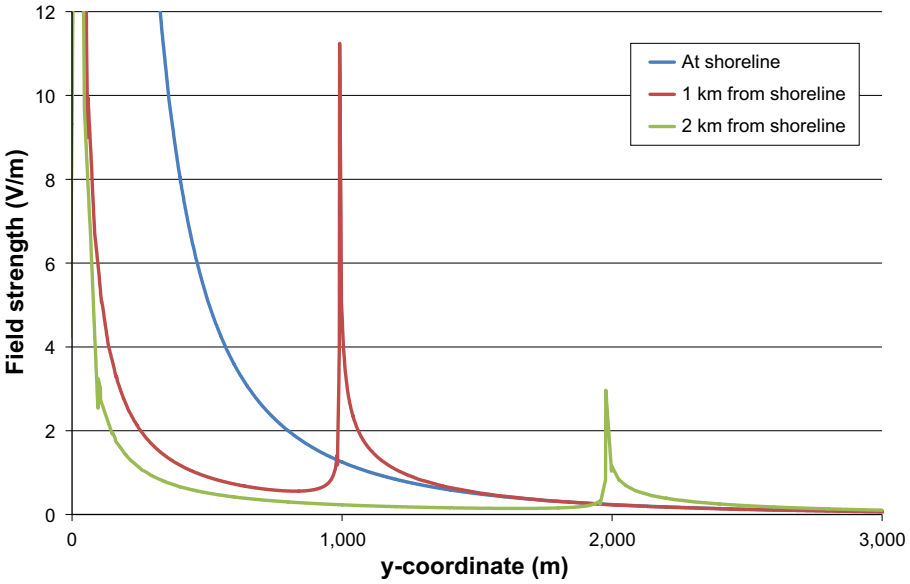

Figure 4-16. *The field strength that arises at ground level in the direction towards land and inland from the shoreline, for different locations of the electrode: 2 km from the shoreline (green), 1 km from the shoreline (red) and at the shoreline (blue). Rock resistivity function f2 is used.*

4.3.5 Potentials and power loss

The calculations that were used for the field strength in Section 4.3.4 are here used to estimate the power loss at the electrode for the alternative locations 2 km from shoreline, 1 km from shoreline and at the shoreline.

Figure 4-17 shows the distribution of the potential around a 2,500 A electrode located 2 km from the shoreline. The curves were cut at a distance of 200 m from the center of the electrode. Within this distance of 200 m, local electrode engineering may affect the potentials but is likely to have small effects at greater distances. As Figure 4-17 shows, potentials of about 1,000 V are required to drive 2,500 A through the electrode. If the electrode is considered to have a radius of 200 m and the potential at the outer boundary of the model sphere is approximated as distant earth, the electrode would have a resistance of 1,000 V/2,500 A=0.4 Ω.

Figure 4-18 shows the distribution of the potential around an electrode located 1 km from the shoreline and Figure 4-19 shows the distribution of the potential around an electrode located at the shoreline. The voltages between electrode and distant earth appear as power losses in the transmission. There is a strong incitement to minimize the power loss.

Comparing the levels of potential between the electrode and distant earth, a location 1 km from the shoreline in Figure 4-18 shows a level of potential of about 1,600 V and for a location at the shoreline Figure 4-19 shows a level of potential of about 6,000 V. Thus in terms of power loss, for a location 1 km from the shoreline the power loss is about 60% higher than for a location 2 km from the shoreline and for a location at the shoreline, the power loss is about 6 times higher.

In absolute terms, the potential difference of 1,000 V for 2,500 A corresponds to a loss of 2.5 MW. Thus it is likely that great efforts will be made to minimize the potentials also for future installations.

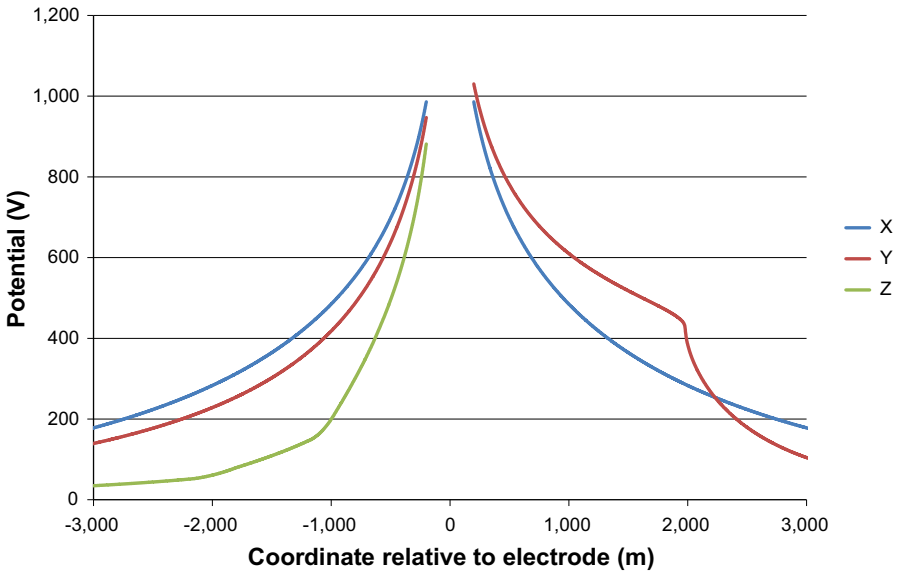

Figure 4-17. *The distribution of the potential around an electrode located 2 km from the shoreline. Positive y-coordinates indicate the direction towards land and on land. Rock resistivity function f2 is used.*

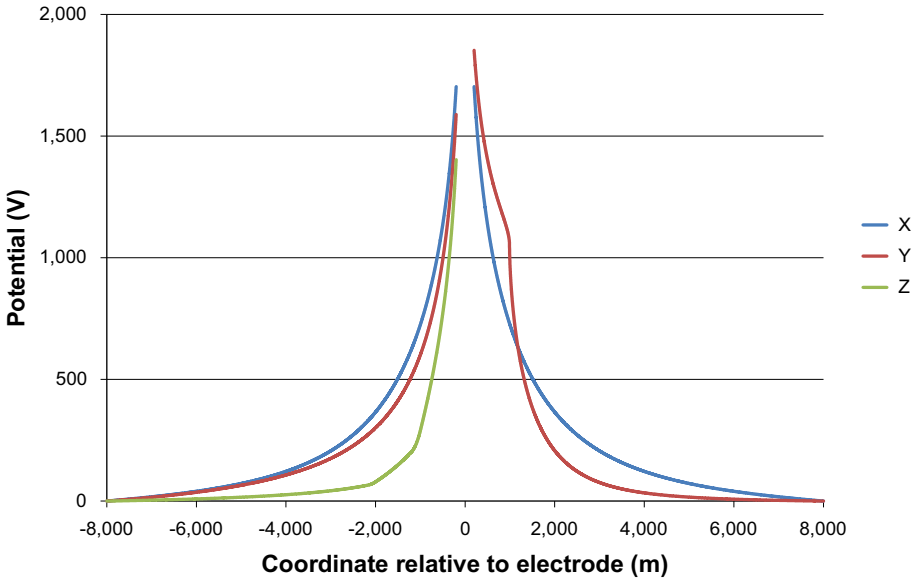

Figure 4-18. *The distribution of the potential around an electrode located 1 km from the shoreline. Positive y-coordinates indicate the direction towards land and on land. Rock resistivity function f2 is used.*

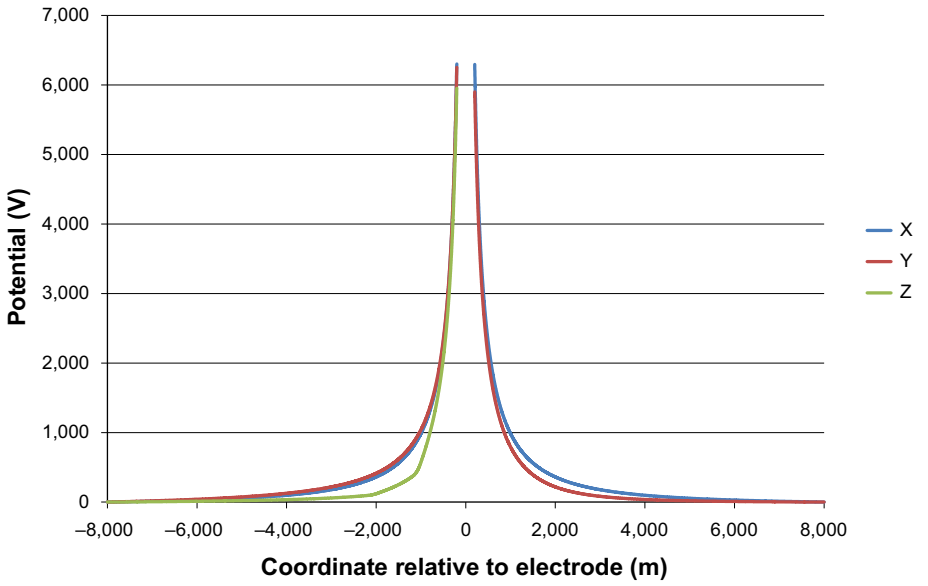

Figure 4-19. *The distribution of the potential around an electrode located at the shoreline. Positive y-coordinates indicate the direction towards land and on land. Rock resistivity function f2 is used.*

4.3.6 Comparison between measured potentials and calculated potentials

A set of calculations was performed to study model predictions for the various functions of rock resistivity relative to the measured potentials illustrated in Figure 4-3. The conditions for the calculation were selected to be similar to the conditions for the Fenno-Skan anode. Thus a current of 1,250 A was fed from a sea-based electrode located 2.3 km from the shoreline. A seawater resistivity of 1.6 Ωm and a slope angle of 1 m/ 1,000 m were used. The radius of the model hemisphere was 32 km.

Figure 4-20 shows the resulting potentials in a direction from the electrode out towards the sea, which is the direction of the field in Figure 4-3. The electrical fields are not symmetrical. For comparison with the observed potentials, approximate values for some selected points were read from Figure 4-3, curve D Fenno-Skan anode, and drawn as connected black circles in Figure 4-20.

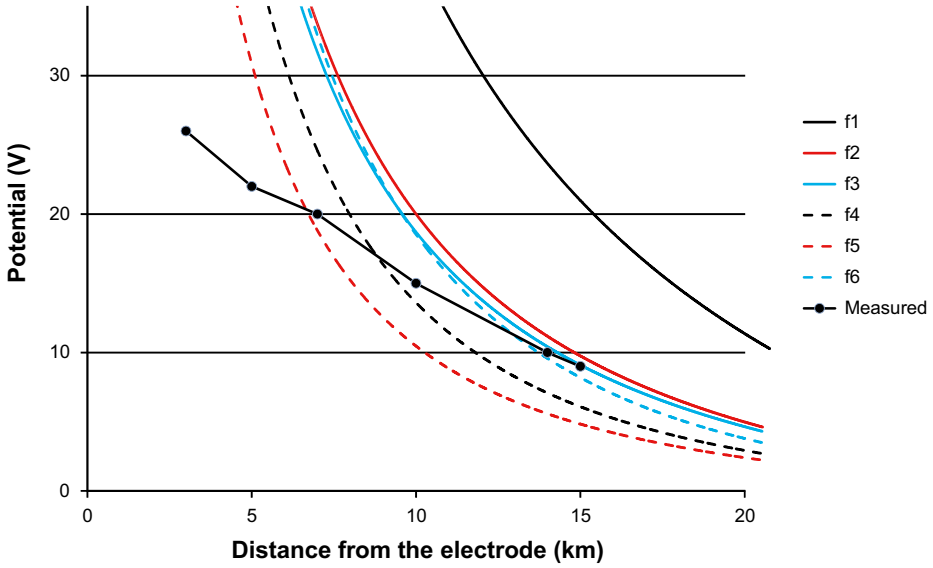

Figure 4-20. *Calculated potentials in the direction out towards the sea for an electrode located 2.3 km from the shoreline using various functions for the rock resistivity, f1 through f6. Current output 1,250 A. Measured values are taken from Figure 4-3, Fenno-Skan.*

Compared to the measured values, resistivity functions *f2*, *f3* and *f6* show good agreement at distances around 15 km from the electrode. At distances lower than about 6 km all resistivity functions give potentials much higher than the measured. The differences between calculated and measured potentials show that the electrical field close to the Fenno-Skan electrode cannot be described using any of the resistivity functions in combination with the used sea water resistivity and constant slope angle.

The calculated results used in Figure 4-20 also provides data for the potential distribution in the opposite direction. Figure 4-21 show the resulting potentials in a direction from the electrode, towards land and finally, at distances higher than 2.3 km, on land. The intention is to compare the calculated results with the measurements performed by Swerea-Kimab and the results have here been rescaled to reflect that the unbalance current was 1,670 A (only Fenno-Skan 2) during the measurements but 1,250 A (only Fenno-Skan 1) for the calculations. The fact that the signs are opposite is neglected and all potentials are presented as positive values.

The difference in potential between the shoreline and a location 5 km from the electrode can be estimated to about 460 V for resistivity function *f1*, and 420 V, 400 V, 370V, 250 V and 500 V, for resistivity function *f2*, *f3*, *f4*, *f5* and *f6*, respectively. These voltages should be compared to the measured value of about 200 V. Clearly, all resistivity functions except *f5* give much higher voltages than the measured.

The differences and similarities between measured values and model values may be understood as a combination of several factors:

- The coast at the location of the electrode is more open than assumed in the model. Figure 4-1 shows that there is open sea not only east-northeast but also due north and to some extent north-northwest.
- The coast is not a straight line. The distance of 2.3 km between the electrode and the shoreline is the shortest distance. For the comparison with model results it would be more relevant to consider the shortest distance to an ‘average shoreline’. No ‘average shoreline’ is estimated here but it is evident that the distance between the electrode and an imagined ‘average shoreline’ is longer than 2.3 km and if a longer distance was introduced in the model, the resulting voltages would be lower and in better agreement with observations.
- The sea water may be deeper at the site of the electrode than average for that distance from the shoreline.

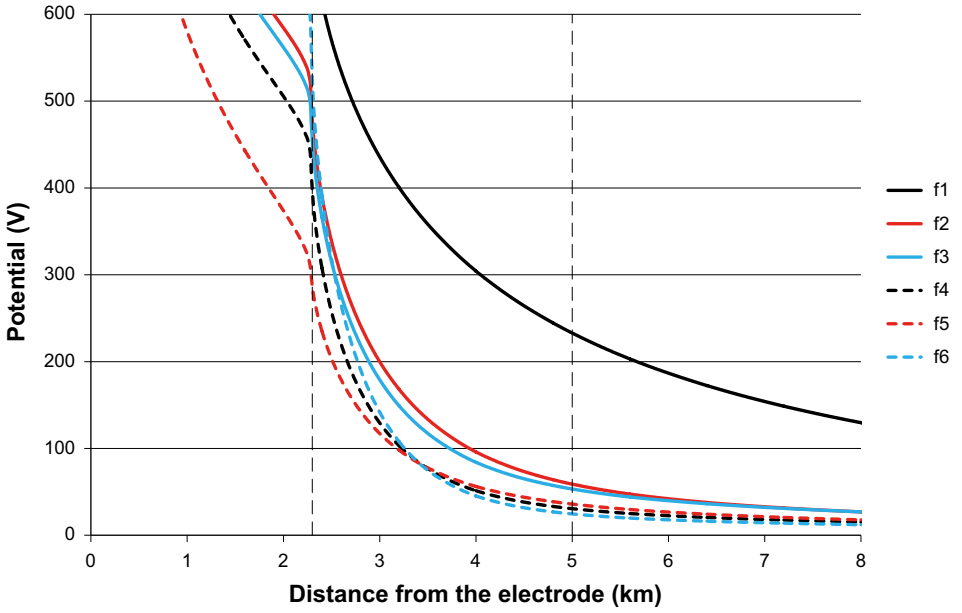

Figure 4-21. *Calculated potentials in the direction towards land and on land for an electrode located 2.3 km from the shoreline using various functions for the rock resistivity, f1 through f6. Current output 1,670 A. The dashed vertical lines indicate the location of the shoreline and a position 5 km from the electrode, respectively.*

These factors may have been of importance for the location of the electrode at the present site since they contribute to decrease the resistive losses in the transmission. It is reasonable that the main difference between observed and measured values decreases at longer distances, as Figure 4-20 shows. At some distance from the electrode, the average depth of the water becomes more important than the local depth because the current spreads in all directions.

In conclusion, the local conditions at the Fenno-Skan electrode and the surroundings, regarding local depth and shoreline profile, have not been introduced model into the model with sufficient resolution to allow better agreement with the observations. The model aims at describing the electrical field surrounding an HVDC electrode at any randomly selected site, here located 2.3 km from the shoreline. The differences between modeling results and measurements may reflect the fact that the location of the present Fenno-Skan electrode was not randomly selected but chosen to give low resistive losses in the transmission.

It should be mentioned that we here apply the model mainly to a possible future electrode located outside Forsmark and located closer to the repository where the description of the present day shoreline as a straight line is better than it is for the present location of the Fenno-Skan electrode, see Figure 4-1.

4.3.7 Results from the finite elements model relative to results for a mathematical solution

Figure 4-22 shows a dashed line, with the legend "R", in addition to the three colored solid lines. This dashed line illustrates the values obtained by using Equation 4-1 with 1.6 Ωm for the sea water resistivity and 10,000 Ωm for the rock resistivity, a slope angle of 1 m/1,000 m and 2,500 A. All parameter values used for the mathematical solution are the same as used in FEM-calculations. The recalculated slope angle and sea water resistivity, according to Section 4.3.3, was applied for the FEM-calculation but not to the mathematical solution. The results in Figure 4-22 are virtually indistinguishable. The potential for the mathematical solution are given relative to the potential at a distance of 8 km, which is the radius of the model sphere used for the FEM-calculations. It is concluded that, for the case where a comparison is possible, the FEM-calculation gives the same results as the mathematical solution.

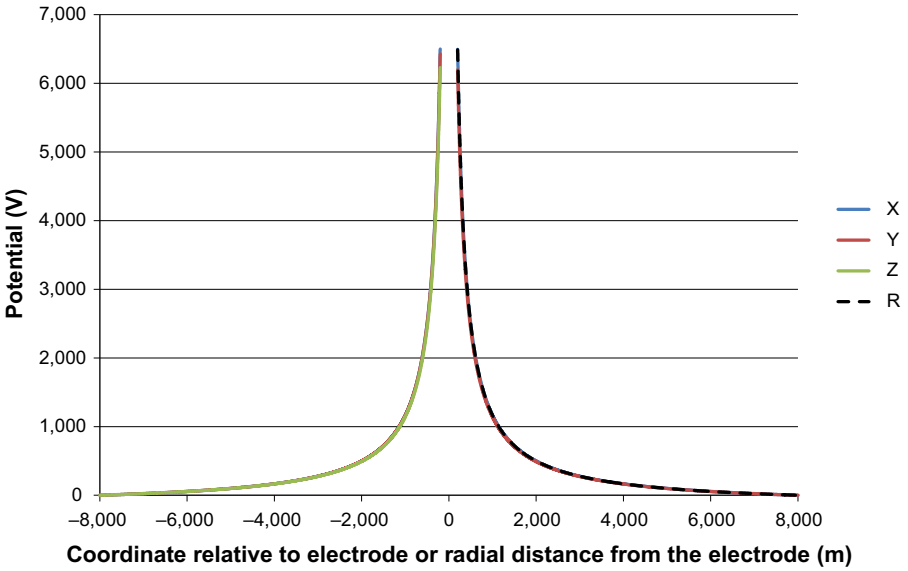

Figure 4-22. *The distribution of the potential around an electrode located at the shoreline. Positive y-coordinates indicate the direction towards land and on land. The dashed line shows the results for the mathematical solution, using Equation 4-1, for the same problem.*

5 Modeling of stray current influence on copper canisters

5.1 Conditions

The following analysis of the stray current interference is based on the layout illustrated in Figure 4-10. The copper canisters are installed in deposition holes and surrounded with bentonite, according to Figures 5-1 to 5-3.

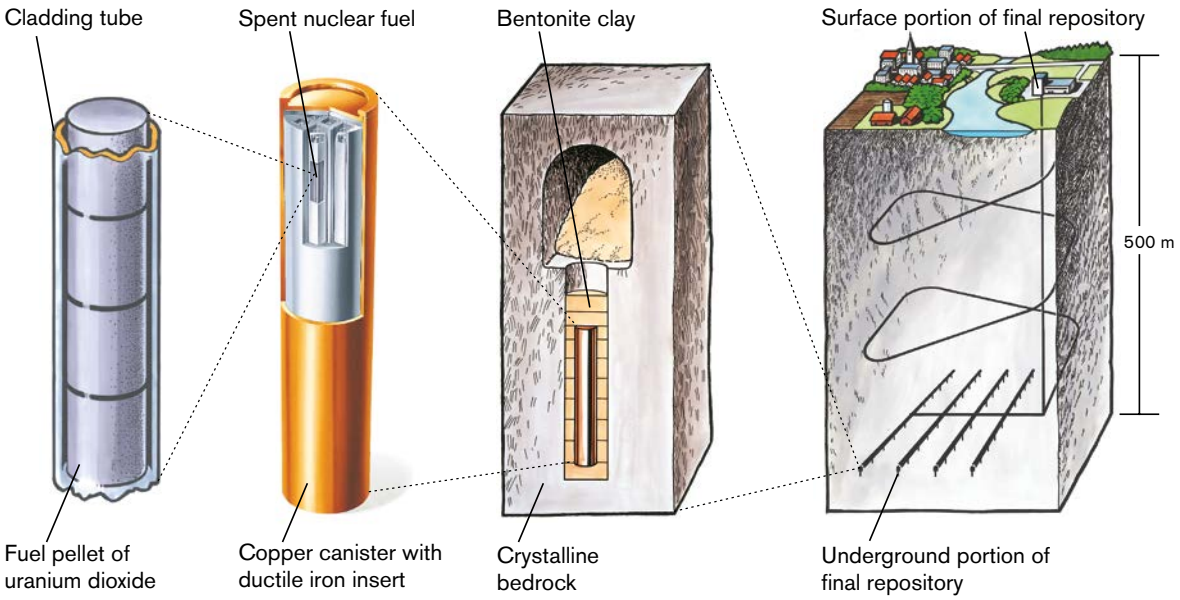

Figure 5-1. *The KBS-3 concept for disposal of spent nuclear fuel (SKB 2011).*

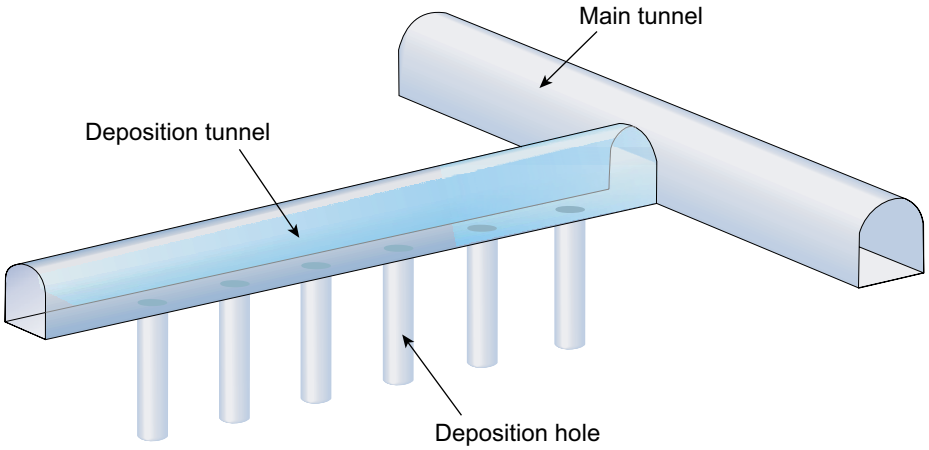

Figure 5-2. *Tunnels and deposition holes.*

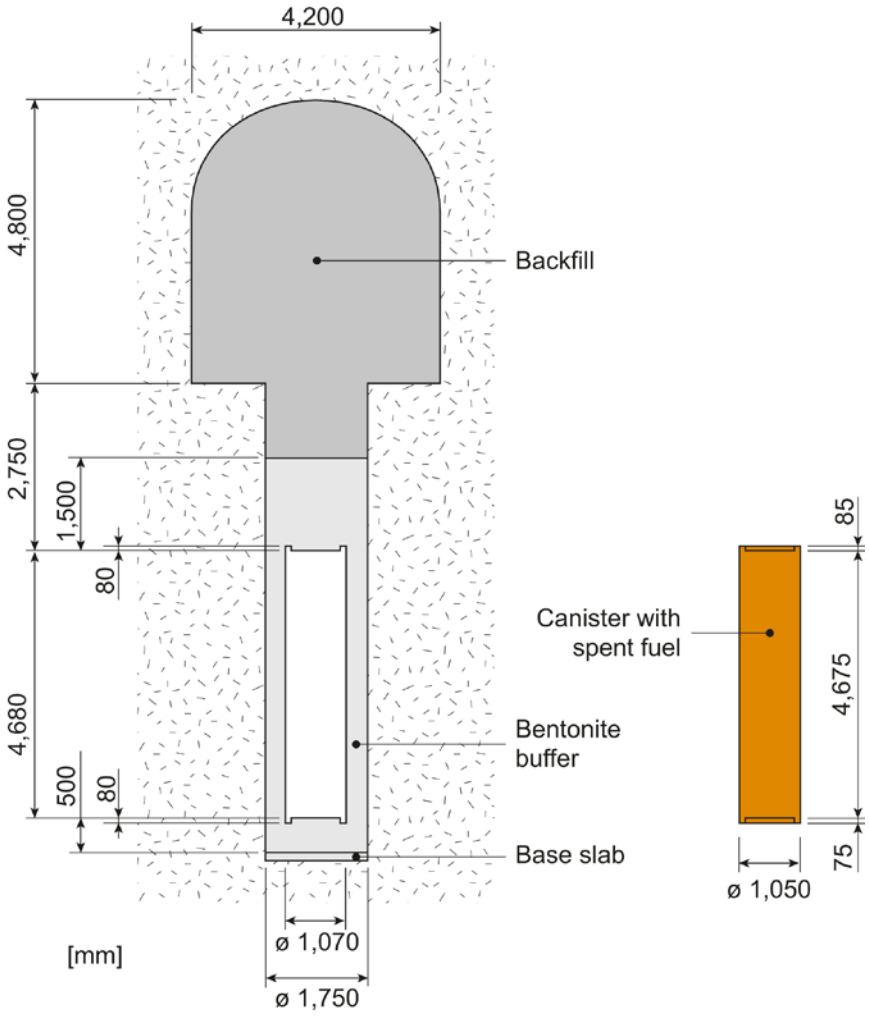

Figure 5-3. *Dimensions of the deposition hole and tunnel (left) and canister (right). The dimensions given for the left hand object refer to the cavity in the bentonite buffer that will be filled by the canister and not to the canister itself. In the modeling the canister height is set to 5 m and the deposition hole depth to 8 m.*

The deposition tunnels, and transport and main tunnels at deposition depth, are filled with bentonite. The bentonite in the deposition tunnels is, for modeling purposes, presumed to be fully water saturated from the start, giving the lowest possible resistivity, in the order of 1 Ωm (SKB 2010a). Rothfuchs et al. (2004) give a lowest resistivity of 1.6 Ωm at a water content of 32.9% at 22°C for MX-80 bentonite. A value of 1 Ωm is used in the modeling for the base case. The bentonite blocks in the deposition holes have a water content of 17%, by weight, when installed (SKB 2010a). The water content will increase as the repository becomes water saturated. A fully water saturated bentonite will have a water content of 28 % by weight. During the saturation stage, the degree of saturation around the canister will vary in time due to heating from the canister. The relationship between the water saturation and the resistivity of the bentonite will be discussed in Chapter 6.

As described in Section 4.2 there are several different cases of influence. While case 3 and 4, an electrode directly on top of the repository or in the close vicinity of the repository, is not anticipated, see Section 4.3, such a location cannot be unconditionally excluded. We therefore treat all separate cases. Case 1 treats a uniform electrical field resulting from a remote electrode. Case 2 treats the effect of the grounding at the Forsmark Power station (or a future corresponding installation) connected to remote grounding sites.

Case 3 and case 4 assume that a hypothetical new sea-based electrode is installed. The distance between the repository and this new electrode is finally varied in order to investigate safe distances with respect to corrosion of the most affected canisters in a repository.

5.2 Calculation steps

As described in Section 2.2 the calculation procedure in the present study is divided in several steps.

1. Calculation of the electrical fields at the repository depth of 500 m. A small part of the tunnel system is included but the deposition holes are not represented. Specifically, the difference in potential between the tunnel floor and 8 m below is calculated. This is the voltage that would be imposed over a deposition hole if the resistivity in the deposition hole was the same as that of the surrounding rock. Calculations are generally made using models that span several kilometers around the HVDC electrode with resistivities intended to represent real conditions at and around Forsmark.
2. Calculation of the effects of the deposition holes on the electrical fields calculated in point 1, above. The deposition holes are here treated as having various conductive properties that decrease the voltage found in point 1. These calculations are generally made using smaller modeling volumes so that the deposition holes can be adequately represented in the model geometry.
3. Calculation of conductive properties of the bentonite in the deposition hole at various degrees of water saturation.
4. The conductance in the bentonite parallel to the canister is together with results from points 1 and 2 used to calculate the voltage along the height of a canister.
5. Estimation of possible corrosion effects of voltages along the height of a canister.

Figure 5-4 shows an equivalent electrical circuit for the effect of an external electrical field on the electrochemical corrosion of a copper canister in a deposition hole.

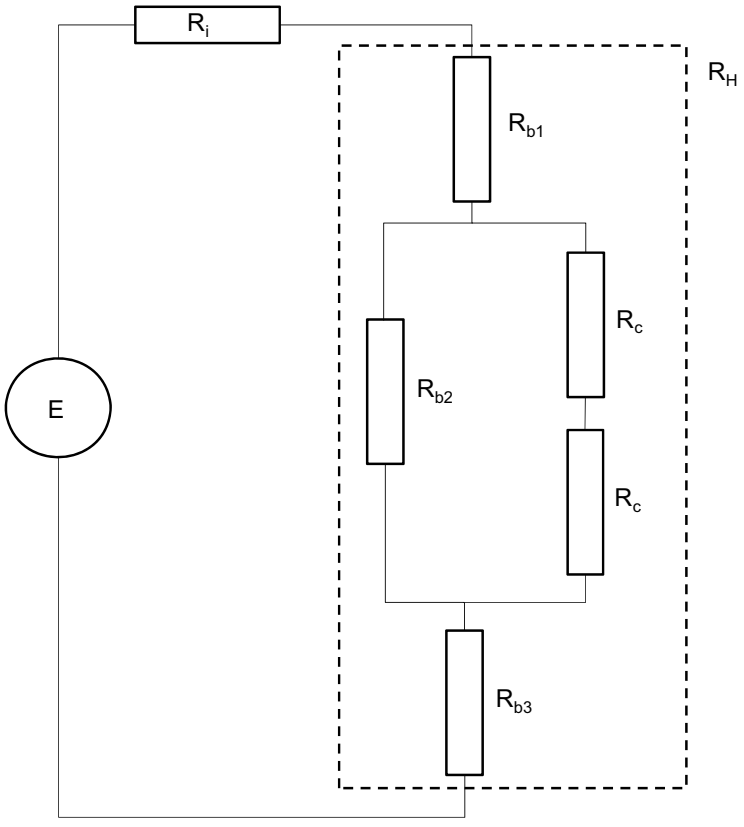

Figure 5-4. *Equivalent electrical circuit for the effect of an external electrical field on the electrochemical corrosion of a copper canister in a deposition hole.*

The electrical circuit consists of a source with a potential, E. This potential source is connected to a resistance, R_H, via an internal resistance, R_i. The source potential is here referred to as electro-motive force, given in V. The internal resistance of the field, R_i, represents the resistance in the current's path, outside of the deposition hole. The resistance R_H represents the resistance between the top and bottom circular end surfaces of the deposition hole. This resistance R_H, is further divided into R_{b1}, R_{b2} and R_{b3} that represent the resistance in bentonite on top of the canister, bentonite surrounding the canister and bentonite below the canister, respectively. R_c represents the resistance for current going into and exiting from the copper canister.

It is found that the voltage that develops along the height of a canister is determined by three parameters, mainly. These are, the electromotive force, E, the internal resistance, R_i and the resistance in the bentonite parallel to the canister, R_{b2}. Equal attention is therefore given to the estimation of values for these three parameters.

The transition from the FEM-model to the equivalent circuit requires some assumptions. Only the current in the direction along the height of the canister is considered relevant. There is also a component of the current in each of the two directions perpendicular to the axis of symmetry of the canister and the deposition hole. The possible effects of these current components are not studied here. The reasons are that the diameter of the hole and of the canister is much smaller than the corresponding height and that the sequence of the resitivities for current passing perpendicular to the axis of symmetry would be determined by rock-deposition hole-rock whereas the sequence of the resitivities for current passing along the axis of symmetry would be determined by tunnel-deposition hole-rock. Both these factors contribute to make the voltages that arise, across a canister, perpendicular to the axis of symmetry much smaller than the voltages that arise along the axis of symmetry.

5.3 Data for sensitivity analysis

Several parameters are varied in this study in order to provide data for a sensitivity analysis:

- rock resistivity,
- location of shoreline in relation to the repository,
- sea water resistivity and slope angle of the sea bed,
- fistance between the HVDC electrode and the repository,
- angle between tunnel and the electrical field,
- edge tunnel or center of three tunnels,
- length of the tunnel system,
- resistivity of the bentonite in the tunnel system and in the deposition hole,
- different positions of the deposition hole relative to the end of a tunnel.

5.4 The model representation of the repository

Several different representations of the repository or parts of the repository are used in this study. A relatively detailed representation of the tunnel system and of the vertical shafts and ramp that connect the repository level and ground level is used for cases where the electrical current in the shaft may be significant (cases 3 and 4). For cases where the electrical current in the shaft is expected to be low (cases 1 and 2), the repository is represented by a set of three 600 m long deposition tunnels interconnected by a main tunnel and by a set of two 1,700 m long deposition tunnels.

Figure 4-10 shows one design of the repository. Figure 5-5 illustrates how the repository may be constructed, including temporary transport tunnels (SKB 2009).

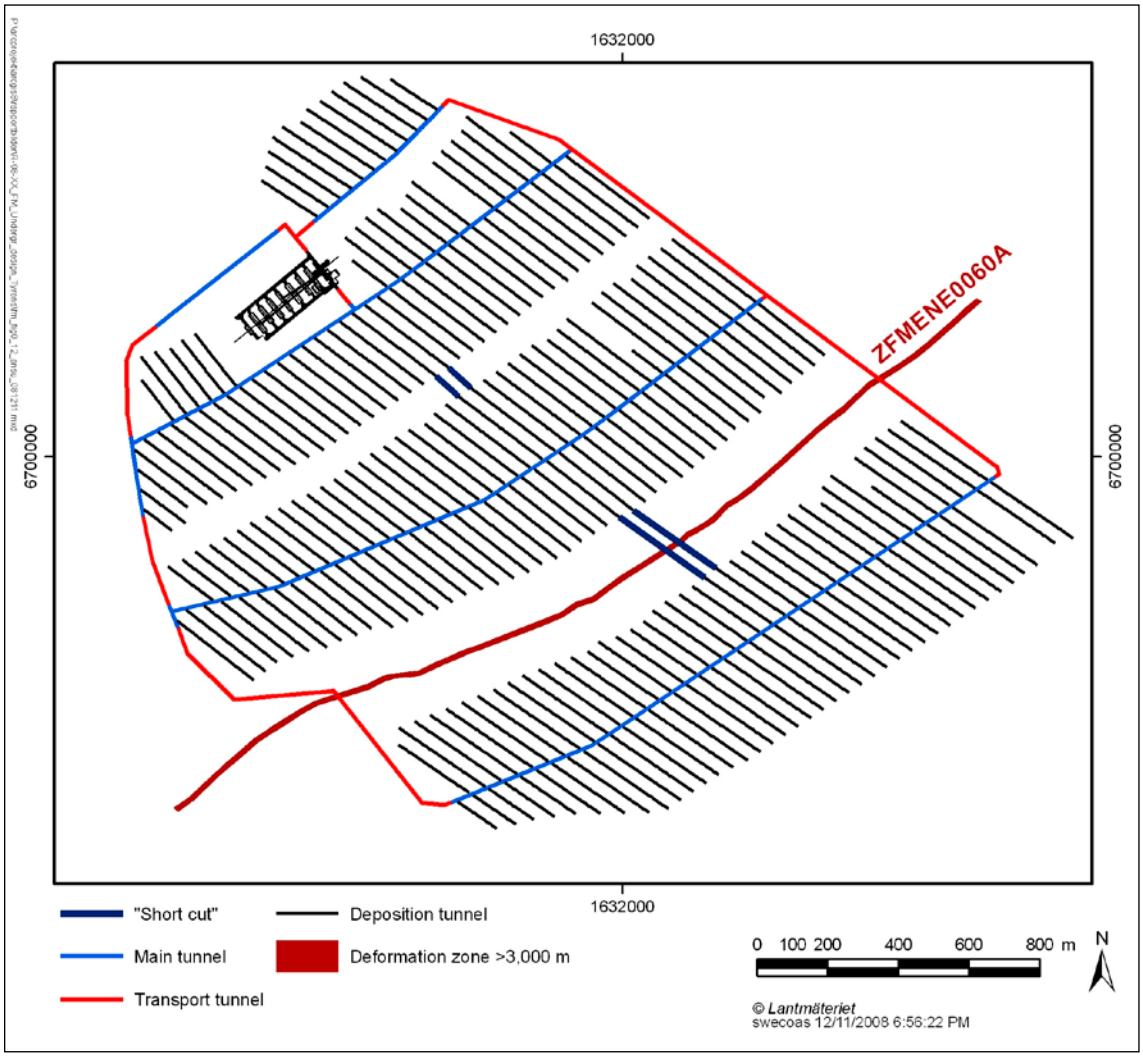

Figure 5-5. *Illustration of the repository with temporary transport tunnels.*

Figure 5-6 shows details of the ramp and vertical shafts at repository level. The various vertical shafts meet the transport tunnel in a rather complicated row of halls. In the model representation of the repository the vertical shafts are collected into one large shaft. The conductivity in the model shaft is adapted to give the same conductance between the repository level and the ground level as the total area of the individual shafts including the ramp.

Figure 5-7 shows the detailed representation of the repository used for cases 3 and 4. The blue lines indicate the main and transport tunnels, the black lines indicate deposition tunnels and the red rectangle represents the set of halls where the various vertical shafts meet the ramp that connects the repository level with the ground level. The model shaft is represented by the black rectangle inside the red rectangle.

The number of tunnels and their location in the model repository were selected to allow the branching of current from an electrode at the ground level conducted by the model shaft into the various deposition tunnels.

For cases 1 and 2, where the current in a shaft would be low, the representation of the repository is simplified further. Two details from Figure 5-7 were selected: a set of three 600 m long deposition tunnels interconnected by a main tunnel and a set of two 1,700 m long deposition tunnels.

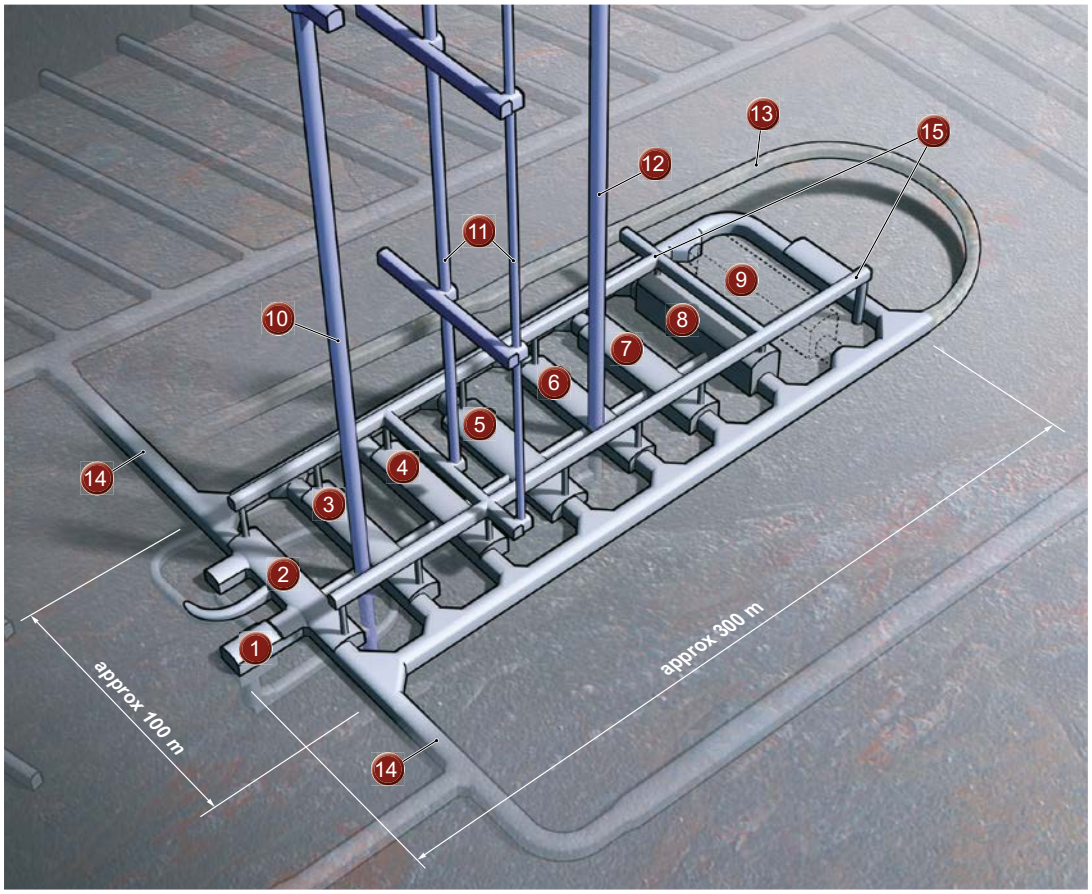

Figure 5-6. *The different parts of the central area at repository level: 1. Rock loading station 2. Rock hall 3. Skip hall 4. Electricalhall 5. Vehicle hall 6. Elevator hall 7. Storage and workshop hall 8. Transloading hall 9. Extra space 10. Skipshaft 11. Ventilation shaft 12. Elevator shaft 13. Ramp 14. Transport tunnels 15. Ventilation tunnels.*

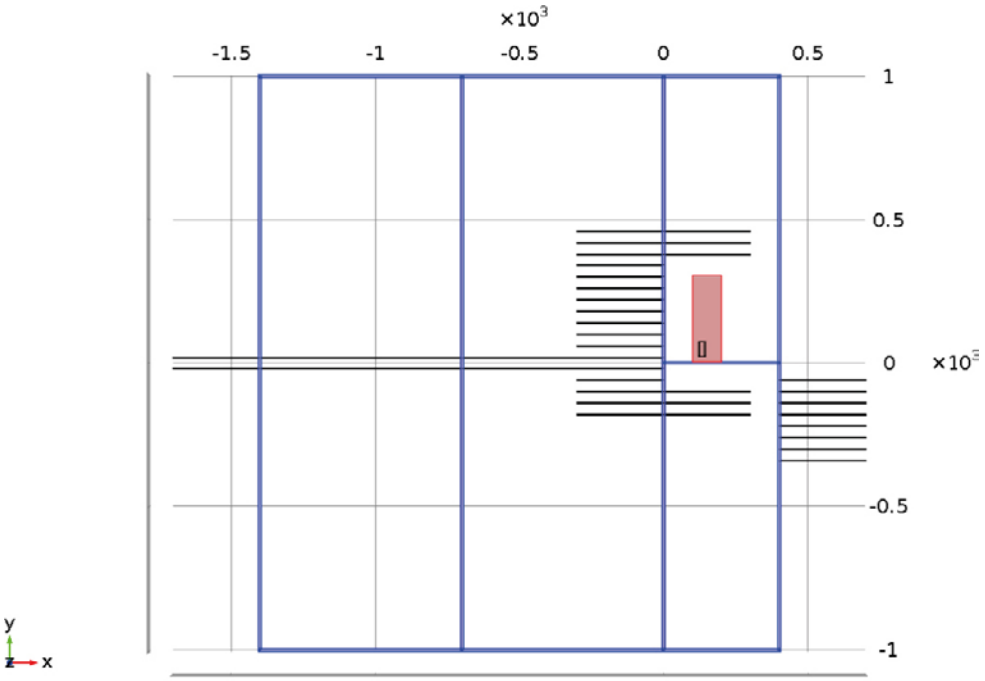

Figure 5-7. *The detailed representation of the repository used for cases 3 and 4. The blue lines indicate main and transport tunnels, the black lines indicate deposition tunnels and the red rectangle represents the set of halls where the various vertical shafts meet the ramp that connects the repository level with the ground level. The model shaft is represented by the black rectangle inside the red rectangle.*

Figure 5-8 shows the representation of the tunnel system with 3 interconnected tunnels. Three 600 m long parallel tunnels with a distance of 40 m between centerlines are used. A larger tunnel (main tunnel) extending a total of 300 m interconnects the three tunnels. The 600 m deposition tunnels have a cross section area of 18.3 m^2. The interconnecting tunnel has a cross section area of 60 m^2 (SKB 2009). The cross sections of the tunnels are only approximately represented. The deposition tunnels are modeled as composed of a rectangle with a triangle on top with a 90° top angle and the interconnecting tunnel has a rectangular cross section. The height of the interconnecting tunnel is the same as the top height of the deposition tunnels.

5.5 The model representation of the HVDC electrode

For the case with a remote electrode, the electrical field is assumed to be constant and not diverging. The actual electrode is not represented for this case. For case 2, Forsmark as a secondary source, the HVDC electrode is not represented and the secondary source is represented as a point current source. For cases 3 and 4 where the HVDC electrode is located directly on top of or close to the repository, the electrode is represented as a ring of 8 sub-electrodes each feeding an equal current. The sub-electrodes are represented as point current sources and the ring has a radius of 100 m. A model electrode smaller or equal in size to the model shaft would allow a large part of the current to be, more or less, directly conducted to the repository level by the high conductivity shaft. A larger model electrode would automatically distribute the current over a wider range and the fraction of the current conducted by the shaft would be smaller. The application of a smaller model electrode thus gives a more pessimistic estimate than a larger model electrode (e.g. the 200 m electrode used for illustration in Section 4.3.5). Figure 5-9 shows the ring of electrodes in red located directly on top of the model shaft in the model repository.

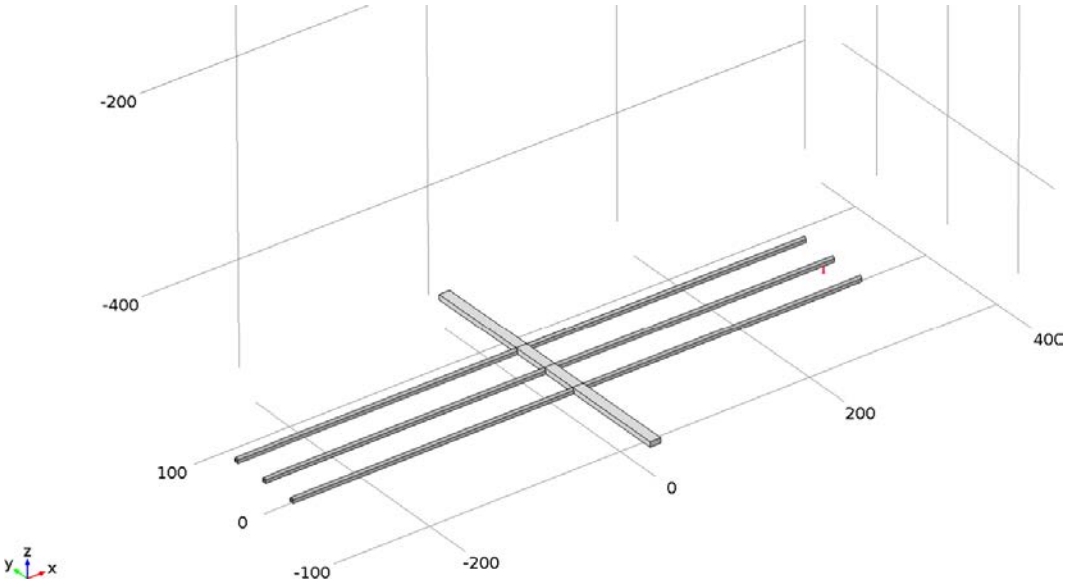

Figure 5-8. *Representation of the 600 m tunnel system. Three 600 m long deposition tunnels are interconnected by a 300 m long, wider tunnel. Here the tunnel system is located with common base plane at 500 m depth, z=–500, with the center point at x=0 and y=0.*

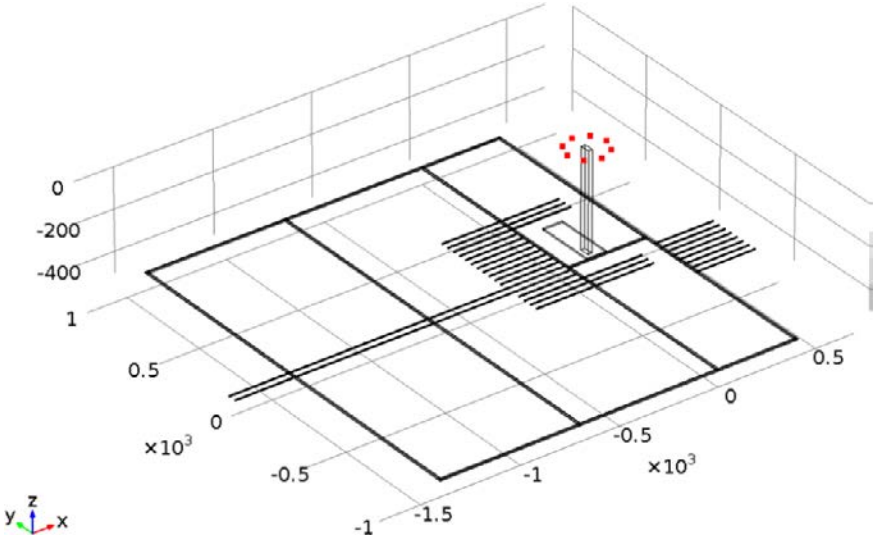

Figure 5-9. *The HVDC electrode represented as a ring of sub-electrodes, in red, located directly on top of the model shaft in the model repository.*

5.6 A uniform electrical field resulting from a remote electrode (Case 1)

The background for this case is personal safety and the grounding of low voltage networks with an extension of about 1 km. Taken together these considerations lead to a reasonable limit for permissible field strength of 50 V/km. A more detailed background is given in Section 4.2. The relatively simple geometry of this case allows the simultaneous representation of the large-scale electrical field and the tunnel system with a deposition hole at various locations. The 600 m long tunnel system illustrated in Figure 5-8 will be studied first (Section 5.6.1–5.6.3), while the 1,700 m long tunnel system is studied in Section 5.6.4.

5.6.1 Tunnels aligned with the electrical field

Figure 5-10 shows a representation of the model geometry for this case. The model is bounded by a box with a length of 3 km, a width of 2 km and a height of 1.5 km. The tunnel system is located in the center of the x-y plane and a depth of 500 m. A voltage of 150 V is applied between the colored face of the model box in Figure 5-10 and the opposing side. All other sides of the box are treated as insulating. This voltage corresponds to a uniform electrical field of 50 V/km.

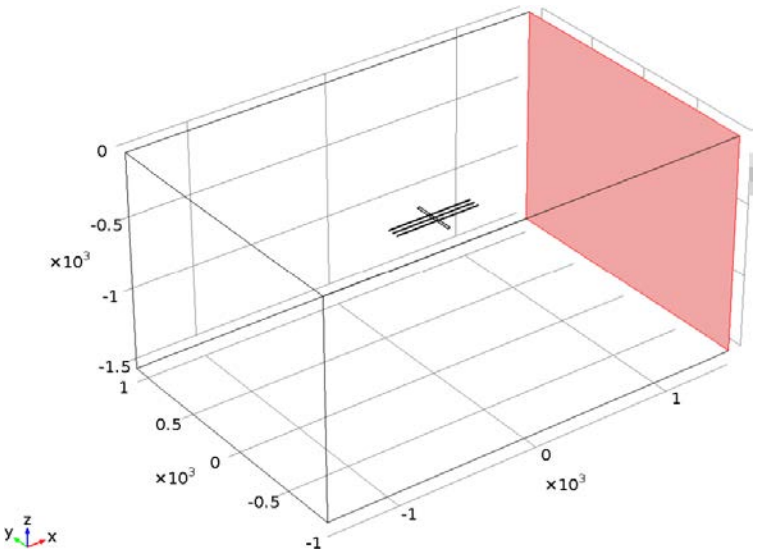

Figure 5-10. *Representation of the model geometry for a uniform electrical field.*

Figure 5-11 shows the potential along the center of the floor of the center tunnel for the resistivity function *f1*. The potential at a level of 8 m below the tunnel floor is also shown.

Figure 5-11 shows that potential differences arise between the tunnel floor and a level of 8 m below the tunnel floor. These are the levels of the upper and lower circular ends of the deposition holes. As the figure shows the differences in potential are highest at the ends of the tunnels. Figure 5-12 shows details from Figure 5-11.

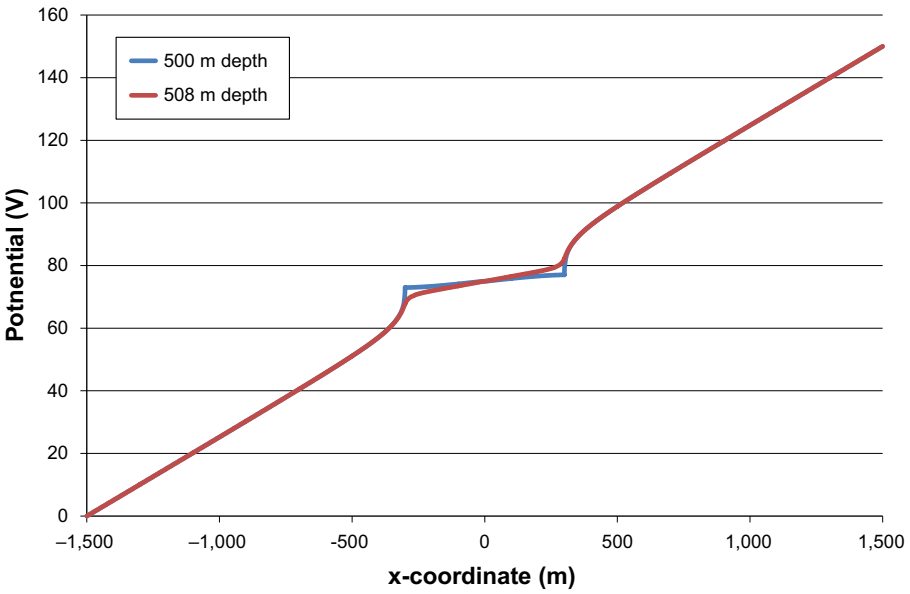

Figure 5-11. *The potential along the center of the floor of the center tunnel for the resistivity function f1. The potential at a level of 8 m below the tunnel floor is also shown.*

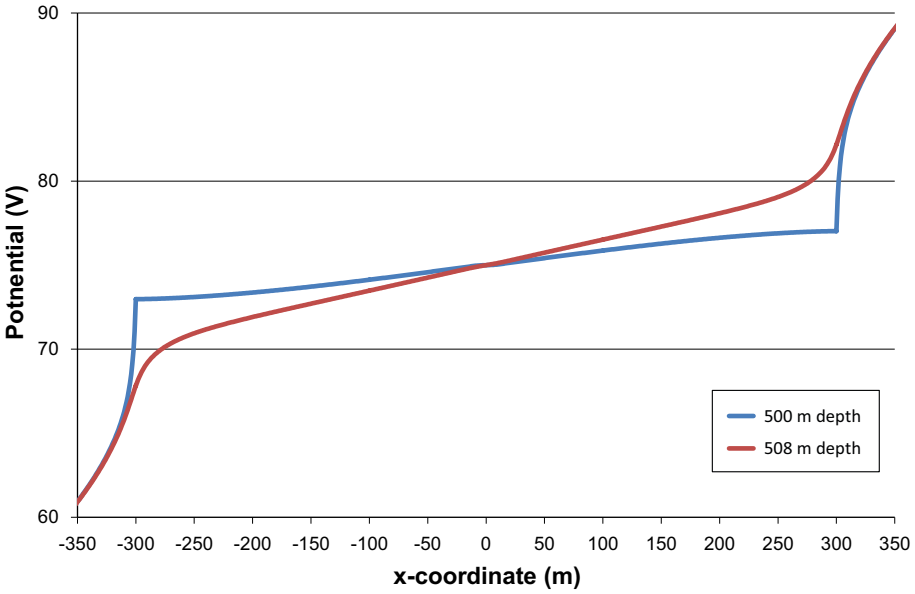

Figure 5-12. *Details from Figure 5-11.*

Tables 5-1 and 5-2 show the voltages at various distances from the tunnel end for the set of functions describing the resistivity of the rock. Table 5-1 shows the results for the center tunnel and Table 5-2 shows the results for an edge tunnel. Symmetry causes the results for the two edge tunnels to be the same.

Tables 5-1 and 5-2 show that the edge tunnel gives the highest voltages and that an increase in the tunnel resistivity from 1 Ωm to 2 Ωm leads to a decrease in the voltage of 10%–20%.

5.6.2 Tunnels not aligned with the electrical field

Various angles are imposed between the tunnel system and the electrical field of 50 V/km. Figure 5-13 shows the geometry for an angle of 20°. Table 5-3 shows the calculated voltages between the upper and lower ends of a deposition hole for angles of 0°, 10° and 20°. The tunnels are numbered so that the center tunnel is number 2, number 1 is one edge tunnel and number 3 is the other edge tunnel.

Table 5-3 shows that there are small changes in the voltage along the height of a deposition hole with changes in the angle between the orientation of the field and the orientation of the model tunnel system. The highest voltage of 4.7 V in Table 5-3 is found for 10° angle. Larger angles between the electrical field and the orientation of the tunnels were not studied, but the voltages are predicted to decrease as the maximum voltage across the model tunnel system decreases with increasing angles. As Table 5-3 shows there seems to be a maximum around an angle of about 10° for the system of three tunnels studied.

5.6.3 Current through deposition holes

Figure 5-12 shows that voltages of several volts could arise between the ends of a deposition hole. However, this voltage will decrease as a representation of the deposition hole and the lower resistivity in the deposition hole is introduced into the FEM-model. Figure 5-14 shows details from the model geometry in Figure 5-8 where a deposition hole located 10 m from the end of the center tunnel has been added.

Table 5-1. Calculated values of the voltage (V) between the upper and lower ends of a deposition hole for various locations of the deposition hole and functions of the rock resistivity, for the center tunnel. The resistivity of the bentonite in the tunnels was set to 1 Ωm unless otherwise stated. The resistivity in the deposition hole is set to be the same as that in the surrounding rock.

	Location of the deposition hole (m from tunnel end)						
Resistivity function	**5**	**10**	**15**	**20**	**25**	**30**	**10 (Tunnel resistivity 2 Ωm)**
f1	4.3	3.8	3.4	3.1	2.9	2.7	3.4
f2	4.4	3.8	3.4	3.1	2.9	2.7	
f3	4.4	3.8	3.4	3.1	2.9	2.7	
f4	4.4	3.8	3.4	3.1	2.9	2.7	
f5	3.9	3.4	3.0	2.8	2.6	2.4	
f6	4.6	4.1	3.7	3.4	3.1	2.9	

Table 5-2. Calculated values of the voltage (V) between the upper and lower ends of a deposition hole for various locations of the deposition hole and functions of the rock resistivity, for an edge tunnel. The resistivity of the bentonite in the tunnels was set to 1 Ωm unless otherwise stated. The resistivity in the deposition hole is set to be the same as that in the surrounding rock.

	Location of the deposition hole (m from tunnel end)						
Resistivity function	**5**	**10**	**10**	**20**	**25**	**30**	**10 (Tunnel resistivity 2 Ωm)**
f1	4.6	4.1	3.7	3.4	3.2	3.0	3.6
f2	4.6	4.1	3.7	3.5	3.2	3.0	
f3	4.6	4.1	3.7	3.5	3.2	3.0	
f4	4.7	4.1	3.7	3.5	3.2	3.0	
f5	4.1	3.6	3.2	3.0	2.8	2.6	
f6	5.0	4.5	4.1	3.8	3.5	3.3	

Table 5-3. Calculated values of the voltage (V) between the upper and lower ends of a deposition hole for various angles between the tunnels and the electrical field. Resistivity function *f1*. The resistivity of the bentonite in the tunnels was set to 1 Ωm. The designations 'near' and 'far' refer to the end of the tunnel that is closest to and farthest away from the high potential boundary, respectively. The resistivity in the deposition hole is set to be the same as that in the surrounding rock.

		Location of the deposition hole (m from tunnel end)											
		5		10		15		20		25		30	
Angle	Tunnel number	near	far	near	far	near	far	near	far	near	far	near	far
0°	1	–4.6	4.6	–4.1	4.1	–3.7	3.7	–3.4	3.4	–3.2	3.2	–3.0	3.0
0°	2	–4.3	4.3	–3.8	3.8	–3.4	3.4	–3.1	3.1	–2.9	2.9	–2.7	2.7
0°	3	–4.6	4.6	–4.1	4.1	–3.7	3.7	–3.4	3.4	–3.2	3.2	–3.0	3.0
10°	1	–4.6	4.6	–4.1	4.1	–3.7	3.7	–3.4	3.4	–3.2	3.2	–3.0	3.0
10°	2	–4.3	4.3	–3.7	3.7	–3.4	3.4	–3.1	3.1	–2.9	2.9	–2.7	2.7
10°	3	–4.4	4.7	–3.9	4.1	–3.6	3.8	–3.3	3.5	–3.1	3.3	–2.9	3.1
20°	1	–4.6	4.1	–4.1	3.6	–3.7	3.3	–3.4	3.1	–3.2	2.8	–3.0	2.7
20°	2	–4.1	4.1	–3.6	3.6	–3.2	3.2	–2.9	2.9	–2.7	2.7	–2.5	2.5
20°	3	–4.1	4.6	–3.6	4.1	–3.3	3.7	–3.1	3.4	–2.8	3.2	–2.7	3.0

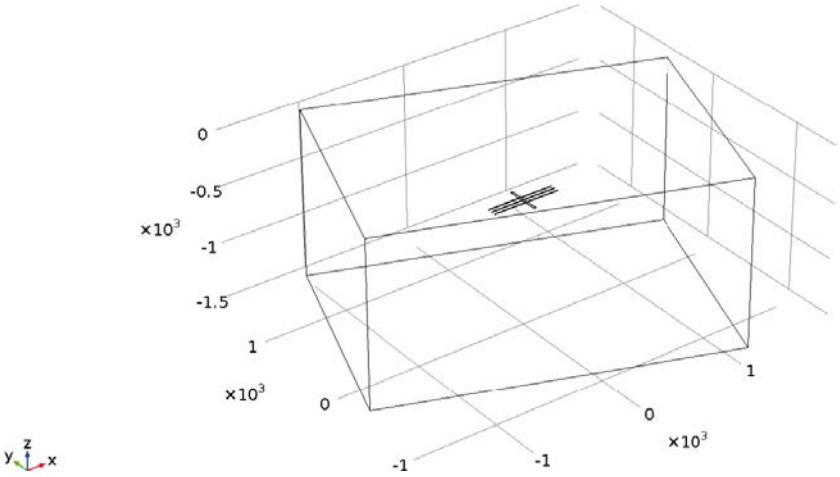

Figure 5-13. *Representation of the model geometry for a uniform electrical field with 20° angle between the orientation of the tunnels and the electrical field.*

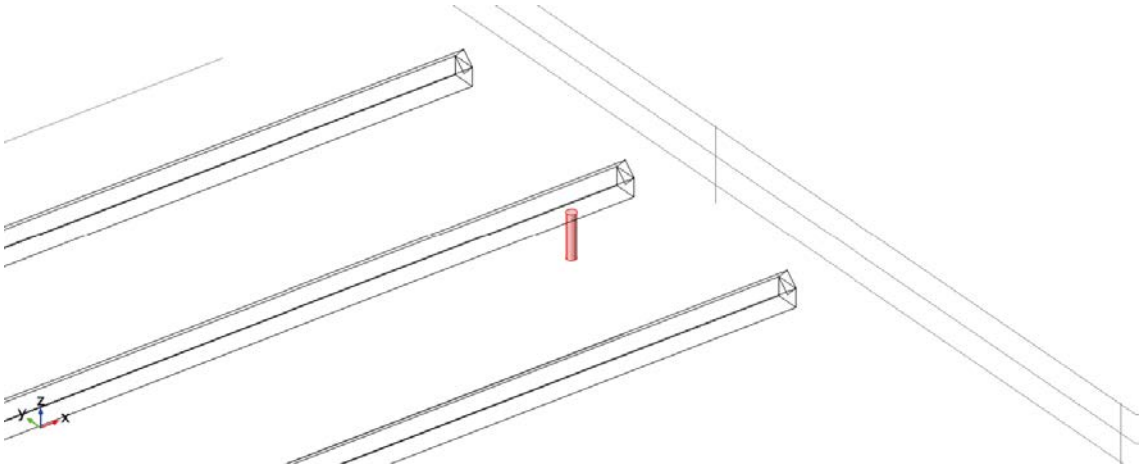

Figure 5-14. *Details from Figure 5-8, showing a representation of an 8 m deep deposition hole located 10 m from the end of the center tunnel.*

The FEM-model now includes the model geometry and boundary conditions from Figure 5-10 as well as the deposition whole depicted in Figure 5-14. Table 5-4 shows the calculated voltages between the upper and lower circular ends of the deposition hole for various assumed resistivities of the medium in the deposition hole and various locations of the deposition hole.

The resistivities of the medium in the hole are used to calculate the resistance between the circular end surfaces. Figure 5-15 shows the dimensions of the deposition hole and illustrates how the resistances are calculated.

Figure 5-16 shows the numerically modeled currents through the deposition holes as a function of the voltage across the holes. The data points are derived by dividing the voltage values in Table 5-4 with the resistance in the hole for each resistivity used (10,000, 100 and 2 Ωm, respectively). The figure shows that when the resistance in the deposition hole is very high, there is a low current and a high voltage, conversely, when there is a low resistance in the deposition hole there is a relatively high current and a low voltage. The lines connecting the data points show a very high degree of linearity.

Referring to the equivalent electrical circuit in Figure 5-4 the intersection of the lines with the x-axis can be identified as the electromotive force, E, for each location of the deposition hole. The slope of the line ($-\Delta U/\Delta i$) has the significance of the internal resistance, Ri. As can be seen in Figure 5-16 the values of E vary with the location of the deposition hole while the value of R_i is virtually independent of the location. Figure 5-16 also shows that the voltages found for a resistivity of 10,000 Ωm (in the large scale models) give good estimates of the value of the electromotive force, E.

Table 5-5 shows values of the internal resistance, R_i, calculated for various locations of the deposition hole and various functions of the resistivity in the rock.

Table 5-5 shows that the value of the internal resistance, R_i, are very similar not only for various locations of the deposition hole but also for several functions of the resistivity of the rock. The values of R_i are the same for resistivity functions *f1*, *f2*, *f3* and *f4*. Also when the resistivity in the tunnel system is increased from 1 Ωm to 2 Ωm, there is a very small change in R_i from 747 Ω to 753 Ω. Thus the value of R_i is determined by the geometry and the resistivity of the rock close to the tunnel system.

Table 5-4. Voltages between between the upper and lower circular ends of the deposition hole for various assumed resistivites of the medium in the deposition hole and various locations of the deposition hole. Center tunnel. Rock resistivity function *f1*.

		Location of the deposition hole (m from tunnel end)		
Resistivity (Ω m)	**Resistance (Ω)**	**10**	**20**	**30**
10,000	33,300	3.8	3.1	2.7
100	333	1.2	0.98	0.85
2	6.67	0.034	0.028	0.024

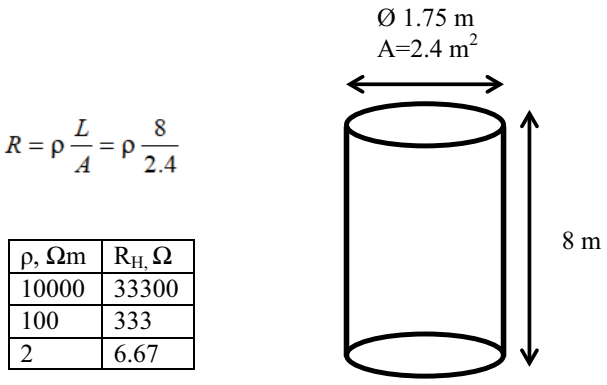

$$R = \rho \frac{L}{A} = \rho \frac{8}{2.4}$$

ρ, Ωm	$R_{H,}$ Ω
10000	33300
100	333
2	6.67

Figure 5-15. *Resistance of the deposition hole.*

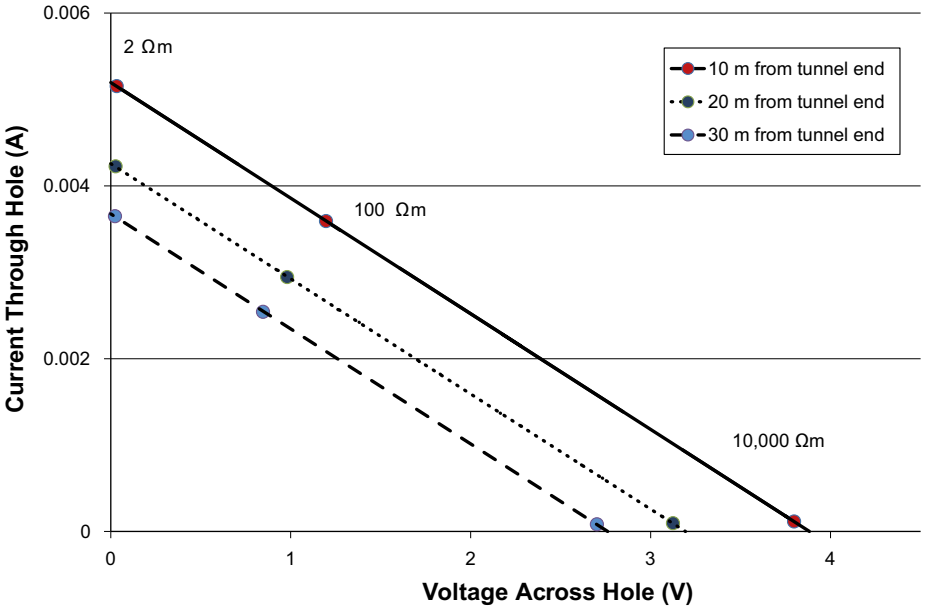

Figure 5-16. *The currents through the deposition holes as a function of the voltage across the holes. Three different locations of the hole are represented. Conditions representing a uniform field strength of 50 V/km assumed and rock resistivity according to function f1.*

Table 5-5. Calculated values of the internal resistance for various locations of the deposition hole and functions of the rock resistivity. The resistivity of the bentonite in the tunnels was set to 1 Ωm. Center tunnel, aligned with the electrical field. Also data for an edge tunnel and tunnel resistivity set to 2 Ωm, for resistivity function *f1*.

	Location of the deposition hole (m from tunnel end)				
Resistivity function	**10**	**20**	**30**	**10 (Edge Tunnel)**	**10 (Tunnel resistivity 2 Ω m)**
f1	747	750	751	746	753
f2	747				
f3	747				
f4	747				
f5	379	380	382		
f6	1,472	1,477	1,479		

Resistivity functions *f5* and *f6* show values of R_i that are close to half and double the value for resistivity function *f1*, respectively.

The currents through the deposition holes as a function of the voltage across the holes for the resistivity functions *f1*, *f5* and *f6* are shown in Figure 5-17.

Figure 5-17 illustrates that although the value of the electromotive force, E, read from the intersection with the x-axis, is higher for resistivity function *f6* than for *f1*, the current that can be drawn is lower. The highest current is instead found for the resistivity function *f5*, which gives the lowest value of E.

5.6.4 Two 1,700 m long tunnels

The temporary transport tunnels combined with deposition tunnels are represented as two 1,700 m long tunnels with the same electrical conductivity as the deposition tunnels. The model geometry used for this case is shown in Figure 5-18. The two tunnels are enclosed in a box with length of 4 km, width of 4 km and a height of 2 km. A voltage of 200 V is imposed between the colored face in Figure 5-18 and the opposing face. The other boundaries are treated as insulating. No deposition hole is represented in the model. Table 5-6 shows the voltages that arise between the tunnel floor and 8 m below the tunnel floor.

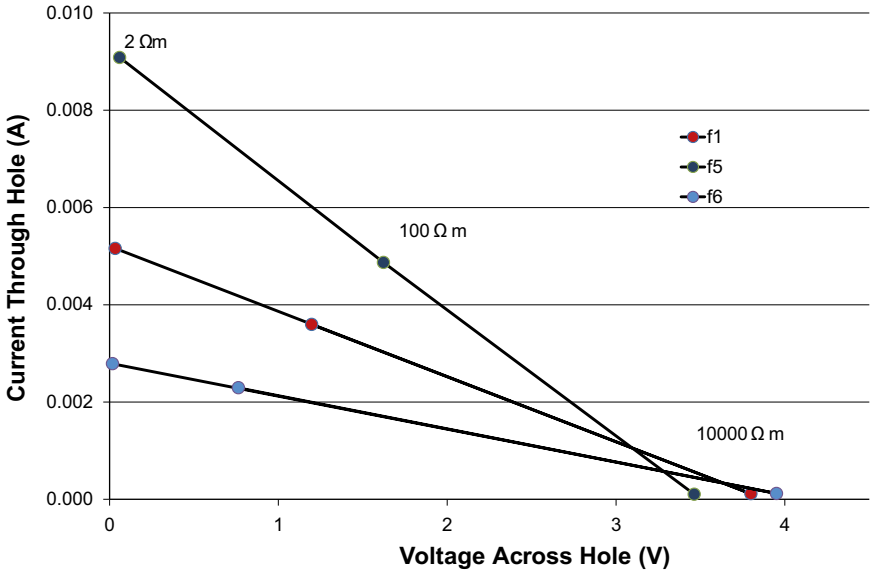

Figure 5-17. *The current through the deposition hole as a function of the voltage across the holes for different rock resistivity functions. The deposition hole is located 10 m from the end of the center tunnel. The texts at each group of points indicate the resistivity of the medium in the deposition hole.*

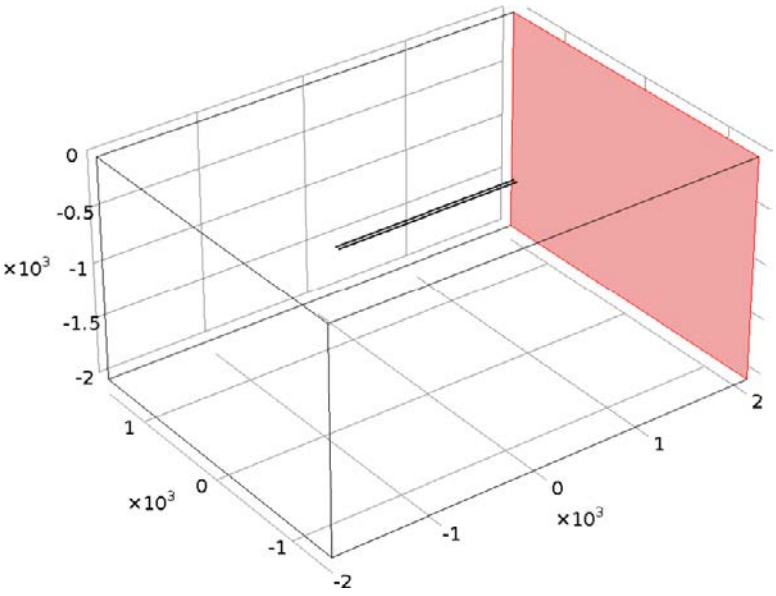

Figure 5-18. *Representation of the 1,700 m tunnel system enclosed in a 4 km long, 2 km deep and 4 km wide box. The tunnels are located with a common base plane at 500 m depth, z=–500, with the center point at x=0 and y=0.*

Table 5-6. Calculated values of the voltage (V) between the upper and lower ends of a deposition hole for various locations of the deposition hole and functions of the rock resistivity. Two 1,700 m long tunnels. The resistivity of the bentonite in the tunnels was set to 1 Ωm. The resistivity in the deposition hole is set to be the same as that in the surrounding rock.

	Location of the deposition hole (m from tunnel end)					
Resistivity function	**5**	**10**	**15**	**20**	**25**	**30**
f1	7.3	6.6	6.0	5.6	5.3	5.1
f2	7.4	6.6	6.1	5.7	5.4	5.1
f3	7.4	6.6	6.1	5.7	5.4	5.1
f4	7.4	6.6	6.1	5.7	5.4	5.1
f5	5.4	4.8	4.4	4.1	3.8	3.6
f6	9.6	8.6	7.9	7.5	7.1	6.8

5.7 Forsmark Power station as a secondary electrode (Case 2)

Forsmark Power station constitutes a grounding site with a relatively low resistance to remote earth. Current is picked up by local grounding lines and transmitted over large distances by overhead power lines to remote sites. Forsmark Power station then acts as an electrode, which always has the opposite polarity to the nearby HVDC electrode. The situation is also used to represent a possible future similar type of installation.

The distance between the repository and Forsmark Power station is approximately 800 m. The maximum possible future voltage level at Forsmark relative to remote earth has been estimated to be in the region of 200 V, see Section 4.2. If we presume a circular grounding with a diameter of 1,000 m this will have a grounding resistance of approximately 5 Ω (R=ρ/(2d)=10^4/(2×1,000)) (von Baeckmann 1989). The 400 kV overhead power line pylons leaving the power plants are grounded and connected to each other by a top wire. If we presume a total resistance for top wires and remote groundings of 5 Ω the maximum current that can be picked up by the grounding system on top of the repository is

I = 200 V/(5+5) Ω = 20 A

Figure 5-19 shows the model geometry used. The effective electrical center of the secondary electrode is here located a horizontal distance of 800 m from the center of the model tunnel system. A rather small model volume with a radius of 3 km is selected so that also the deposition hole can be represented with good resolution. The model tunnel system is set to be aligned with the electrical field.

A total of 20 A is fed from the point current source to the boundary of the hemisphere which is attributed ground potential. The circular upper surface is treated as insulating.

The effect of the sea, which could influence the uppermost part of the model volume, is neglected for this case.

Calculations of the potential differences that arise between the levels of 500 m and 508 m depth were made for various functions of rock resistivity. Particular attention is given to the ends of the tunnels because that is where the highest voltages arise. Table 5-7 shows the calculated voltages for the case where the deposition holes have the same properties as the surrounding rock. There are two cases for each distance from a tunnel end. The designation “near” in Table 5-7 refers to the tunnel end closest to the point current source (Forsmark) and ‘far’ refers to the opposite tunnel end.

The internal resistance was determined for various locations of a deposition hole by changing the resistivity of the hole in the same way as described in Section 5.6.3. The result is shown in Table 5-8 which also includes variations in the rock resistivity.

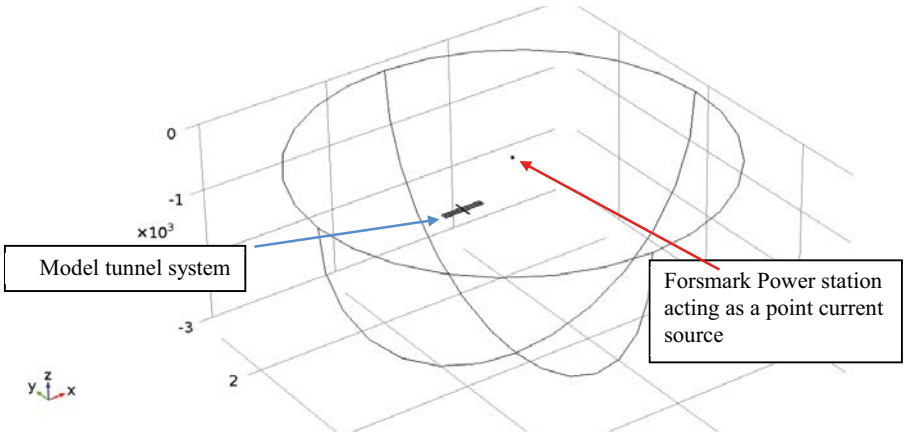

Figure 5-19. *Model geometry for studying effects of Forsmark Power station as a secondary electrode.*

Table 5-7. Calculated values of the voltage (V) between the upper and lower ends of a deposition hole for various locations of the deposition hole and functions of the rock resistivity. The resistivity of the bentonite in the tunnels was set to 1 Ωm. Center tunnel. The notation 'near' and 'far' refer to the end of the tunnel that is closest to and farthest away from the current source, respectively. The resistivity in the deposition hole is set to be the same as that in the surrounding rock.

	Location of the deposition hole (m from tunnel end)											
	5		10		15		20		25		30	
Resistivity function	near	far	near	far	near	far	near	far	near	far	near	far
f1	–3.0	2.5	–2.6	2.2	–2.3	2.0	–2.1	1.9	–1.9	1.8	–1.8	1.7
f2	–2.8	2.2	–2.4	2.0	–2.1	1.8	–1.9	1.7	–1.7	1.6	–1.6	1.5
f3	–2.7	2.2	–2.3	1.9	–2.1	1.8	–1.9	1.7	–1.7	1.6	–1.6	1.5
f4	–2.4	1.9	–2.1	1.7	–1.9	1.6	–1.7	1.5	–1.5	1.4	–1.4	1.4
f5	–1.1	0.9	–1.0	0.8	–0.9	0.7	–0.8	0.7	–0.7	0.7	–0.6	0.6
f6	–5.0	4.0	–4.3	3.6	–3.8	3.3	–3.5	3.1	–3.2	3.0	–2.9	2.9

Table 5-8. Calculated values of the internal resistance for various locations of the deposition hole and functions of the rock resistivity. The resistivity of the bentonite in the tunnels was set to 1 Ωm. Center tunnel, aligned with the electrical field.

	Location of the deposition hole (m from tunnel end)		
Resistivity function	10	20	30
f1	738	740	740
f2	737		
f3	737		
f4	735		
f5	372		
f6	1,451		

5.8 A possible future HVDV-electrode at various distances from the tunnel system (Cases 3 and 4)

Figure 5-20 shows a representation of a possible future situation. If the sea rises to a level where the entire footprint of repository is submerged, it may be feasible to locate a HVDV electrode in the immediate vicinity of the repository. Figure 5-20 illustrates such a situation where the repository, shown as a network of tunnels, has its center about 2 km from the shoreline. The colored disc represents the sea. The black dot at the center of the hemisphere represents the electrode and is located directly on top of the opening of the shafts and the ramp that connect repository level with ground (now seabed).

The model volume is here limited to a hemisphere with a radius of 4 km. The electrode is located 2 km from the shoreline. With an assumed slope angle of the seabed of 1 m/1,000 m, the water depth at the site of the electrode would be about 2 m.

5.8.1 The HVDC electrode located directly on top of the repository (Case 3)

Model setup

The geometrical model used for this case is depicted in Figure 5-7. Thus the HVDC electrode is represented as a ring of 8 sub-electrodes located in a ring with a radius of 100 m placed directly on top of the model shaft.

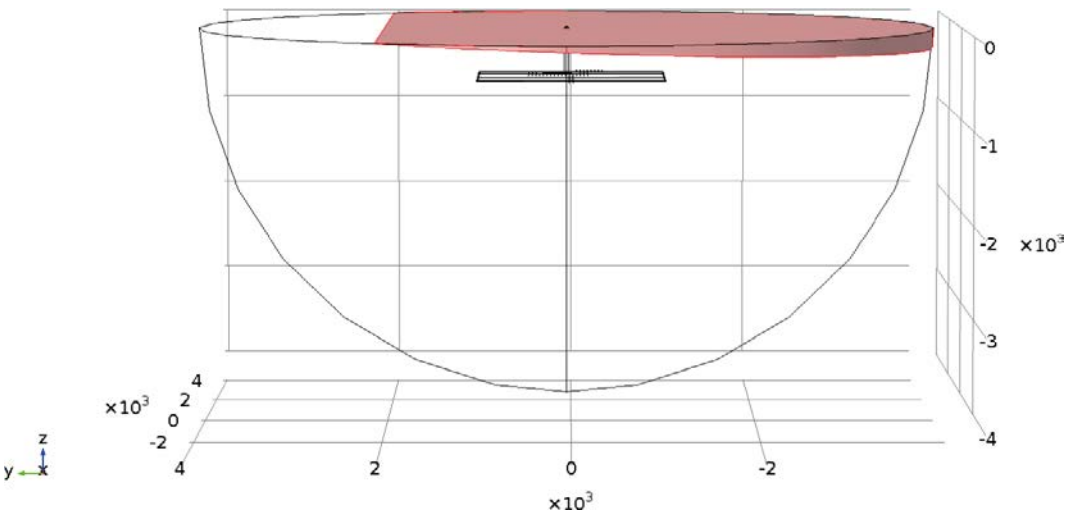

Figure 5-20. *A representation of a possible future situation where the sea, shown as a colored disc, covers the entire repository.*

Properties of the model shaft

In addition to the transport tunnel or ramp that winds its way over several kilometers to reach a depth of 500 there are several vertical shafts. Drawings for the repository (SKB 2009) contain four different shafts with diameters, 6 m, 5 m, 3.5 m and 3.5 m, respectively, where the 6 m and 5 m diameters are given as minimum values. Together these four vertical shafts give a cross section of about 67 m^2. The profile of the ramp varies with the curvature of the winding path but it is approximated as 7×5 m = 35 m^2. The length of the ramp has been estimated to about 4,700 m. The ramp as well as the shafts will be filled by bentonite from 200 m downwards and by crushed rock above that level (SKB 2011). A porosity of 40% has been estimated for the crushed rock, although 100 % porosity is assumed for the top 10 cm along the ramp. Approximating the ramp as a 5 m high and 7 m wide rectangle, 7×0.1×100%+7×4.9×40% is water. That gives about 14.4 m^2 area of water for the upper part of the ramp. For the vertical shafts this area would be 40% of 67 m^2 =26.8 m^2. Below the level of 200 m the ramp as well as shafts can be assumed to have the properties of the repository tunnels.

Summary:

0–200 depth: 26.8 m^2 water, vertical + 14.4 m^2 water, winding
200–500 depth 67 m^2 bentonite, vertical + 35 m^2 bentonite, winding

Thus, the conductance in the vertical shafts is much higher than that in the ramp.

The properties of the water may vary with the depth. We assume here a high conductivity of 5 S/m due to possible presence of saline water. The water saturated bentonite is assumed to have a conductivity of 1 S/m.

For modeling purposes there is approximately 28 m^2 of water with a conductivity of 5 S/m for the top 200 m (26.8+14.4×500/4,700 = 28.3 m^2). Between 200 and 500 m depth there is about 71 m^2 of bentonite (67+35×500/4,700 = 70.7).

Since there are several separate shafts that constitute the total area, we represent the average conductivity over a larger area. A model shaft having the same area as the sum of the separate shafts would allow current from a small electrode located directly on top of the model shaft to be conducted directly to the repository. The results would be very sensitive to the exact location of the electrode in relation to the model shaft. Because there is some distance between the separate shafts, this extreme sensitivity to exact location would be an artifact. The use of a wider model shafts attempts to preclude such artifacts from arising. With a wider model shaft the sensitivity to the exact location of the electrode in relation to the model shaft becomes smaller.

From Figure 5-6 the shafts seem confined to within an area of about 20 m × 50 m. Using an area of 20×50 = 1,000 m^2, to represent the paths to the repository, the top 200 m are given a conductivity of 0.14 S/m ($5\times28+10^{-4}\times972)/1{,}000 = 0.140$). The conductivity below that level is set to 0.071 S/m ($(1\times71+10^{-4}\times929)/1{,}000 = 0.0711$). The part of the cross section that is not water or bentonite, respectively, is here rock with a conductivity of 10^{-4} S/m. Rock resistivity functions *f5* and *f6* have conductivities that differ from 10^{-4} S/m also in the range of the shaft, the top 500 m, but the difference in the conductivity in the average model shaft is so small that the same values are used for all resistivity functions.

Figure 5-21 illustrates the conductivity in the vertical shaft representing several parallel paths connecting the repository level and ground level. From ground level down to about –69 m the conductivity is relatively low corresponding to the recalculation of the seawater resistivity of 1.6 Ωm over an angle of 0.0573° to an average conductivity of 2° as described in Section 4.3.3. From –69 m down to –200 m the conductivity of saline water (5 S/m) is used but recalculated to an average conductivity over the cross sectional area of the model shaft. From –200 m down to about –495 m the conductivity represents that of bentonite with 1 S/m recalculated from 71 m^2 to 1,000 m^2, as described above. At repository depth, between –492 m and –500 m, the conductivity is that of the tunnel system. A total of 8 m is allowed for the height of the 'hall' where the shaft reaches repository level.

Calculations

A current of 2,500 A is fed from the point current sources that represent the HVDC electrode. The potentials that arise in the tunnels and the voltages between the levels of –500 m and –508 m were charted for various positions of the tunnels and various functions of rock resistivity.

Figure 5-22 shows a projection of the model repository and Figure 5-23 shows how the various tunnels are labeled in the presentation of the results.

Figure 5-23 shows the deposition tunnels in the model repository in the coordinates used. The line style and color will be used in following diagrams. The letters *A* through *I* indicate tunnel ends for which the voltages will be studied in some detail. These tunnel ends were selected for detailed studies because the highest voltages are likely to occur at sites where a high conductivity path from the electrode ends and the current is forced into rock.

The shaft has its center at coordinates 130, 50 m. For the case studied here where the electrode is located directly above the shaft, the center of the ring of sub-electrodes is also located at coordinates 130, 50 m.

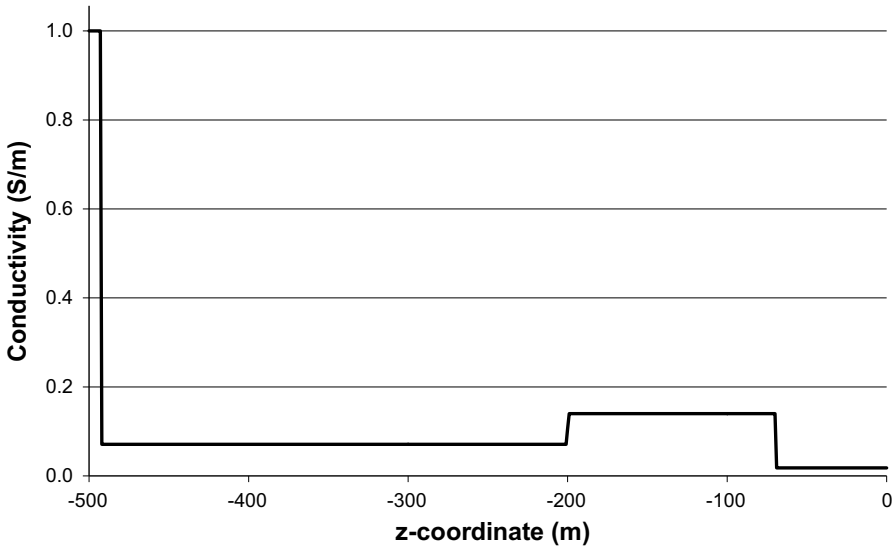

Figure 5-21. *Conductivity in the vertical shaft representing several parallel paths connecting the repository level and ground level.*

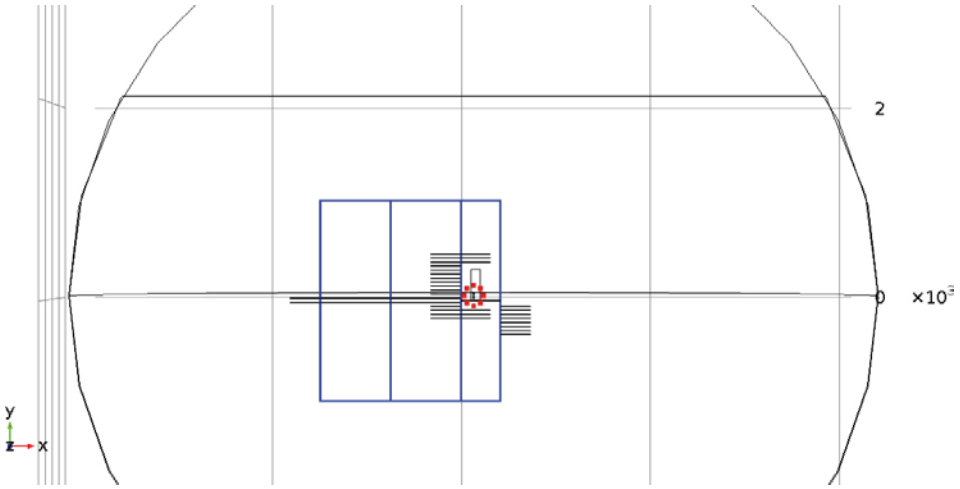

Figure 5-22. *Projection of the model repository with the ring of sub-eletrodes centered around the opening of the model shaft. The outer circle indicates the outer boundary of the geometric model.*

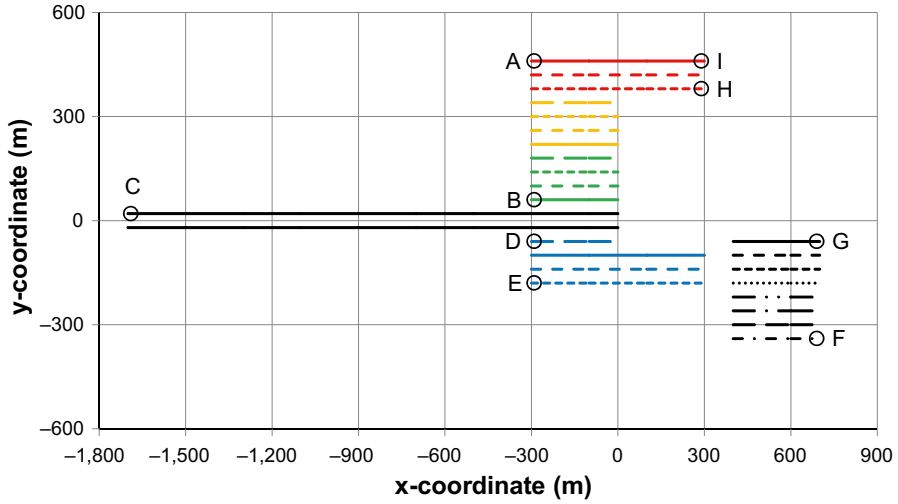

Figure 5-23. *Location of the deposition tunnels in the model repository in the coordinates used. The line style and color will be used in following diagrams. The letters A through I indicate tunnel ends for which the voltages will be studied in some detail.*

Figure 5-24 shows the voltages that would arise along the height of a deposition hole as function of the x-coordinate of the deposition hole. The line style and color from Figure 5-23 is used for the tunnels and the legend in Figure 5-24 indicates the y-coordinate of the tunnel. The voltages at positions *A* through *I* in Figure 5-23 are shown in Figure 5-24 as rings labeled with the corresponding letter. A distance of 10 m from the tunnel end was selected for the labeled rings in Figure 5-24.

Table 5-9 shows the same data in table form for the tunnels labeled *A* through *I* and for each of the resistivity functions *f1* through *f6*. Rock resistivity function *f2* was selected in Figure 5-24 as an example only. There are only minor differences in the values found for the different resistivity functions. The general shape of the curves in Figure 5-24 is the same for all different resistivity functions.

A repository at greater depth

The model tunnel system and the model repository have all been located at 500 m below, present day, ground. In this example the whole repository has been shifted 200 m downwards so that the tunnel floor is located at a depth of 700 m. Figure 5-25 shows the voltages that would arise along the height of a deposition hole as function of the x-coordinate of the deposition hole.

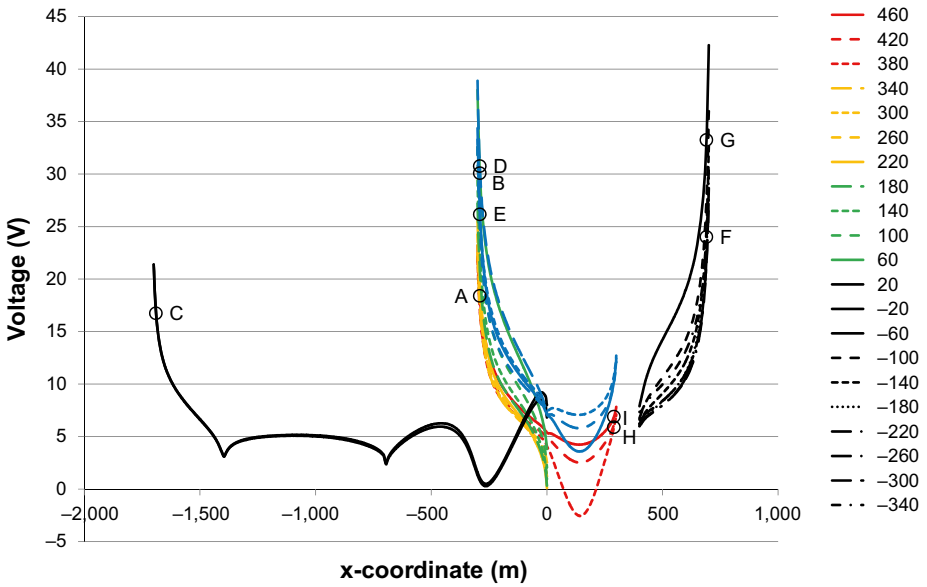

Figure 5-24. *The voltages that would arise along the height of a deposition hole as function of the x-coordinate of the deposition hole. The line style and color from Figure 5-23 is used for the tunnels and the legend indicates the y-coordinate of the tunnel. The voltages at positions A through I in Figure 5-23 are shown in Figure 5-24 as rings with the corresponding letter. A distance of 10 m from the tunnel end was selected for the labeled rings in Figure 5-24. Resistivity function f2. The resistivity in the deposition hole is set to be the same as in the surrounding rock. The electrode is centered around x=130 m.*

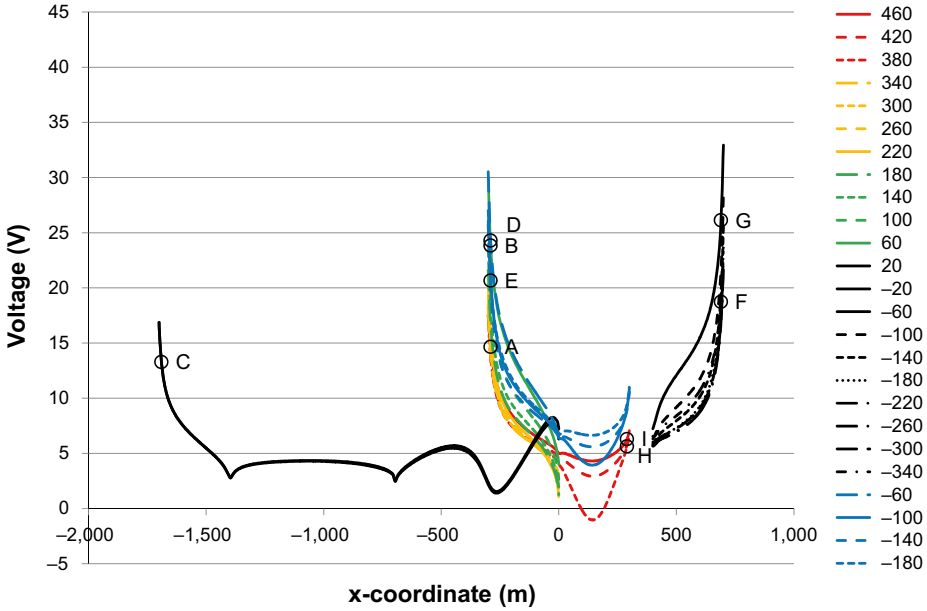

Figure 5-25. *The voltages that would arise along the height of a deposition hole as function of the x-coordinate of the deposition hole. The line style and color from Figure 5-23 is used for the tunnels and the legend indicates the y-coordinate of the tunnel. The voltages at positions A through I in Figure 5-23 are shown in Figure 5-25 as rings with the corresponding letter. A distance of 10 m from the tunnel end was selected for the labeled rings in Figure 5-25. Resistivity function f2. The resistivity in the deposition hole is set to be the same as in the surrounding rock. The electrode is centered around x=130 m. Repository level 700 m below ground.*

Table 5-9. Voltages along the height of a deposition hole at various tunnel ends indicated by the letters *A* through *I*. Various distances from the tunnel ends are included and the resistivity functions *f1* through *f6*. The electrode is centered at the shaft. The resistivity in the deposition hole is set to be the same as in the surrounding rock.

Distance from tunnel end (m)	Resistivity Function	A	B	C	D	E	F	G	H	I
5	*f1*	18.2	30.9	20.6	31.7	26.8	25.4	34.4	4.5	5.3
10	*f1*	16.4	27.9	18.5	28.6	24.1	22.8	31.0	4.0	5.0
15	*f1*	15.1	25.8	17.1	26.5	22.2	21.0	28.6	3.6	4.7
20	*f1*	14.2	24.3	16.0	24.9	20.8	19.7	26.9	3.2	4.5
25	*f1*	13.4	23.1	15.1	23.6	19.6	18.6	25.5	2.8	4.3
30	*f1*	12.7	22.0	14.4	22.6	18.7	17.7	24.4	2.5	4.2
5	*f2*	20.3	33.2	18.6	34.0	29.0	26.6	36.8	6.4	7.3
10	*f2*	18.4	30.1	16.7	30.7	26.1	24.0	33.2	5.9	6.9
15	*f2*	17.1	27.9	15.5	28.6	24.2	22.2	30.8	5.4	6.6
20	*f2*	16.1	26.3	14.6	26.9	22.7	20.9	29.1	5.0	6.4
25	*f2*	15.3	25.1	13.8	25.6	21.6	19.8	27.7	4.6	6.2
30	*f2*	14.6	24.0	13.3	24.6	20.6	18.9	26.5	4.2	6.0
5	*f3*	20.9	33.8	18.0	34.6	29.6	27.0	37.4	7.0	7.8
10	*f3*	18.9	30.7	16.3	31.3	26.7	24.3	33.9	6.4	7.4
15	*f3*	17.6	28.5	15.1	29.1	24.8	22.6	31.5	5.9	7.1
20	*f3*	16.6	26.9	14.2	27.5	23.3	21.2	29.7	5.4	6.9
25	*f3*	15.8	25.6	13.5	26.2	22.1	20.2	28.3	5.0	6.7
30	*f3*	15.1	24.6	12.9	25.1	21.2	19.3	27.1	4.6	6.5
5	*f4*	22.1	35.3	16.4	36.0	31.0	27.5	38.8	8.5	9.3
10	*f4*	20.2	32.1	14.9	32.7	28.1	24.9	35.2	7.8	8.9
15	*f4*	18.8	29.9	13.9	30.4	26.1	23.2	32.8	7.3	8.5
20	*f4*	17.8	28.3	13.1	28.8	24.6	21.9	31.0	6.8	8.3
25	*f4*	17.0	27.0	12.5	27.5	23.4	20.8	29.6	6.4	8.1
30	*f4*	16.3	25.9	12.0	26.4	22.4	20.0	28.4	6.0	7.9
5	*f5*	15.1	24.2	10.7	24.3	20.1	16.5	24.7	6.8	6.3
10	*f5*	13.7	22.0	9.6	22.0	18.2	14.9	22.4	6.3	6.0
15	*f5*	12.7	20.4	8.9	20.5	16.8	13.8	20.8	5.8	5.7
20	*f5*	12.0	19.2	8.4	19.3	15.8	13.0	19.6	5.4	5.5
25	*f5*	11.4	18.3	8.0	18.4	15.0	12.3	18.7	5.0	5.3
30	*f5*	10.9	17.6	7.6	17.7	14.3	11.8	17.9	4.6	5.1
5	*f6*	33.8	48.1	27.3	49.7	46.9	46.1	58.7	13.6	16.1
10	*f6*	30.8	43.7	24.8	45.2	42.5	41.8	53.2	12.6	15.3
15	*f6*	28.8	40.8	23.1	42.1	39.6	38.9	49.6	11.8	14.7
20	*f6*	27.3	38.6	21.8	39.9	37.4	36.7	46.9	11.2	14.3
25	*f6*	26.1	36.9	20.9	38.1	35.7	35.0	44.8	10.6	14.0
30	*f6*	25.1	35.5	20.1	36.7	34.3	33.6	43.0	10.1	13.7

Compared to the results for a location 500 m below ground (Figure 5-24), the voltage has decreased from about 33 V for position *G* to about 26 V for the same position when the repository is located at 700 m below ground.

Table 5-10 shows the voltages along the deposition holes for this case, 700 m blow ground. The results can be compared with the results in Table 5-9, for the corresponding conditions at 500 m below ground.

Compared to the results for a location 500 m below ground (Table 5-9), the voltage has decreased from about 59 V for position *G*, resistivity function *f6* to about 50 V, for the same position and resistivity function when the repository is located at 700 m below ground.

Table 5-10. Voltages along the height of a deposition hole at various tunnel ends indicated by the letters *A* through *I*. Various distances from the tunnel ends are included and the resistivity functions *f1* through *f6*. The electrode is centered at the shaft. The resistivity in the deposition hole is set to be the same as in the surrounding rock. Repository level 700 m below ground.

Distance from tunnel end (m)	Resistivity Function	A	B	C	D	E	F	G	H	I
5	*f1*	13.8	23.7	17.8	24.3	20.3	19.5	26.2	3.7	4.2
10	*f1*	12.4	21.4	16.0	21.9	18.3	17.5	23.6	3.3	3.9
15	*f1*	11.5	19.8	14.7	20.3	16.9	16.2	21.8	3.0	3.8
20	*f1*	10.8	18.7	13.8	19.1	15.8	15.1	20.5	2.7	3.6
25	*f1*	10.2	17.8	13.1	18.2	14.9	14.3	19.5	2.4	3.5
30	*f1*	9.7	17.0	12.5	17.4	14.2	13.7	18.7	2.2	3.4
5	*f2*	16.1	26.2	14.7	26.7	22.8	20.7	28.8	6.1	6.6
10	*f2*	14.7	23.8	13.3	24.3	20.7	18.7	26.1	5.6	6.3
15	*f2*	13.7	22.2	12.3	22.6	19.2	17.4	24.3	5.2	6.1
20	*f2*	12.9	21.0	11.6	21.4	18.1	16.4	23.0	4.9	5.9
25	*f2*	12.3	20.0	11.0	20.4	17.2	15.6	21.9	4.6	5.7
30	*f2*	11.8	19.3	10.6	19.6	16.5	15.0	21.0	4.3	5.6
5	*f3*	16.7	26.9	13.8	27.4	23.5	21.0	29.6	6.7	7.3
10	*f3*	15.3	24.5	12.5	25.0	21.3	19.1	26.8	6.3	6.9
15	*f3*	14.3	22.9	11.6	23.3	19.8	17.8	25.0	5.9	6.7
20	*f3*	13.5	21.7	11.0	22.0	18.7	16.8	23.6	5.5	6.5
25	*f3*	12.9	20.7	10.5	21.1	17.8	16.0	22.6	5.2	6.4
30	*f3*	12.4	19.9	10.1	20.2	17.1	15.3	21.7	4.8	6.2
5	*f4*	17.8	28.5	11.4	28.8	24.9	21.2	30.8	9.0	9.3
10	*f4*	16.4	26.1	10.4	26.4	22.7	19.3	28.1	8.4	8.9
15	*f4*	15.4	24.4	9.7	24.7	21.3	18.1	26.3	8.0	8.6
20	*f4*	14.7	23.2	9.2	23.5	20.2	17.2	25.0	7.6	8.5
25	*f4*	14.1	22.3	8.8	22.5	19.3	16.4	23.9	7.2	8.3
30	*f4*	13.6	21.5	8.5	21.7	18.6	15.9	23.1	6.9	8.2
5	*f5*	11.3	18.0	8.0	18.0	14.9	12.1	18.1	6.1	5.6
10	*f5*	10.3	16.5	7.3	16.5	13.6	11.1	16.5	5.7	5.3
15	*f5*	9.7	15.4	6.8	15.4	12.7	10.3	15.4	5.3	5.1
20	*f5*	9.2	14.6	6.4	14.6	12.0	9.8	14.6	5.0	5.0
25	*f5*	8.8	14.0	6.1	14.0	11.4	9.3	14.0	4.8	4.9
30	*f5*	8.5	13.4	5.8	13.4	11.0	9.0	13.5	4.5	4.8
5	*f6*	30.0	42.3	18.1	43.4	41.2	37.8	50.4	16.1	17.6
10	*f6*	27.6	38.8	16.5	39.7	37.6	34.5	45.9	15.1	16.8
15	*f6*	25.9	36.4	15.5	37.2	35.2	32.3	43.0	14.4	16.2
20	*f6*	24.7	34.6	14.7	35.4	33.5	30.7	40.9	13.8	15.9
25	*f6*	23.7	33.2	14.1	34.0	32.1	29.4	39.2	13.2	15.6
30	*f6*	23.0	32.1	13.6	32.8	31.0	28.4	37.9	12.8	15.4

5.8.2 The HVDC electrode located at variable distance from the repository (Case 4)

The dependence of the voltage along the height of a deposition hole on the distance between the center of the electrode and the model shaft was studied. A relatively large set of variations were made in the x-direction and more limited set of variations were made in the y-direction. These variations were made in order to estimate the extent of a possible risk area with respect to canister corrosion.

x-direction

Figure 5-26 shows the model repository with the HVDC electrode represented as a ring of sub-electrodes at two alternative locations in relation to the repository. The left hand figure shows a location where the x-coordinate of the electrode is –3,000 m relative to the center of the shaft. The right hand figure shows a location where the x-coordinate of the electrode is +1,500 m relative to the center of the shaft.

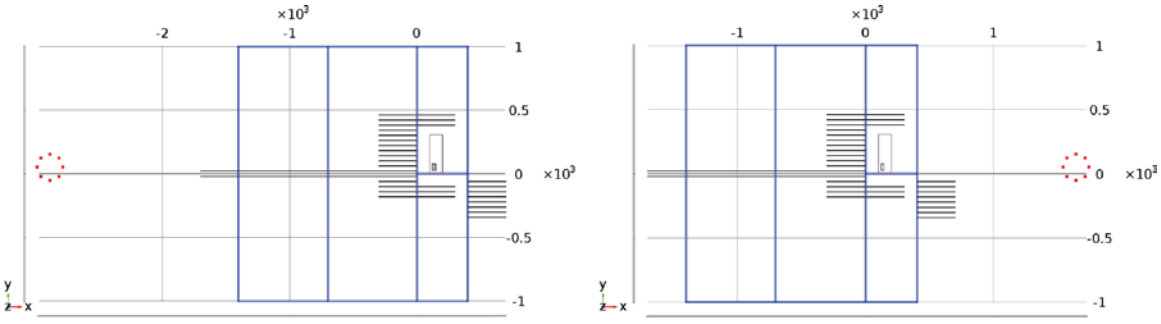

a. *The x-coordinate of the electrode is -3,000 m relative to the center of the shaft.*

b. *The x-coordinate of the electrode is +1,500 m relative to the center of the shaft.*

Figure 5-26. *The model repository with the HVDC electrode represented as a ring of sub-electrodes at two alternative locations in relation to the repository. Variations in the x-direction.*

Calculations of the voltages that would arise along the height of a deposition hole as function of the x-coordinate of the deposition hole for the various tunnels were made for the two geometries illustrated in Figure 5-26 and for several intermediate locations of the electrode. Calculations were made for locations of electrode at –3,000 m, –2,500 m, –2,000 m, –1,500 m, –1,000 m, –500 m, –100 m, +100 m, +500 m, +1,000 m and +1,500 m difference in x-coordinate relative to the center of the shaft. The extent of the model volume used is given by a hemisphere with a radius of 4 km for all locations except the locations of –3,000 m, –2,500 m and +1,500 m where the radius was set to 5 km. The model hemisphere was always centered at the center of the electrode.

In order to visualize the results, the voltages that arise at the locations *A* through *I*, in Figure 5-23, are shown for a distance of 10 m from the tunnel end.

Figure 5-27a shows the voltages that arise at position *A* at 10 m from the tunnel end as function of the difference in x-coordinate between the center of the electrode and the center of the shaft. Figures 5-27b through 5-27i show the corresponding results for positions *B* through *I*, respectively. The diagrams show results for resistivity functions *f1* through *f6* as indicated by the legends. The data points for the case where the electrode is located directly on top of the shaft are included in the diagrams.

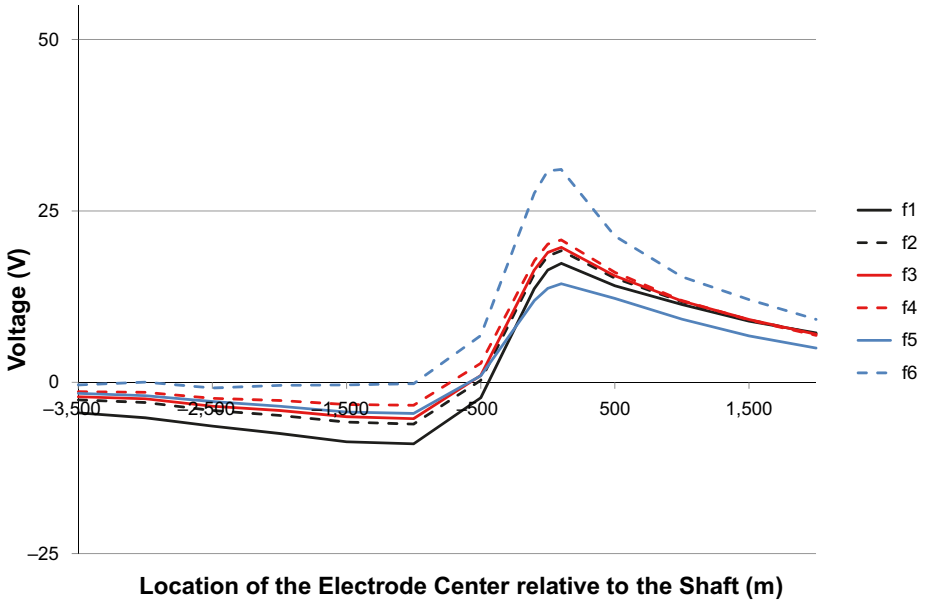

Figure 5-27a. *The voltages that arise at position* A *at 10 m from the tunnel end as function of the difference in x-coordinate between the center of the electrode and the center of the shaft.*

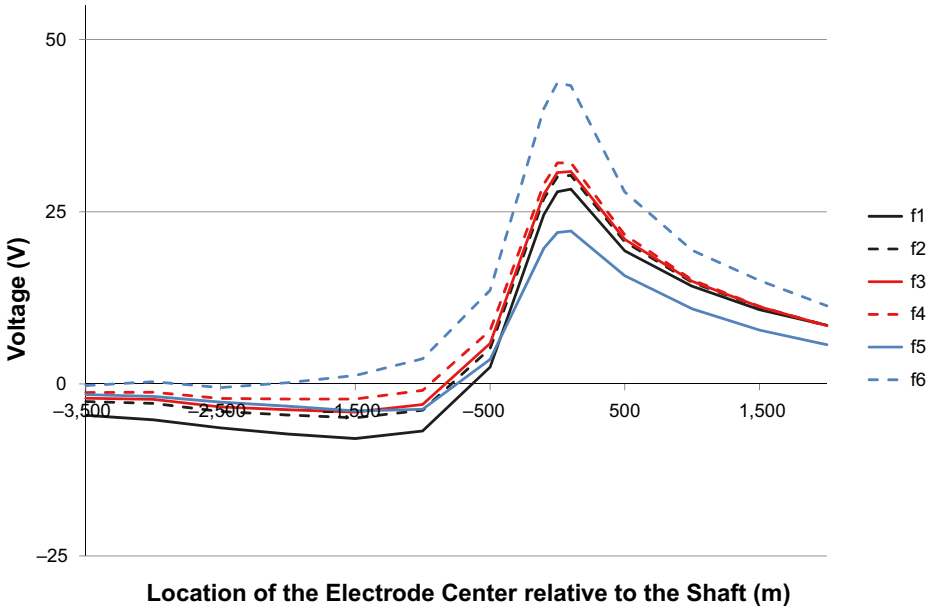

Figure 5-27b. *The voltages that arise at position* B *at 10 m from the tunnel end as function of the difference in x-coordinate between the center of the electrode and the center of the shaft.*

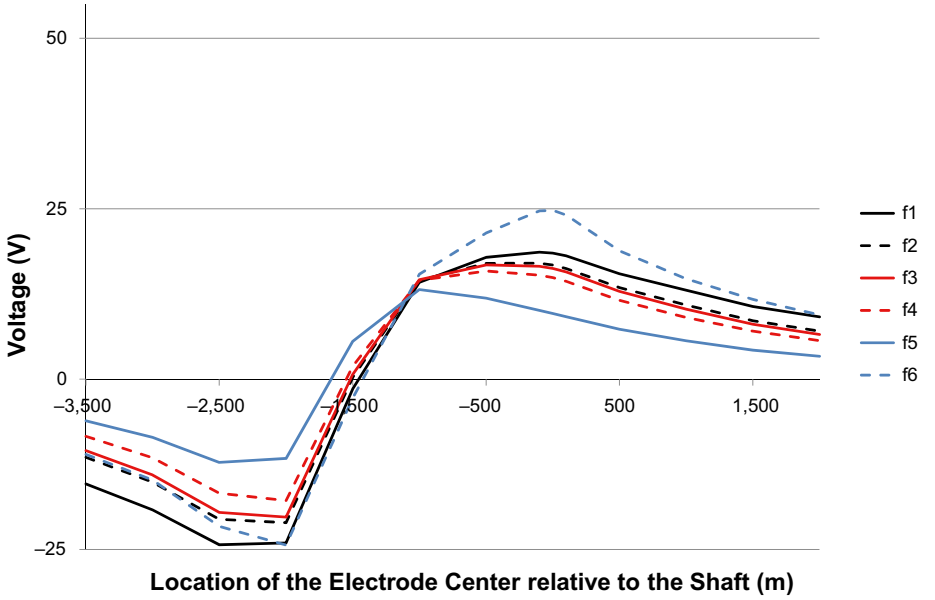

Figure 5-27c. *The voltages that arise at position* C *at 10 m from the tunnel end as function of the difference in x-coordinate between the center of the electrode and the center of the shaft.*

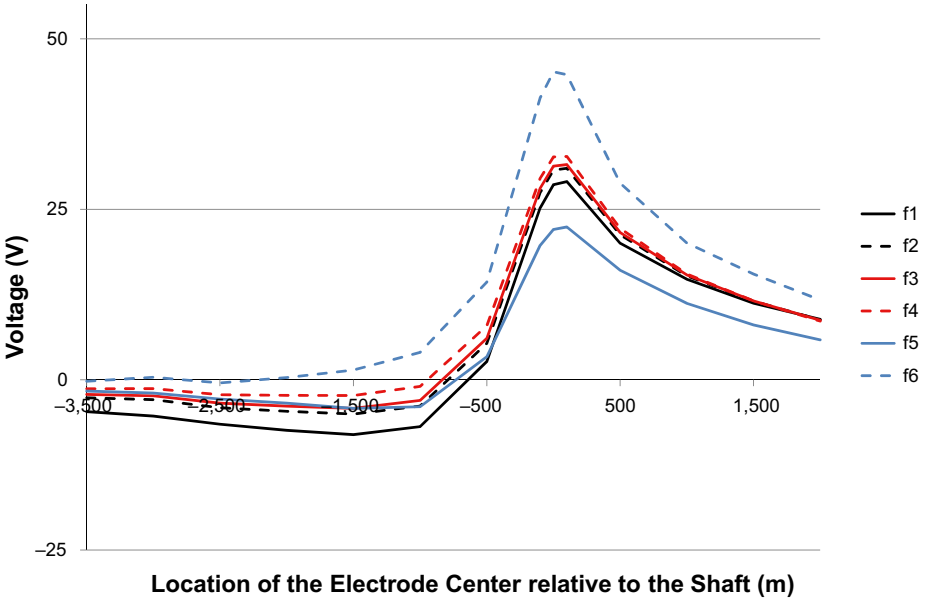

Figure 5-27d. *The voltages that arise at position* D *at 10 m from the tunnel end as function of the difference in x-coordinate between the center of the electrode and the center of the shaft.*

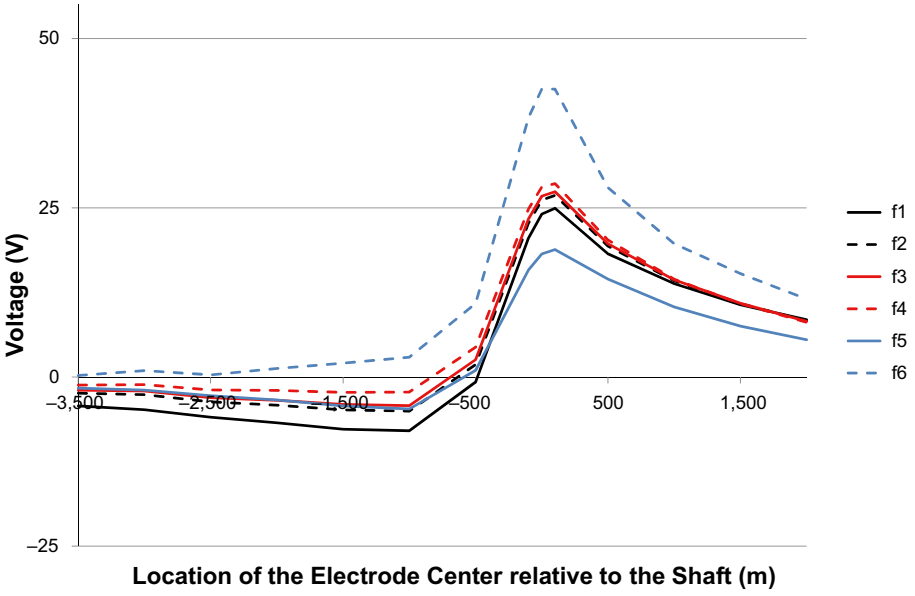

Figure 5-27e. *The voltages that arise at position* E *at 10 m from the tunnel end as function of the difference in x-coordinate between the center of the electrode and the center of the shaft.*

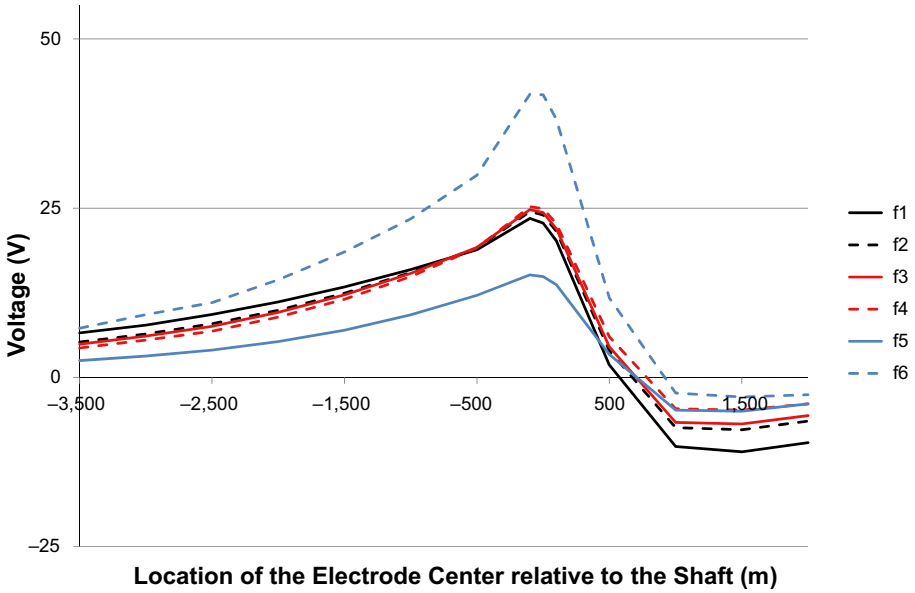

Figure 5-27f. *The voltages that arise at position* F *at 10 m from the tunnel end as function of the difference in x-coordinate between the center of the electrode and the center of the shaft.*

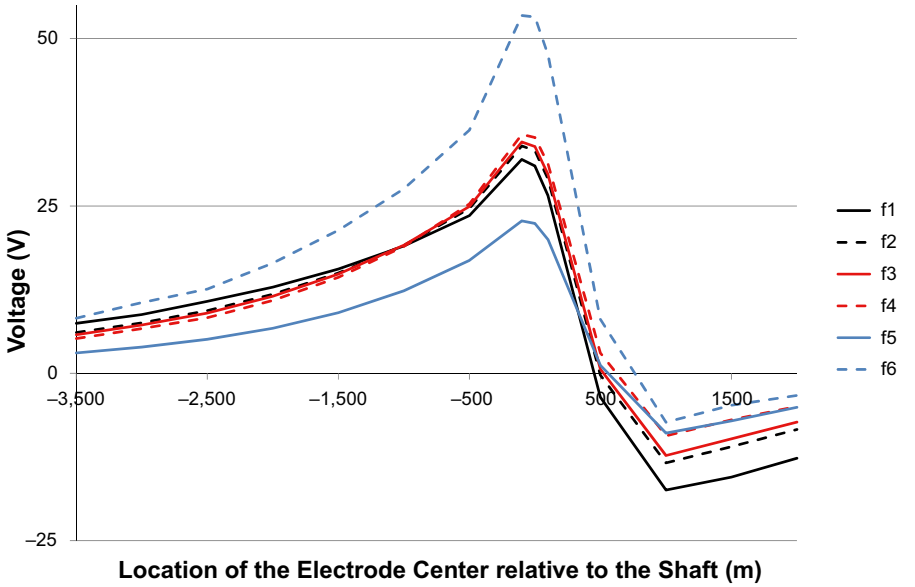

Figure 5-27g. *The voltages that arise at position* G *at 10 m from the tunnel end as function of the difference in x-coordinate between the center of the electrode and the center of the shaft.*

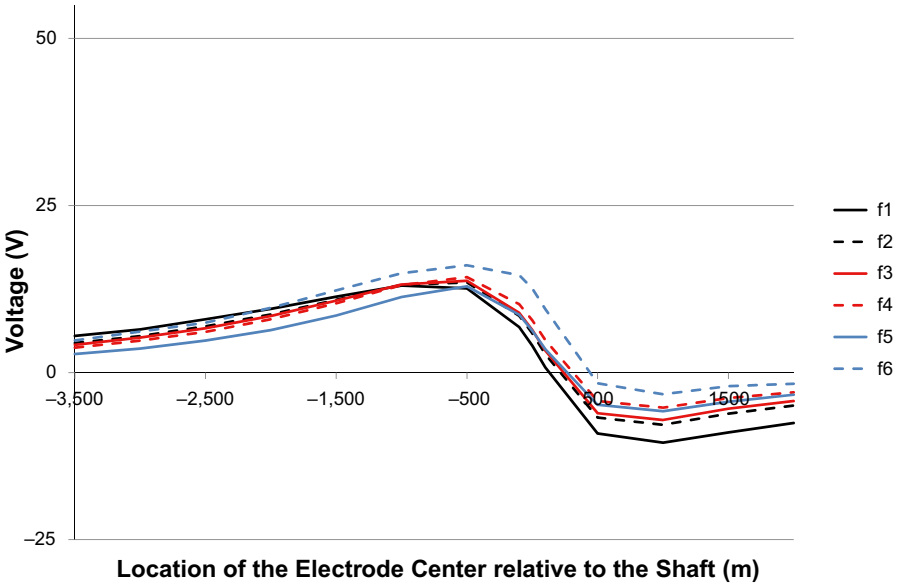

Figure 5-27h. *The voltages that arise at position* H *at 10 m from the tunnel end as function of the difference in x-coordinate between the center of the electrode and the center of the shaft.*

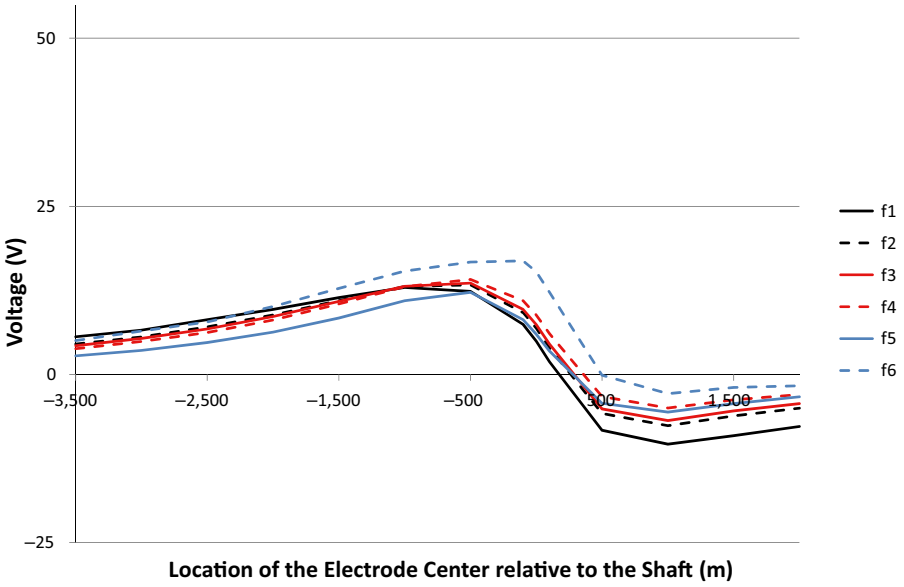

Figure 5-27i. *The voltages that arise at position* I *at 10 m from the tunnel end as function of the difference in x-coordinate between the center of the electrode and the center of the shaft.*

Figures 5-27a through 5-27i show that there is a rather complicated dependence of the voltage on the location of the electrode center relative to the shaft on the resistivity function and the position in the model repository. When the electrode center is located close to the shaft, position *G* gives the highest voltages (Figure 5-27g). When the electrode center is located at large negative coordinates relative to the shaft, position *C* gives the highest values of the potential, although the polarity is reversed (Figure 5-27c).

Figure 5-28 shows the maximum absolute value of the voltage for positions *A* through *I*. The diagram was constructed by linear interpolation of the voltages to a resolution of 100 m in the x-coordinate, for each resistivity function, calculating the absolute values of these voltages and selecting the highest absolute value and plotting these values as function of the difference in x-coordinate between the shaft and the electrode. Values for a location of the deposition hole 10 m from the end of the tunnel were selected for all cases. The highest value (position G) is slightly less than the highest value in Table 5-9, but quite close.

y-direction

Figure 5-29 shows the model repository with the HVDC electrode represented as a ring of sub-electrodes at two alternative locations in relation to the repository. The left hand figure shows a location where the y-coordinate of the electrode is –200 m relative to the center of the shaft. The right hand figure shows a location where the y-coordinate of the electrode is +500 m relative to the center of the shaft.

Calculations of the voltages that would arise along the height of a deposition hole as function of the y-coordinate of the deposition hole for the various tunnels were made for the two geometries illustrated in Figure 5-29 and for several intermediate locations of the electrode. Calculations were made for locations of electrode at –500 m, –200 m, +200 m and +500 m difference in y-coordinate relative to the center of the shaft. The voltages that arise at the locations *A* through *I*, in Figure 5-23, are shown for a distance of 10 m from the tunnel end.

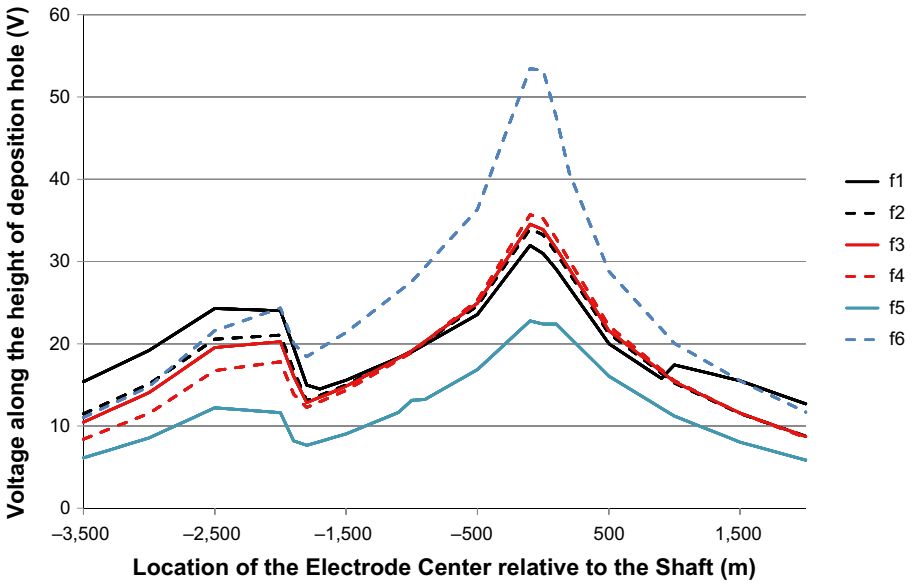

Figure 5-28. *Maximum absolute values of the voltage along the height of a deposition hole as function of the location of electrode center relative to the shaft. The resistivity in the deposition hole is set to be the same as in the surrounding rock.*

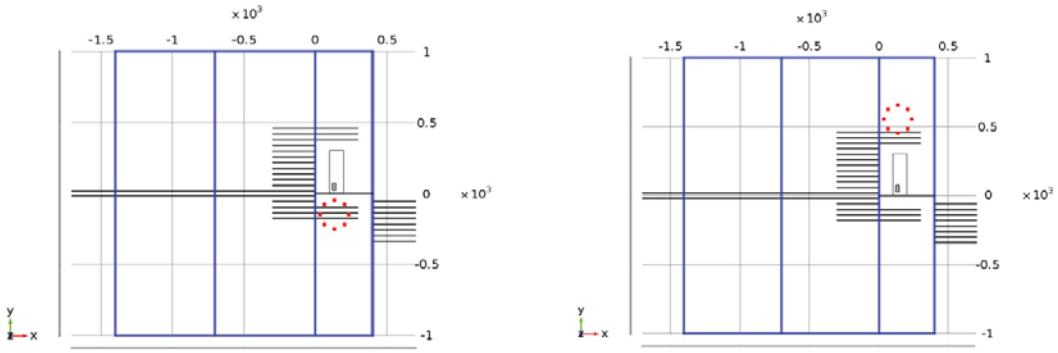

a. *The x-coordinate of the electrode is –200 m relative to the center of the shaft.*

b. *The x-coordinate of the electrode is +500 m relative to the center of the shaft.*

Figure 5-29. *The model repository with the HVDC electrode represented as a ring of sub-electrodes at two alternative locations in relation to the repository. Variations in the y-direction.*

Figure 5-30a shows the voltages that arise at position *A* at 10 m from the tunnel end as function of the difference in x-coordinate between the center of the electrode and the center of the shaft. Figures 5-30b through 5-30i show the corresponding results for positions *B* through *I*, respectively. The diagrams show results for resistivity functions *f1* through *f6* as indicated by the legends. The data points for the case where the electrode is located directly on top of the shaft are included in the diagrams. Although the range of variation in location in the y-direction is much smaller in Figure 5-30 than the range of variation in x-direction in Figure 5-27, the same scale is maintained to facilitate comparison of peak widths between variations in x-direction and variations in the y-direction.

As the Figures 5-30a through 5-30i show, position *G* in Figure 5-30g gives the highest voltage for all resistivity functions. It can also be seen that the variation in y-direction of the location of the electrode gives a simpler pattern than for the variation in x-direction, with the location of the electrode on top of close to the shaft gives the highest voltages. The width of the peaks in voltage across a deposition hole in Figures 5-30a through 5-30i are relatively similar to the widths in Figures 5-27a through 5-27i, where comparisons are possible. Thus for locations of the electrode center close to the shaft the extent of the peaks in the voltage along the height of a deposition hole is approximately the same for a variation in the y-direction as in the x-direction.

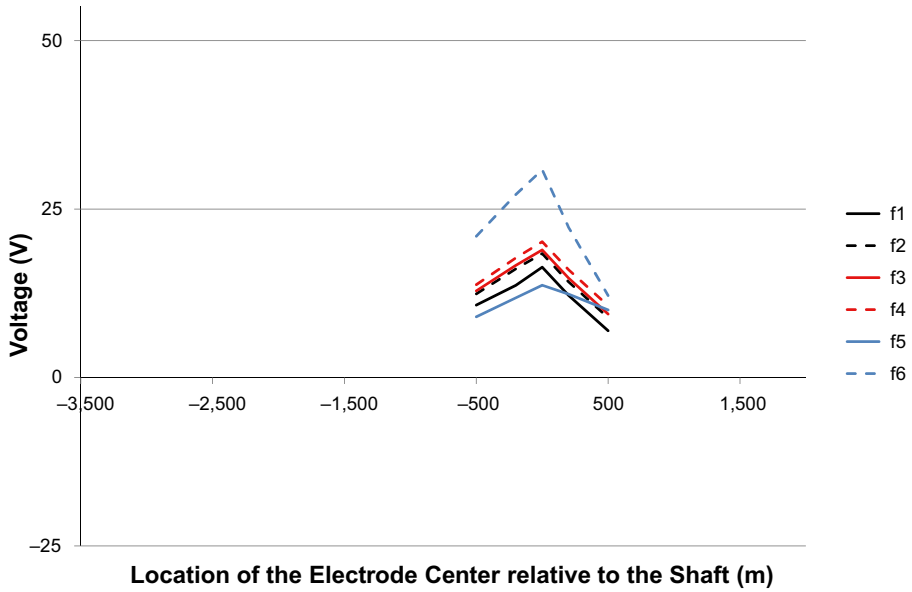

Figure 5-30a. *The voltages that arise at position* A *at 10 m from the tunnel end as function of the difference in y-coordinate between the center of the electrode and the center of the shaft.*

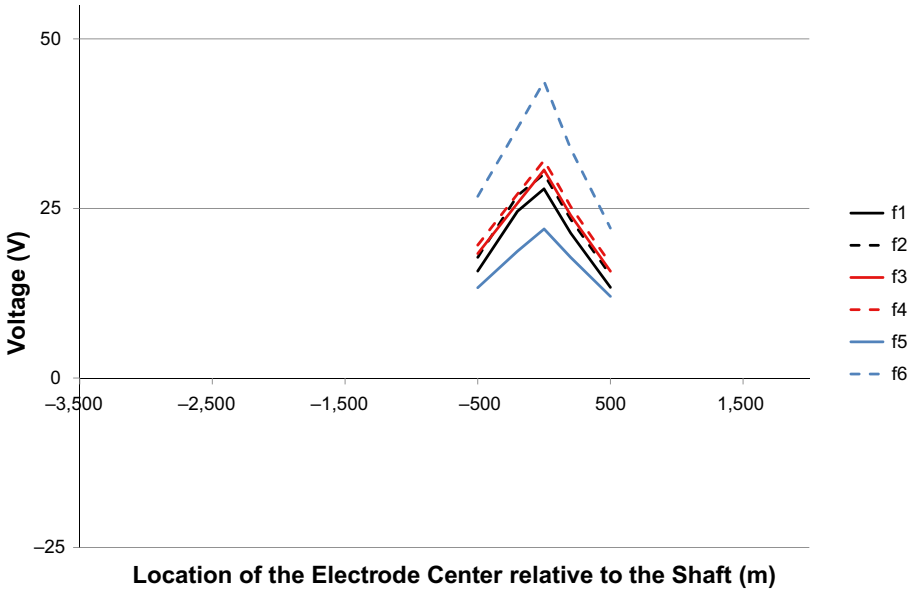

Figure 5-30b. *The voltages that arise at position* B *at 10 m from the tunnel end as function of the difference in y-coordinate between the center of the electrode and the center of the shaft.*

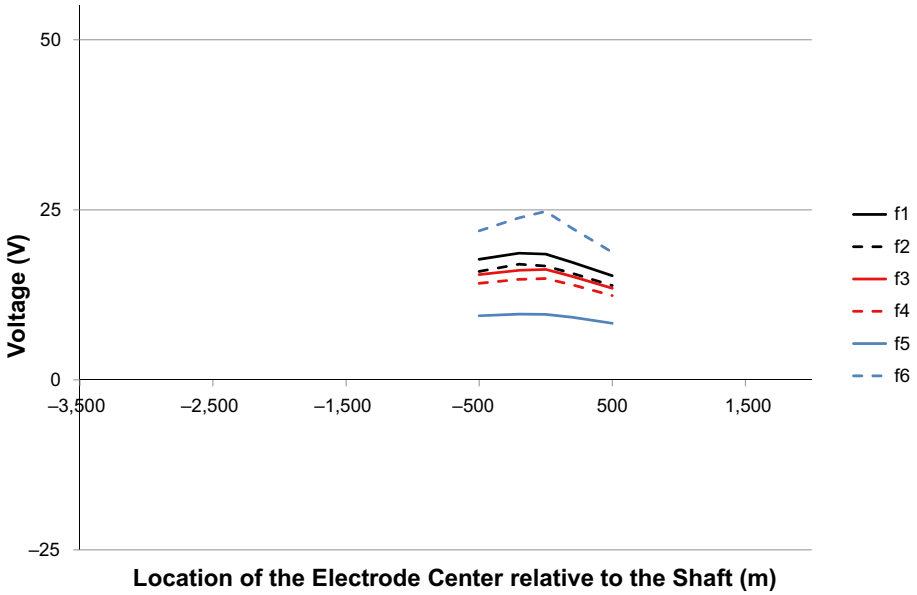

Figure 5-30c. *The voltages that arise at position* C *at 10 m from the tunnel end as function of the difference in y-coordinate between the center of the electrode and the center of the shaft.*

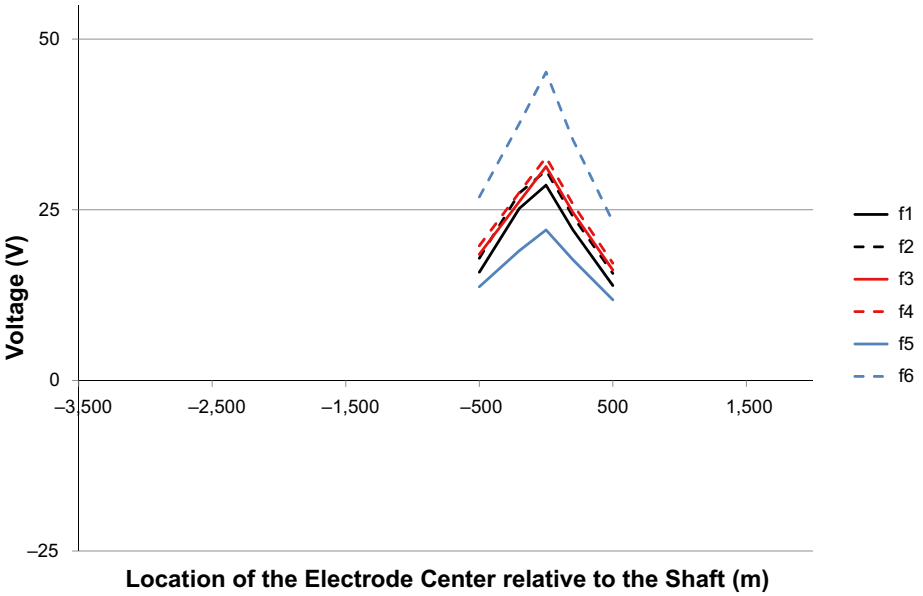

Figure 5-30d. *The voltages that arise at position* D *at 10 m from the tunnel end as function of the difference in y-coordinate between the center of the electrode and the center of the shaft.*

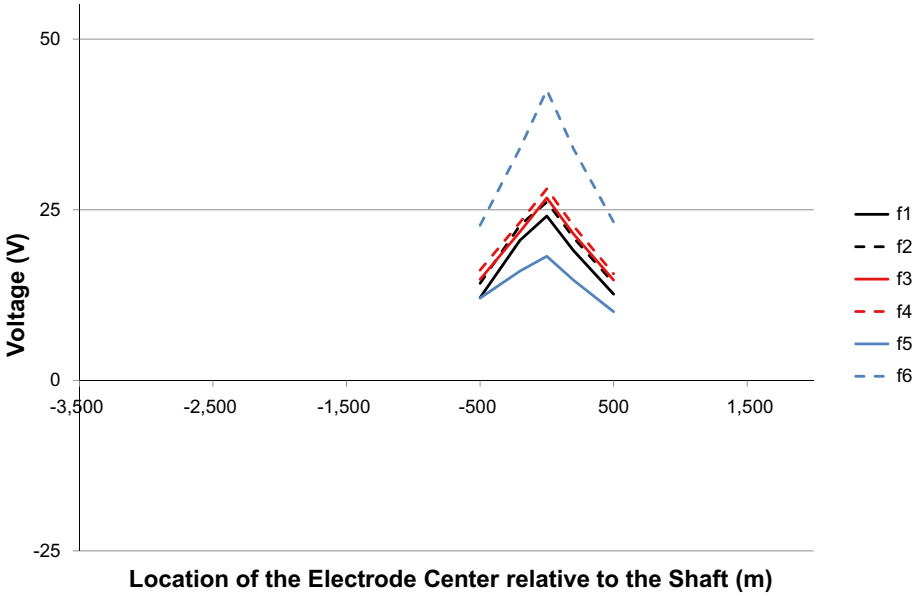

Figure 5-30e. *The voltages that arise at position* E *at 10 m from the tunnel end as function of the difference in y-coordinate between the center of the electrode and the center of the shaft.*

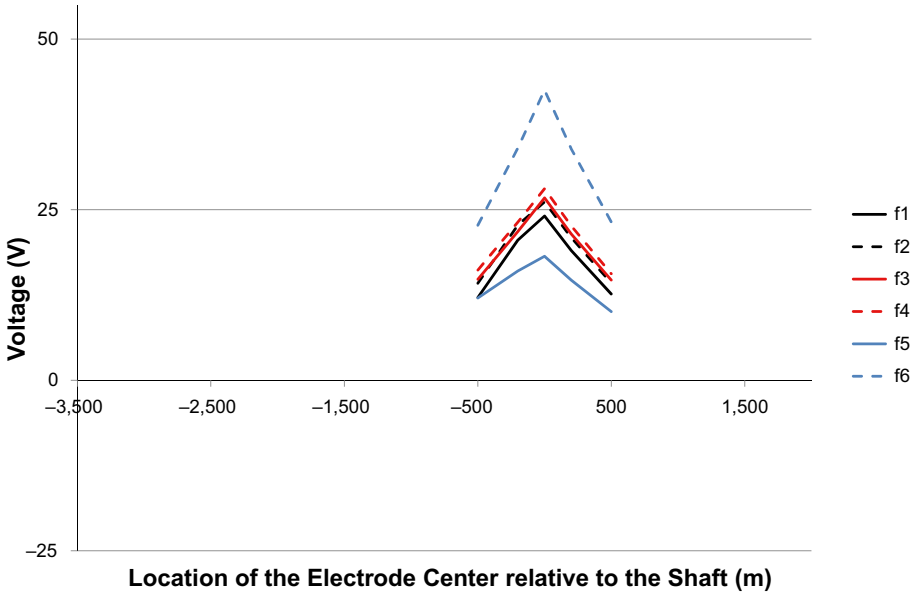

Figure 5-30f. *The voltages that arise at position* F *at 10 m from the tunnel end as function of the difference in y-coordinate between the center of the electrode and the center of the shaft.*

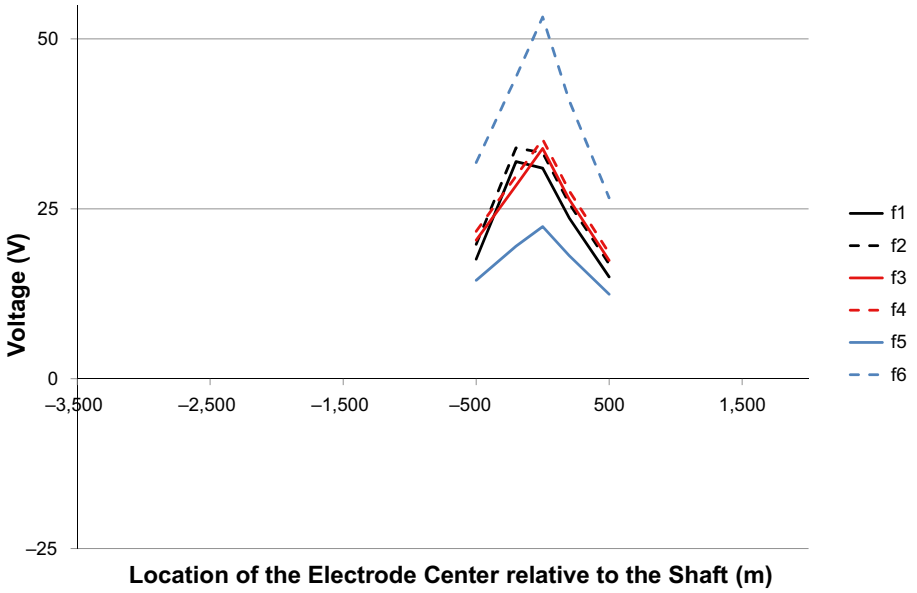

Figure 5-30g. *The voltages that arise at position* G *at 10 m from the tunnel end as function of the difference in y-coordinate between the center of the electrode and the center of the shaft.*

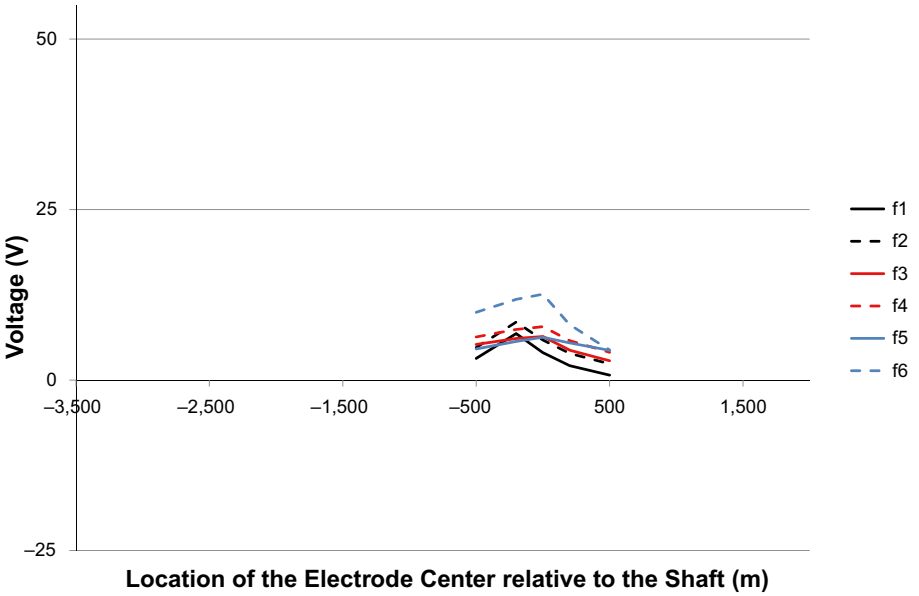

Figure 5-30h. *The voltages that arise at position* H *at 10 m from the tunnel end as function of the difference in y-coordinate between the center of the electrode and the center of the shaft.*

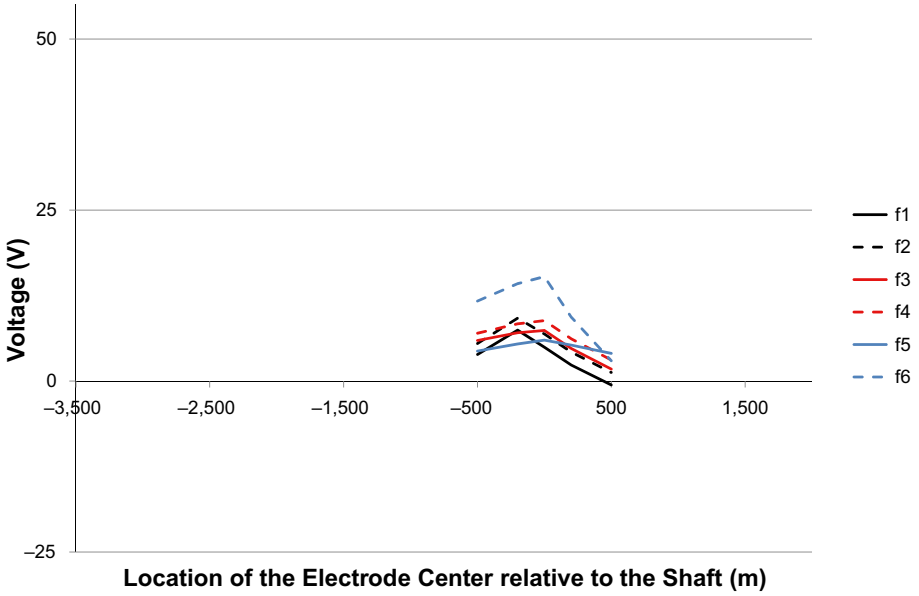

Figure 5-30i. *The voltages that arise at position* I *at 10 m from the tunnel end as function of the difference in y-coordinate between the center of the electrode and the center of the shaft.*

Simultaneous variations in x- and y-directions

Comparing the layout of the planned repository in Figure 5-5 with the model repository in Figure 5-7, it is apparent that not all tunnels are represented in the model repository. Figure 5-31 shows the model repository and ranges where the tunnels are planned but not represented in the model repository. These ranges are labeled J, K and L in Figure 5-31.

Canisters in deposition holes located in deposition tunnels at positions *J*, *K* or *L* may suffer corrosion because of the proximity to the HVDC electrode although the influence of the shaft is negligible. This situation is not treated by the other cases and is therefore treated here. The reduced tunnel system with three interconnected 600 m long tunnels, illustrated in Figure 5-8, is used. Thus, the most of the net of transport tunnels as well as the shaft is neglected in this study. Also, when the effect at position *J* is studied, tunnels at locations *K* and *L* are neglected. The x-coordinate of the center of the electrode relative to the location of the shaft was varied: 0 m, 100 m, 200 m, 300 m, 400 m, 500 m, 1,000 m, 1,500 m and 2,000 m for the cases where the tunnels are aligned with the electrical field from electrode and 100 m, 300 m, 500 m and 800 m for the case where the tunnels are not aligned with the electrical field. For the latter case there is a 500 m difference in the y-coordinate.

Translations of the tunnel system in the y-direction allow practically all tunnels in the repository to be included in the analysis. The electrode can also be translated to agree with the assumptions of location of the electrode relative to the center of the tunnel system and to satisfy the assumption of alignment between the orientation of the tunnel system in the electrical field.

Each set of three 600 m long tunnels contains 6 tunnel ends and the highest of the values of the voltages at locations 10 m from the tunnel ends are reported, for each distance. Figure 5-32 shows the voltages along the height of a deposition hole as function of the distance between the center of the tunnel system and the center of the electrode. The electrode is aligned with the tunnels for the blue curves. Figure 5-32a shows the voltage for resistivity function *f1*. Figures 5-32b through 5-32f show the voltage for resistivity functions *f2* through *f6*.

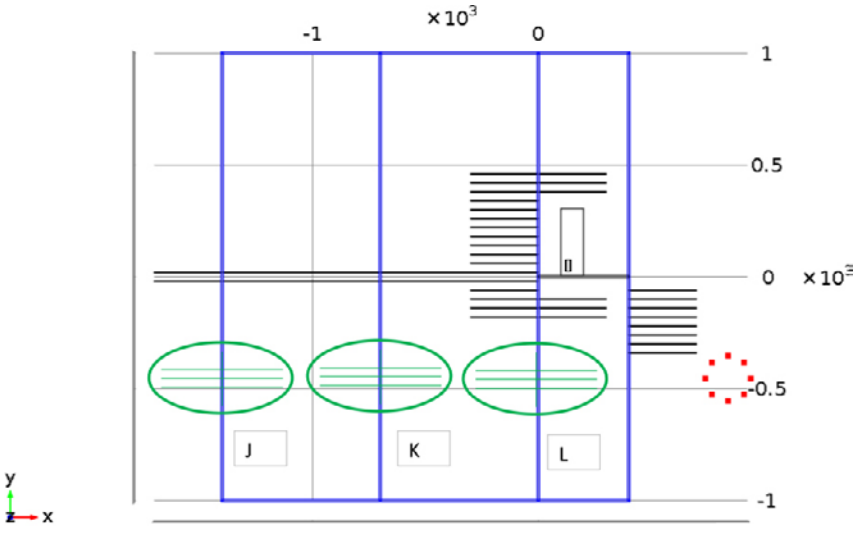

Figure 5-31. *Ranges where the planned repository contains deposition tunnels are not represented in the model repository. The tunnels are aligned with the electrical field from the electrode.*

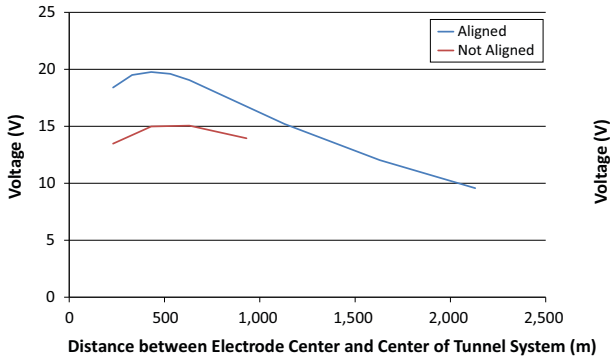

a. *Resistivity Function f1.*

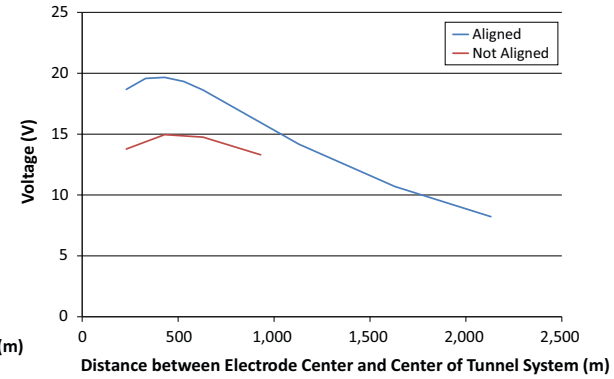

b. *Resistivity Function f2*

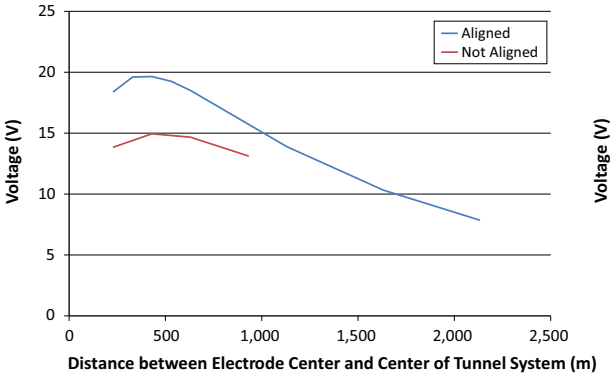

c. *Resistivity Function f3*

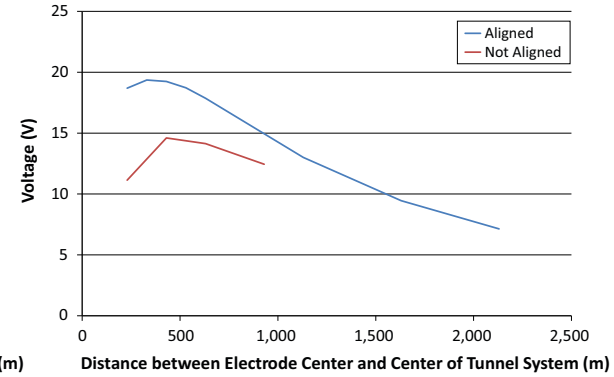

d. *Resistivity Function f4*

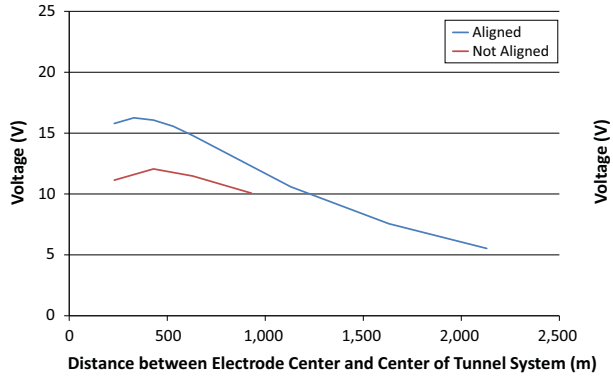

e. *Resistivity Function f5*

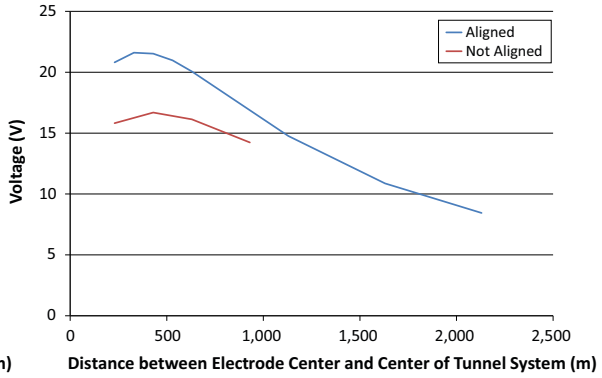

f. *Resistivity Function f6*

Figure 5-32. *The maximum voltage arising 10 m from a tunnel end as function of the distance in the x-direction between the electrode center and the center of the tunnel system. For the case where the electrode is not aligned with the tunnels, the separation in the y-coordinate is 500m.*

Figure 5-32a through 5-32c show that a voltage of about 20 V is predicted for resistivity function *f1* through *f4* when the electrode is located within about 500 m from the center of the tunnel system (3 interconnected 600 m long tunnels), if the field from the electrode is aligned with the tunnels and about 15 V if there is a 500 m difference in the y-coordinate between the location of electrode and the tunnel center. For resistivity function *f5* the voltage is slightly lower and for resistivity function *f6* the voltage is slightly higher. The maximum value is though lower than the highest values for variation of the electrode positon in x-direction (Figure 5-28) or for the electrode on top of the repository (Table 5-9).

6 Vertical conductance in the bentonite parallel to the canister

The present study is made under the premises that there will be no significant loss of water from a bentonite block. Water may be redistributed within a block so that parts closest to the canister become dryer than the initial state and the parts of the same bentonite block further away from the canister get increased water content.

For simplicity, the bentonite around the canister is treated as having no vertical gradients in water content. With this simplification the hollow cylinder that the bentonite around the canister constitutes may be divided into a number of cylindrical shells. The conductance, C, of such a shell is given by Equation 6-1.

$$C = \frac{\pi (r_o^2 - r_i^2)}{h} \kappa \qquad (6\text{-}1)$$

where r_o is the outer radius of the shell and r_i is the inner radius of the shell, h is the height of the shells which is equal to the height of the canister. The parameter κ is the local conductance of the bentonite in this shell. The total conductance is the sum of the contributions from each small shell. In order to calculate the total conductance we need to consider the dependence of the conductance in bentonite as a function of water content, in some detail.

6.1 Conductance in compacted bentonite as a function of water content

Figure 6-1 shows a diagram of measured conductivities for two different bentonite qualities as function of water content. Data is taken from Rothfuchs et al. (2004).

The data for MX-80 at 22°C is the most extensive data set. The data points form a line that seems to justify the application of linear regression. The regression line for this data set is also drawn in the figure.

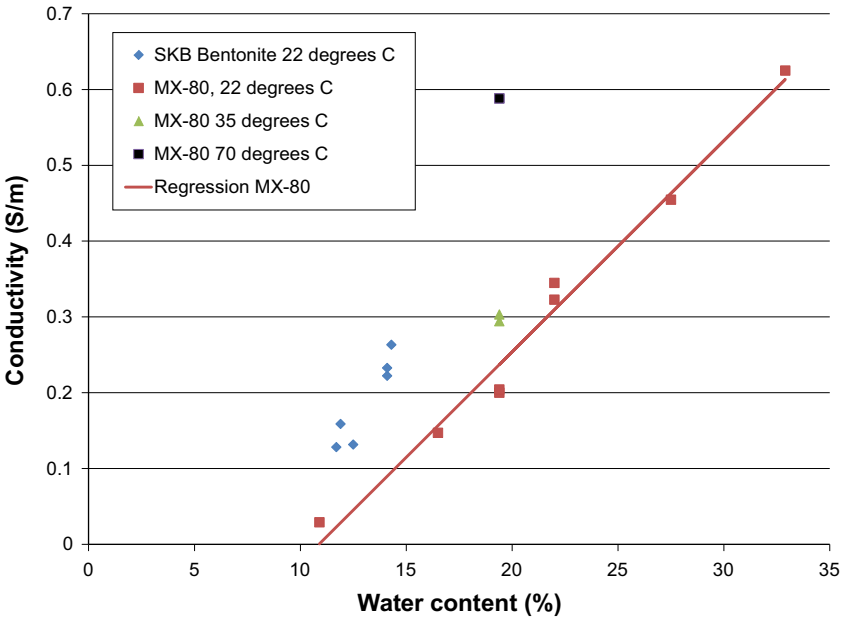

Figure 6-1. *Conductivity of bentonite as a function of water content. The regression line for MX-80 bentonite at 22°C is also shown.*

In approximate terms, the conductivity for MX-80 at 22°C can be expressed as

$$\kappa = C_{wc}\,(wc - 10.88) \qquad (6\text{-}2)$$

for water contents higher than 10.88%. *wc* is the water content in percent and C_{wc} is the coefficient describing the dependence of conductivity on water content. The value of C_{wc} found from linear regression is 0.02786 S/m.

If the small shell closest to the canister looses a certain amount of water to the neighboring shell, the conductance in the innermost shell will decrease and that of the neighboring shell will increase. In order to quantify the effects it is useful to divide the bentonite into *N* small shells such that the volume of each small shell is the same.

A loss of 68.67 g water per kg bentonite, with the initial water content of 17%, from the inner shell would decrease the conductivity to almost zero ((170–68.67)/(1,000–68.67)×100%=10.88). If this amount of water is collected in the neighboring shell the resulting water content would become about 22.33 % ((170+68.67)/(1,000+68.67)×100 %= 22.33).

Using these figures and four shells as an example:

Initially the four shells have identical water content and conductivity = $\kappa 1 = \kappa 2 = \kappa 3 = \kappa 4$ = 0.02786×(17–10.88) = 0.1705 S/m

After drying the different shells have the conductivity:

$\kappa 1$ = 0.02786×(10.88–10.88) = 0 S/m

$\kappa 2$ = 0.02786×(22.33–10.88) = 0.3190 S/m

$\kappa 3$ = 0.02786×(17–10.88) = 0.1705 S/m

$\kappa 4$ = 0.02786×(17–10.88) = 0.1705 S/m

The average conductivity after drying is 0.165 S/m. The relative decrease in conductivity caused by such an extreme drying of a large part of the bentonite close to the canister gives rise to a decrease in the average conductivity of about 3% ((0.1705–0.1650)/0.1705=0.032). If the water from the innermost shell is distributed evenly in the three outer shells the decrease in average conductivity would be less than 3%. When more shells than four are considered, say 10–20 shells, the relative decrease in conductivity becomes negligible if the innermost of these shells becomes non-conducting because of redistribution of the water content.

It is correct to regard average conductivity because only the conductivity parallel to the canister is considered and each shell is given an equal statistical weight because they were given an equal volume. By assuring that the shells have the same volume we also assure that they contribute equally much to the total conductance.

If the innermost shell is severely dried so that the water content drops below 10.88 %, this shell will not contribute significantly to the total conductance. If the water content drops to about 5% the paradoxical situation arises that the water constituting the difference between 10.88% and 5% water contents has been shifted from a place where is does not convey any conductance to places where there is a positive influence of water on the conductance. Thus, if the water content drops below about 10 % the conductance of the bentonite parallel to the canister actually increases. A premise is of course that the water is just relocated, radially, within the block.

The most pessimistic case from Figure 6-1 seems to be bentonite of the MX-80 quality. In view of the scatter in data points it is reasonable to estimate conductivities at a certain water content from the regression line rather than from interpolation between single data points. An initial water content of 17% would give a conductivity of 0.17 S/m for MX-80 at 22°C. Higher temperatures and the bentonite provided by SKB would give higher values of the conductance. According to the findings above, the conductivity of the bentonite parallel to the canister will not decrease to lower values than the initial state of a uniform water content of 17%.

6.2 Resistances in the bentonite parallel to the canister as a function of water content

Table 6-2 shows the calculated resistances for R_{b2} in Figure 5-4. The values are calculated according to Figure 6-2.

A maximum water content of 28% is considered since this corresponds to a fully water saturated bentonite buffer in the deposition hole.

Table 6-2. Conductivity of bentonite and resistance parallel to the canister for various values of the water content in the bentonite.

Water content	17%	22%	28%
Conductivity (S/m)	0.170	0.393	0.533
Resistance parallel to canister (Ω)	19.1	10.5	6.8

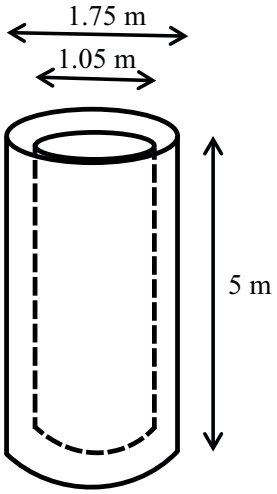

$$A = \pi\,(0.875^2 - 0.525^2) = 0.49\pi$$

$$R_2 = \rho\,\frac{5}{0.49\cdot\pi} \quad 3.25\cdot\rho \quad \frac{3.25}{\kappa}$$

Figure 6-2. *The resistance of the bentonite surrounding the canister.*

6.3 Resistances in the bentonite in the deposition hole over and under the canister

In the modeling, 8 m deep deposition holes are considered and the canister is 5 m in height. Thus there is a total of 3 m of bentonite over and under the canister. The geometry for this resistance is that of Figure 5-15 with the difference that the cylinder is only 3 m high. The sum of the resistances R_{b1} and R_{b3}, in Figure 5-4 is thus:

$$R_{b1} + R_{b3} = \rho \cdot \frac{3}{2.4}$$

In the electrical circuit in Figure 5-4, the resistances R_{b1} and R_{b3} appear in series with the internal resistance R_i. Resistances connected in series can be directly added and comparing the values of R_{b1} and R_{b3} in Table 6-3 with the values of R_i in Tables 5-5 and 5-8 it is found that the values of R_i are much higher. The maximum current through the deposition hole is thus determined by the resistance in the rock and tunnels and not by the situation in the deposition hole.

Table 6-3. Conductivity of bentonite and resistance in the deposition hole over and under the canister for various values of the water content in the bentonite.

Water content	17%	22%	28%
Conductivity (S/m)	0.170	0.393	0.533
Resistances R_{b1}+R_{b3} (Ω)	7.4	3.2	2.3

7 Combinations of HVDC field cases and bentonite saturation cases

7.1 Equivalent electrical circuit

7.1.1 The corrosion current

For the full electrical circuit we also need the resistances for current going in and out of the copper canister. Over a limited voltage range this value is equal to R_c. The polarization resistance has been measured to 3,100 Ω m^2 (Taxén 2011), for nominally oxygen free conditions. For an area of the circular end of the canister the resistance is about 3,580 Ω.

It is now possible to study different combinations of electrical fields resulting from HVDC electrodes and cases with different saturation of the bentonite around the canister.

Using Figure 5-4, we can now begin to simplify the circuit. First it is observed that the value of R_c is much higher than the value than the value of R_{b2}. This means that the total current in the circuit can be estimated as the current through R_{b2}.

$$I_{tot}=E/(R_i+R_{b1}+R_{b2}+R_{b3}) \quad (7\text{-}1)$$

The voltage that can arises along the height of a canister, U_2, is equal the voltage over R_{b2} and is calculated as

$$U_2= R_{b2}/(R_i+R_{b1}+R_{b2}+R_{b3})\times E \quad (7\text{-}2)$$

The corrosion current, I_{corr}, is the small part of the total current that passes in and out of the canister is calculated as

$$I_{corr}=U_2/(2\times R_c) \quad (7\text{-}3)$$

The values of the voltages that can arise along the height of a canister are here presented under the assumption of linear behavior of the polarization resistance. That is, R_c is assumed to be constant, independently of the voltage. This may not always be the case and the extent of the linear region will be further discussed in Section 8.1.

7.1.2 The internal resistance, R_i

As discussed in Section 5.6.3 and 5.7 values of R_i are calculated for two different cases, but gives nearly the same values (Tables 5-5 and 5-8). Thus the following will used: a value R_i of 730 Ω for the resistivity functions *f1*, *f2*, *f3*, *f4*, a value of 370 Ω for resistivity function *f5* and a value of 1,450 Ω for function *f6*.

7.1.3 The voltage along the height of a canister

The electromotive force, E, is defined as the voltage along the height of a deposition hole for the case where there is no current through the hole. Tabulated values of the calculated voltages for the various cases refer to conditions where the medium in the deposition hole is the same as that of the surrounding rock. Thus, the values of the electromotive force, E, should be recalculated from the tabulated values, U_1, by the expression:

$$E=U_1\times(R_{H1}+ R_i)/R_{H1} \quad (7\text{-}4)$$

Then, the actual voltages along the height of a canister, U_2, is calculated from the tabulated values of the calculated voltages for the various cases, U_1, by compensating for the difference in the resistivity in the deposition hole. i.e. by combining Equation (7-2) and (7-4):

$$U_2= (R_{H1}+R_i)/R_{H1}\times R_{b2}/(R_i+R_{1b}+ R_{2b}+R_{3b})\times U_1 \quad (7\text{-}5)$$

The resistivity functions *f1* through *f4* use a value of 10,000 Ωm for the resistivity of the rock at repository depth. Figure 5-15 shows that the value of R_{H1} is about 33,300 Ω for this case. For function *f5* the value of R_{H1} is about 16,700 Ω and for function *f6* the value is 66,600 Ω.

When the extent of the electrical field is calculated the value of R_H is that given by Figure 5-15, with a resistivity that is the same as in the surrounding rock (R_{H1}). The values of U_1 for the different cases are given in Tables 5-1, 5-2, 5-3, 5-6, 5-7, 5-9 and 5-10.

The values of R_{b2} are given in Table 6-2 for three different water contents of the bentonite. Table 6-3 shows the corresponding value for the sum of R_{b1} and R_{b3}. The voltages along the height of a canister, U_2, is calculated from Equation 7-5.

7.2 A uniform electrical field resulting from a remote electrode

Tables 5-2 and 5-6 in Section 5.5 show the voltages that would arise between the positions of the circular end surfaces of the deposition hole for the case where the conductivity of the deposition hole is the same as in the surrounding rock. Table 5-2 shows the results for the 600 m long tunnels and Table 5-6 shows the results for 1,700 m long tunnels. These values can now be used to calculate the voltages that would arise along the height of a copper canister in these deposition holes when the canisters are surrounded by bentonite.

7.2.1 600 m long tunnels

As-deposited bentonite

Table 7-1 shows the calculated values of the voltage along a copper canister for various locations of the deposition hole and functions of the rock resistivity. The resistivity of the bentonite in the tunnels was set to 1 Ωm unless otherwise stated. Three 600 m long tunnels were studied and the values for an edge tunnel are presented. As-deposited bentonite with 17% water content is considered.

Table 7-1 shows that the highest voltage along the height of a canister would occur for resistivity function *f5*. Location of a deposition hole 5 m from the end of a tunnel would give a voltage of 0.20 V along the height of a canister.

Water saturated bentonite

Table 7-2 shows the corresponding values to Table 7-1 but for conditions where the bentonite surrounding the canister is water saturated with 28% water content. As expected the voltages are lower with higher water content in the bentonite.

Table 7-1. Calculated values of the voltage (V) along a copper canister for various locations of the deposition hole and functions of the rock resistivity. The resistivity of the bentonite in the tunnels was set to 1 Ωm unless otherwise stated. Three 600 m long tunnels, edge tunnel. As-deposited bentonite with 17% water content.

	Location of the deposition hole (m from tunnel end)						
Resistivity function	**5**	**10**	**15**	**20**	**25**	**30**	**10 (Tunnel resistivity 2 Ωm)**
f1	0.12	0.11	0.10	0.09	0.08	0.08	0.09
f2	0.12	0.11	0.10	0.09	0.08	0.08	
f3	0.12	0.11	0.10	0.09	0.08	0.08	
f4	0.12	0.11	0.10	0.09	0.08	0.08	
f5	0.20	0.18	0.16	0.15	0.14	0.13	
f6	0.07	0.06	0.05	0.05	0.05	0.04	

Table 7-2. Calculated values of the voltage (V) along a copper canister for various locations of the deposition hole and functions of the rock resistivity. The resistivity of the bentonite in the tunnels was set to 1 Ωm unless otherwise stated. Three 600 m long tunnels, edge tunnel. Saturated bentonite with 28% water content.

	Location of the deposition hole (m from tunnel end)						
Resistivity function	**5**	**10**	**15**	**20**	**25**	**30**	**10 (Tunnel resistivity 2 Ωm)**
f1	0.04	0.04	0.03	0.03	0.03	0.03	0.03
f2	0.04	0.04	0.03	0.03	0.03	0.03	
f3	0.04	0.04	0.03	0.03	0.03	0.03	
f4	0.04	0.04	0.03	0.03	0.03	0.03	
f5	0.08	0.07	0.06	0.06	0.05	0.05	
f6	0.02	0.02	0.02	0.02	0.02	0.02	

7.2.2 1,700 m long tunnels

Table 7-3 and 7-4 show the voltages that arise along the height of a canister in deposition holes located at the ends of a 1,700 m long tunnel. The resulting voltages are slightly higher than for shorter tunnels (Table 7-1 and 7-2).

As-deposited bentonite

Table 7-3. Calculated values of the voltage (V) along a copper canister for various locations of the deposition hole and functions of the rock resistivity. The resistivity of the bentonite in the tunnels was set to 1 Ωm. Two 1,700 m long tunnels. As-deposited bentonite with 17% water content.

	Location of the deposition hole (m from tunnel end)					
Resistivity function	**5**	**10**	**15**	**20**	**25**	**30**
f1	0.19	0.17	0.15	0.14	0.14	0.13
f2	0.19	0.17	0.16	0.15	0.14	0.13
f3	0.19	0.17	0.16	0.15	0.14	0.13
f4	0.19	0.17	0.16	0.15	0.14	0.13
f5	0.27	0.24	0.22	0.20	0.19	0.18
f6	0.13	0.11	0.10	0.10	0.09	0.09

Water saturated bentonite

Table 7-4. Calculated values of the voltage (V) along a copper canister for various locations of the deposition hole and functions of the rock resistivity. The resistivity of the bentonite in the tunnels was set to 1 Ωm. Two 1,700 m long tunnels. Saturated bentonite with 28% water content.

	Location of the deposition hole (m from tunnel end)					
Resistivity function	**5**	**10**	**15**	**20**	**25**	**30**
f1	0.07	0.06	0.06	0.05	0.05	0.05
f2	0.07	0.06	0.06	0.05	0.05	0.05
f3	0.07	0.06	0.06	0.05	0.05	0.05
f4	0.07	0.06	0.06	0.05	0.05	0.05
f5	0.10	0.09	0.08	0.08	0.07	0.07
f6	0.05	0.04	0.04	0.04	0.03	0.03

7.3 Forsmark Power station as a secondary electrode (Case 2)

As-deposited bentonite

Table 7-5 shows the calculated values of the voltage along a copper canister for various locations of the deposition hole and functions of the rock resistivity, using the data in Table 5-7. The resistivity of the bentonite in the tunnels was set to 1 Ωm. As-deposited bentonite with 17% water content is considered.

Table 7-5 shows that the highest voltage along the height of a canister would occur for resistivity functions *f1* and *f6*. A location of a deposition hole 5 m from the end of a tunnel would give a voltage of 0.08 V along the height of a canister for the end closest to the secondary electrode.

Water saturated bentonite

Table 7-6 shows the corresponding values to Table 7-5 but for conditions where the bentonite surrounding the canister is water saturated with 28% water content. Again the voltages are lower with higher water content of the bentonite.

Table 7-5. Calculated values of the voltage (V) along a copper canister for various locations of the deposition hole and functions of the rock resistivity. The resistivity of the bentonite in the tunnels was set to 1 Ωm. Center tunnel. The notation 'near' and 'far' refer to the end of the tunnel that is closest to and farthest away from the current source, respectively. Edge tunnel. As-deposited bentonite with 17% water content.

	Location of the deposition hole (m from tunnel end)											
	5		10		15		20		25		30	
Resistivity function	near	far	near	far	near	far	near	far	near	far	near	far
f1	–0.08	0.06	–0.07	0.06	–0.06	0.05	–0.05	0.05	–0.05	0.05	–0.05	0.04
f2	–0.07	0.06	–0.06	0.05	–0.05	0.05	–0.05	0.04	–0.04	0.04	–0.04	0.04
f3	–0.07	0.06	–0.06	0.05	–0.05	0.05	–0.05	0.04	–0.04	0.04	–0.04	0.04
f4	–0.06	0.05	–0.05	0.04	–0.05	0.04	–0.04	0.04	–0.04	0.04	–0.04	0.04
f5	–0.05	0.04	–0.05	0.04	–0.04	0.03	–0.04	0.03	–0.03	0.03	–0.03	0.03
f6	–0.08	0.06	–0.07	0.06	–0.06	0.05	–0.05	0.05	–0.05	0.05	–0.05	0.04

Table 7-6. Calculated values of the voltage (V) along a copper canister for various locations of the deposition hole and functions of the rock resistivity. The resistivity of the bentonite in the tunnels was set to 1 Ωm. Center tunnel. The notation 'near' and 'far refer to the end of the tunnel that is closest to and farthest away from the current source, respectively. Edge tunnel. Saturated bentonite with 28% water content.

	Location of the deposition hole (m from tunnel end)											
	5		10		15		20		25		30	
Resistivity function	near	far	near	far	near	far	near	far	near	far	near	far
f1	–0.03	0.02	–0.02	0.02	–0.02	0.02	–0.02	0.02	–0.02	0.02	–0.02	0.02
f2	–0.03	0.02	–0.02	0.02	–0.02	0.02	–0.02	0.02	–0.02	0.01	–0.01	0.01
f3	–0.02	0.02	–0.02	0.02	–0.02	0.02	–0.02	0.02	–0.02	0.01	–0.01	0.01
f4	–0.02	0.02	–0.02	0.02	–0.02	0.01	–0.02	0.01	–0.01	0.01	–0.01	0.01
f5	–0.02	0.02	–0.02	0.01	–0.02	0.01	–0.01	0.01	–0.01	0.01	–0.01	0.01
f6	–0.03	0.02	–0.02	0.02	–0.02	0.02	–0.02	0.02	–0.02	0.02	–0.02	0.02

7.4 The HVDC electrode located directly on top of the repository (Case 3)

A case of a future HVDC electrode on top of the repository assumes a rise of the sea level so that the water depth is about 2 m at the site of the repository. This scenario would seem to be likely only after times when full saturation of the bentonite has been reached. Only the case for water-saturated bentonite parallel to the canisters will therefore be considered. Figure 7-1 shows the voltages along the height of a deposition hole from Figure 5-24 recalculated to voltages along the height of a canister according to Equation 7-5. The labels *A* through *I* indicate the tunnel ends in Figure 5-23. The rings at each label show the voltage at a deposition hole located 10 m from the tunnel end.

Table 7-7 shows the calculated values of voltage along the height of a copper canister, using the data in Table 5-9 where all resistivity functions *f1* through *f6* are included.

Table 7-7 shows that the highest voltage along the height of a canister would occur for resistivity function *f5*. A location of a deposition hole 5 m from the end of a tunnel would give a voltage of 0.46 V along the height of a canister.

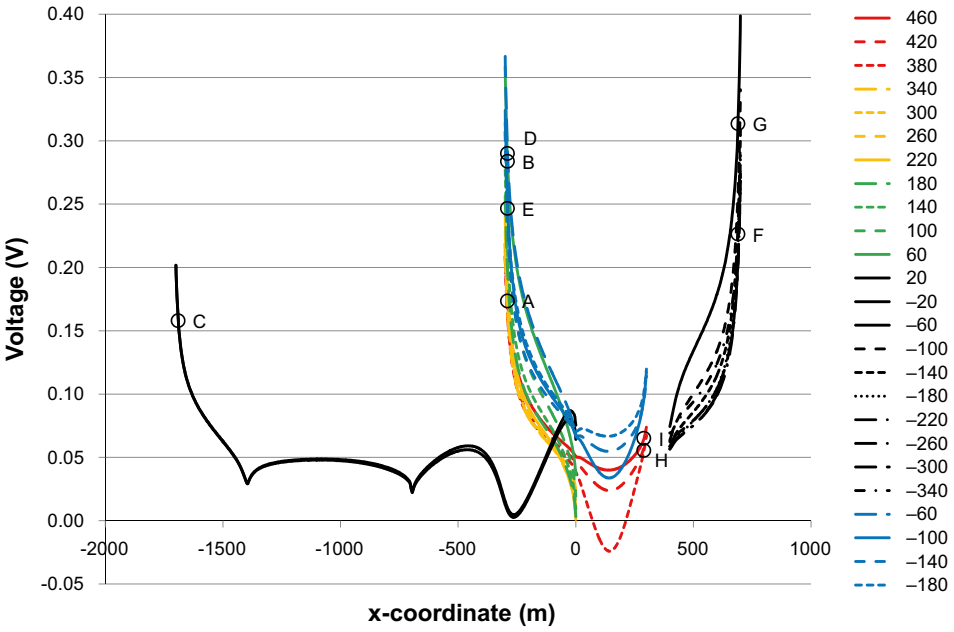

Figure 7-1. *The voltages that would arise along the height of a canister as function of the x-coordinate of the deposition hole. The line style and color from Figure 5-23 is used for the tunnels and the legend indicates the y-coordinate of the tunnel. The voltages at positions A through I in Figure 5-23 are shown in Figure 7-1 as rings with the corresponding letter. A distance of 10 m from the tunnel end was selected for the labeled rings in Figure 7-1. The electrode is centered around x=130 m. Resistivity function f2 is used. The conductivity in the bentonite surrounding the canister is set 0.53 S/m corresponding to saturated bentonite with 28% water content.*

Table 7-7. Calculated values of the voltage (V) along a copper canister for various locations of the deposition hole and functions of the rock resistivity. The resistivity of the bentonite in the tunnels was set to 1 Ωm. The column headings *A* through *I* indicate the tunnel ends in Figure 5-23. Saturated bentonite with 28% water content.

Distance from tunnel end (m)	Resistivity Function	A	B	C	D	E	F	G	H	I
5	*f1*	0.17	0.29	0.19	0.30	0.25	0.24	0.32	0.04	0.05
10	*f1*	0.15	0.26	0.17	0.27	0.23	0.22	0.29	0.04	0.05
15	*f1*	0.14	0.24	0.16	0.25	0.21	0.20	0.27	0.03	0.04
20	*f1*	0.13	0.23	0.15	0.23	0.20	0.19	0.25	0.03	0.04
25	*f1*	0.13	0.22	0.14	0.22	0.18	0.18	0.24	0.03	0.04
30	*f1*	0.12	0.21	0.14	0.21	0.18	0.17	0.23	0.02	0.04
5	*f2*	0.19	0.31	0.18	0.32	0.27	0.25	0.35	0.06	0.07
10	*f2*	0.17	0.28	0.16	0.29	0.25	0.23	0.31	0.06	0.07
15	*f2*	0.16	0.26	0.15	0.27	0.23	0.21	0.29	0.05	0.06
20	*f2*	0.15	0.25	0.14	0.25	0.21	0.20	0.27	0.05	0.06
25	*f2*	0.14	0.24	0.13	0.24	0.20	0.19	0.26	0.04	0.06
30	*f2*	0.14	0.23	0.13	0.23	0.19	0.18	0.25	0.04	0.06
5	*f3*	0.20	0.32	0.17	0.33	0.28	0.25	0.35	0.07	0.07
10	*f3*	0.18	0.29	0.15	0.30	0.25	0.23	0.32	0.06	0.07
15	*f3*	0.17	0.27	0.14	0.27	0.23	0.21	0.30	0.06	0.07
20	*f3*	0.16	0.25	0.13	0.26	0.22	0.20	0.28	0.05	0.07
25	*f3*	0.15	0.24	0.13	0.25	0.21	0.19	0.27	0.05	0.06
30	*f3*	0.14	0.23	0.12	0.24	0.20	0.18	0.26	0.04	0.06
5	*f4*	0.21	0.33	0.15	0.34	0.29	0.26	0.37	0.08	0.09
10	*f4*	0.19	0.30	0.14	0.31	0.27	0.23	0.33	0.07	0.08
15	*f4*	0.18	0.28	0.13	0.29	0.25	0.22	0.31	0.07	0.08
20	*f4*	0.17	0.27	0.12	0.27	0.23	0.21	0.29	0.06	0.08
25	*f4*	0.16	0.25	0.12	0.26	0.22	0.20	0.28	0.06	0.08
30	*f4*	0.15	0.24	0.11	0.25	0.21	0.19	0.27	0.06	0.07
5	*f5*	0.28	0.45	0.20	0.45	0.37	0.30	0.46	0.13	0.12
10	*f5*	0.25	0.41	0.18	0.41	0.34	0.27	0.41	0.12	0.11
15	*f5*	0.23	0.38	0.16	0.38	0.31	0.25	0.38	0.11	0.11
20	*f5*	0.22	0.35	0.15	0.36	0.29	0.24	0.36	0.10	0.10
25	*f5*	0.21	0.34	0.15	0.34	0.28	0.23	0.34	0.09	0.10
30	*f5*	0.20	0.32	0.14	0.33	0.26	0.22	0.33	0.08	0.09
5	*f6*	0.16	0.23	0.13	0.24	0.22	0.22	0.28	0.06	0.08
10	*f6*	0.15	0.21	0.12	0.22	0.20	0.20	0.25	0.06	0.07
15	*f6*	0.14	0.19	0.11	0.20	0.19	0.19	0.24	0.06	0.07
20	*f6*	0.13	0.18	0.10	0.19	0.18	0.18	0.22	0.05	0.07
25	*f6*	0.12	0.18	0.10	0.18	0.17	0.17	0.21	0.05	0.07
30	*f6*	0.12	0.17	0.10	0.18	0.16	0.16	0.21	0.05	0.07

A repository at greater depth

Figure 7-2 shows the results corresponding to Figure 7-1 but where the repository level has been shifted downwards from 500 m to 700 m below, present day, ground.

Table 7-8 shows the calculated values of voltage along a copper canister, using the data in Table 5-10, for the case where the repository level has been shifted to 700 m below ground.

Table 7-8 shows that the highest voltage along the height of a canister would occur for resistivity function *f5*. A location of a deposition hole 5 m from the end of a tunnels *D* and *G* would give a voltage of 0.33 V along the height of a canister for the case where the repository level is 700 m below ground. Generally the voltage over the canister decrease with a deeper location of the repository, but the effects are rather small. For the canisters with the highest voltage (the same at both depths) the decrease is close to 30 %.

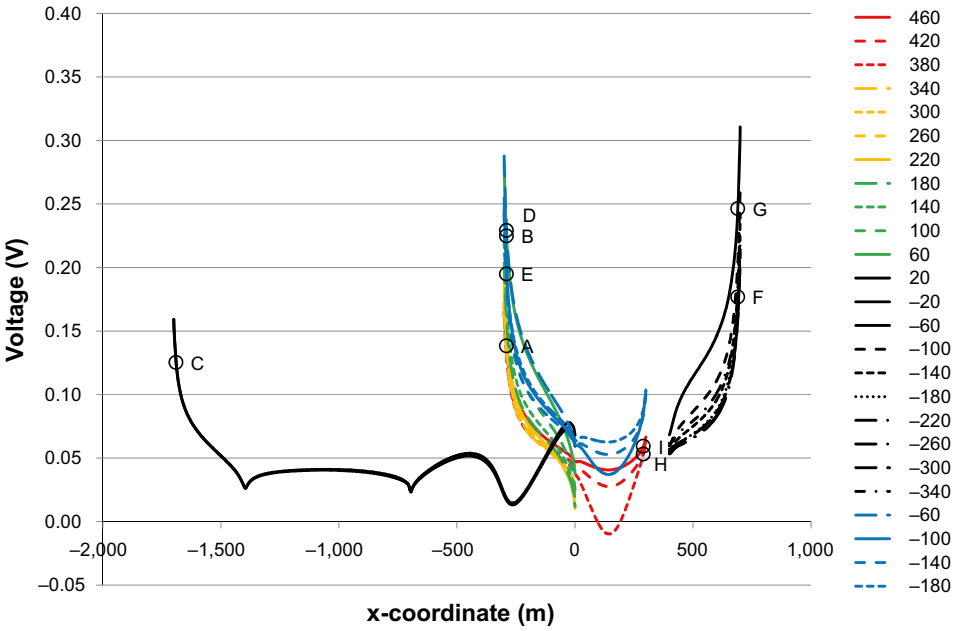

Figure 7-2. *The voltages that would arise along the height of a canister as function of the x-coordinate of the deposition hole. Repository level 700 m below ground.*

Table 7-8. Calculated values of the voltage (V) along a copper canister for various locations of the deposition hole and functions of the rock resistivity. The resistivity of the bentonite in the tunnels was set to 1 Ωm. The column headings *A* through *I* indicate the tunnel ends in Figure 5-23. Saturated bentonite with 28% water content. Repository level 700 m below ground.

Distance from tunnel end (m)	Resistivity Function	A	B	C	D	E	F	G	H	I
5	*f1*	0.13	0.22	0.17	0.23	0.19	0.18	0.25	0.03	0.04
10	*f1*	0.12	0.20	0.15	0.21	0.17	0.17	0.22	0.03	0.04
15	*f1*	0.11	0.19	0.14	0.19	0.16	0.15	0.21	0.03	0.04
20	*f1*	0.10	0.18	0.13	0.18	0.15	0.14	0.19	0.03	0.03
25	*f1*	0.10	0.17	0.12	0.17	0.14	0.13	0.18	0.02	0.03
30	*f1*	0.09	0.16	0.12	0.16	0.13	0.13	0.18	0.02	0.03
5	*f2*	0.15	0.25	0.14	0.25	0.22	0.20	0.27	0.06	0.06
10	*f2*	0.14	0.22	0.13	0.23	0.20	0.18	0.25	0.05	0.06
15	*f2*	0.13	0.21	0.12	0.21	0.18	0.16	0.23	0.05	0.06
20	*f2*	0.12	0.20	0.11	0.20	0.17	0.15	0.22	0.05	0.06
25	*f2*	0.12	0.19	0.10	0.19	0.16	0.15	0.21	0.04	0.05
30	*f2*	0.11	0.18	0.10	0.18	0.16	0.14	0.20	0.04	0.05
5	*f3*	0.16	0.25	0.13	0.26	0.22	0.20	0.28	0.06	0.07
10	*f3*	0.14	0.23	0.12	0.24	0.20	0.18	0.25	0.06	0.07
15	*f3*	0.13	0.22	0.11	0.22	0.19	0.17	0.24	0.06	0.06
20	*f3*	0.13	0.20	0.10	0.21	0.18	0.16	0.22	0.05	0.06
25	*f3*	0.12	0.20	0.10	0.20	0.17	0.15	0.21	0.05	0.06
30	*f3*	0.12	0.19	0.10	0.19	0.16	0.14	0.20	0.05	0.06
5	*f4*	0.17	0.27	0.11	0.27	0.23	0.20	0.29	0.08	0.09
10	*f4*	0.15	0.25	0.10	0.25	0.21	0.18	0.27	0.08	0.08
15	*f4*	0.15	0.23	0.09	0.23	0.20	0.17	0.25	0.08	0.08
20	*f4*	0.14	0.22	0.09	0.22	0.19	0.16	0.24	0.07	0.08
25	*f4*	0.13	0.21	0.08	0.21	0.18	0.15	0.23	0.07	0.08
30	*f4*	0.13	0.20	0.08	0.20	0.18	0.15	0.22	0.07	0.08
5	*f5*	0.21	0.33	0.15	0.33	0.27	0.22	0.33	0.11	0.10
10	*f5*	0.19	0.30	0.13	0.30	0.25	0.20	0.30	0.11	0.10
15	*f5*	0.18	0.28	0.13	0.28	0.23	0.19	0.28	0.10	0.09
20	*f5*	0.17	0.27	0.12	0.27	0.22	0.18	0.27	0.09	0.09
25	*f5*	0.16	0.26	0.11	0.26	0.21	0.17	0.26	0.09	0.09
30	*f5*	0.16	0.25	0.11	0.25	0.20	0.17	0.25	0.08	0.09
5	*f6*	0.14	0.20	0.09	0.21	0.20	0.18	0.24	0.08	0.08
10	*f6*	0.13	0.19	0.08	0.19	0.18	0.16	0.22	0.07	0.08
15	*f6*	0.12	0.17	0.07	0.18	0.17	0.15	0.21	0.07	0.08
20	*f6*	0.12	0.17	0.07	0.17	0.16	0.15	0.20	0.07	0.08
25	*f6*	0.11	0.16	0.07	0.16	0.15	0.14	0.19	0.06	0.07
30	*f6*	0.11	0.15	0.06	0.16	0.15	0.14	0.18	0.06	0.07

7.5 The HVDC electrode at variable distance from the repository (Case 4)

x-direction

Figure 5-27a through 5-27i showed the voltages that would arise at the various positions *A* through *I* as function of the x-coordinate of the electrode relative to the shaft. Figure 5-28 showed the maximum voltage for all positions (*A* through *I*) as function of the x-coordinate of the electrode relative to the shaft. Figure 7-3 shows the voltages that would arise along the height of a canister surrounded by water saturated bentonite as function of the x-coordinate of the electrode relative to the shaft. The values were calculated from those in Figure 5-28 by application of Equation 7-5, for each resistivity function.

The highest values are seen when the electrod is close to the shaft, and for resistivity function f5. The top values are though slightly smaller than for case 3.

y-direction

As noted in Section 5.8.2 the width of the peaks in voltage across a deposition hole in Figures 5-30a through 5-30i are relatively similar to the widths in Figures 5-27a through 5-27i. Thus for locations of the electrode center close to the shaft the extent of the peaks in the voltage across a canister is approximately the same for a variation in the y-direction as in the x-direction. The curves in Figure 7-3 can be seen as representing also variations in the location in the y-direction from –500 m to +500 m.

Simultaneous variations in x- and y-directions

Positions *J*, *K* and *L* in Figure 5-31 are considered and the reduced tunnel system with 3 interconnected tunnels is studied. The voltages over a deposition hole in Figures 5-32a through 5-32d are recalculated to voltages along the height of a canister in water saturated bentonite by application of Equation 7-5. Figures 7-4a through 7-4d show the voltages for resistivity function *f1* through *f6*, respectively.

From Figure 7-4 it can be seen that the highest values are achieved for resistivity function *f5*, as for case 3 with the electrode directly on top of the shaft. The maximum value is slightly smaller.

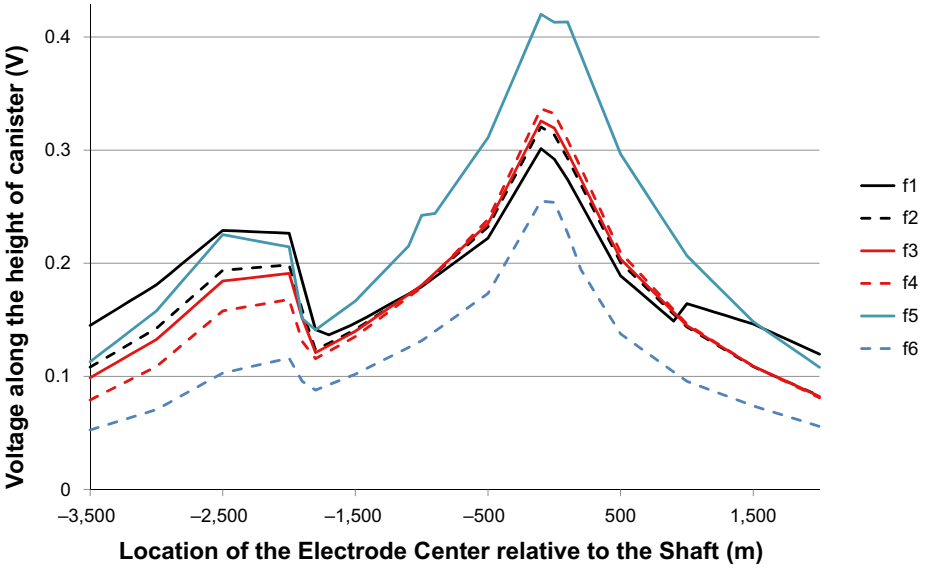

Figure 7-3. *The voltages that would arise along the height of a canister. The maximum voltage for any canister (positions A through I) in the model repository is drawn as function of the x-coordinate of the deposition hole. A distance of 10 m from the tunnel end was selected. The conductivity in the bentonite surrounding the canister is set 0.53 S/m corresponding to saturated bentonite with 28% water content.*

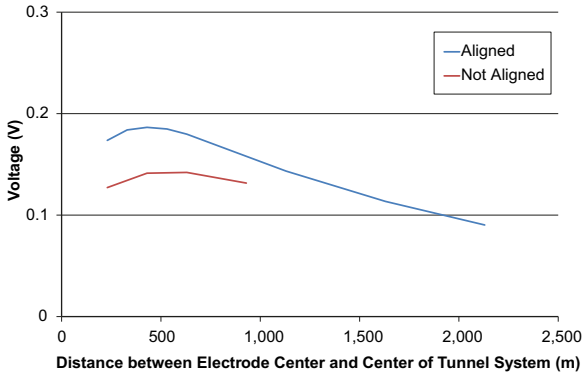

a. *Resistivity function f1*

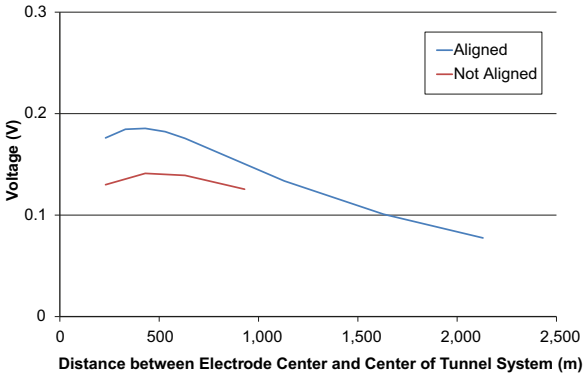

b. *Resistivity function f2*

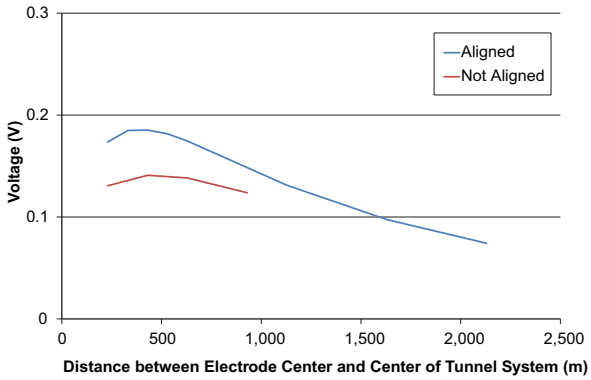

a. *Resistivity function f3*

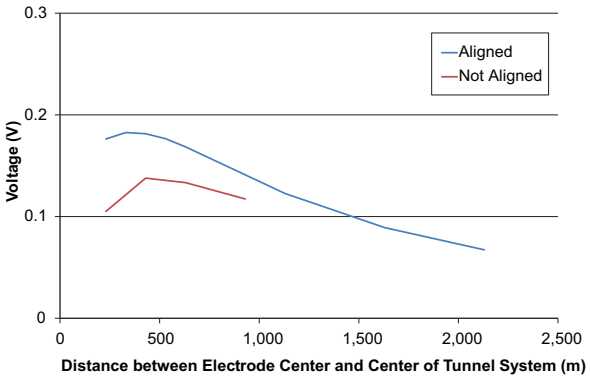

b. *ResistivityfFunction f4*

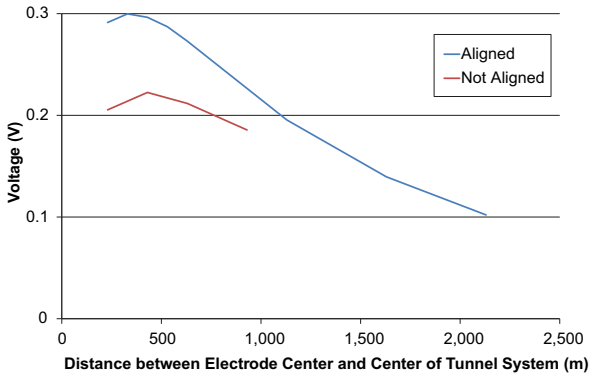

a. *Resistivity function f5*

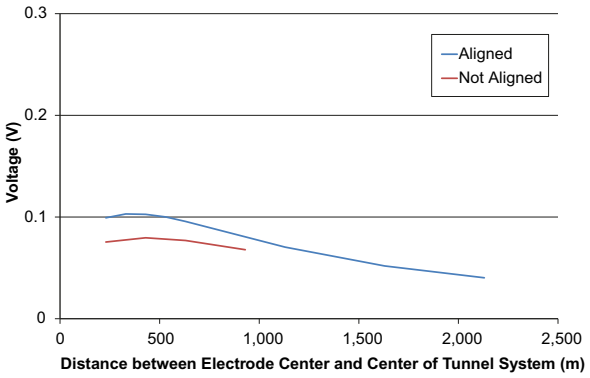

b. *Resistivity function f6*

Figure 7-4. *The maximum voltage across a canister arising 10 m from a tunnel end as function of the distance in the x-direction between the electrode center and the center of the tunnel system. For the case where the electrode is not aligned with the tunnels, the separation in the y-coordinate is 500m.*

8 Possible corrosion effects on the copper canisters

8.1 Limits for the application of linear polarization resistance

The process of electrical current going into and exiting from the copper canister in bentonite can be described using electrical equivalents. Corrosion occurs where current exits the canister. The simplest electrical equivalent is a resistor so that a doubling of the voltage leads to a doubling of the current. However, the representation with a resistor is not a good approximation at large voltages. The voltage range where the approximation can be justified is referred to as the linear region and this resistance is termed the polarization resistance.

The value of the polarization resistance and the extent of the potential range over which it is applied must be regarded together with the chemical environment it is intended to represent. Under oxygen rich conditions the polarization resistance may be very low and the linear range short, but except for the initial phase after deposition and closure of the repository the conditions are expected to become virtually oxygen free. This corresponds approximately to the conditions prevailing during measurement of the polarization resistance.

The value of the polarization resistance used in this study was determined by application of a potential difference of 0.365 V around the corrosion potential (Taxén 2011). Outside the linear range, the currents may increase exponentially rather than linearly with the voltage. A useful analogy is that of one or more diodes. Below a certain threshold potential the diodes are essentially non-conducting. Above the threshold potential, an increase in the potential causes a disproportionately large increase in current.

Figures 8-1 and 8-2 show some experimental polarization curves that illustrate the situation (King and Tang 1998). Figure 8-1 shows a sequence of four potential scans while Figure 8-2 shows only the two last scans. We will use these curves as an illustration of the currents through a copper canister and let the first two scans represent short term behavior and the two last scans represent the behavior in a longer time perspective. No precise limits for ‘long’ and ‘short’ time perspectives can be given. The transition from short time behavior to long time behavior will depend on the amount of corrosion products on the copper surface and the magnitude of the current.

Strongly non-linear behavior is observed at potentials higher than about –0.2 V. Following scan 1 towards more negative potentials, a reduction peak is observed at about –0.9 V. The magnitude and location of this peak shifts for the subsequent scans.

The cases we consider in this study imply that one end of the canister is subjected to an increased potential and the other end is subjected to a negative potential by an electrical field. A constraint is that the positive current at the positive side of the canister is balanced by an equal negative current at the negative side. If we now for the sake of the argument, consider a large positive current at the positive end of the canister, say 100 μA. According to Figure 8-2 we have to go down to potentials below –1.0 V to produce a cathodic current of –100 μA. But for short-term behavior, Figure 8-1, we only have to go down to about –0.8 V to produce a cathodic current of –100 μA.

The interpretation is that for short-term processes, non-linear behavior (diode behavior), at the anodic side can be observed at much smaller voltage differences than long-term processes. What determines the time scales ‘short’ and ‘long’, here is the amount of corrosion products that can be reduced before the potential at the cathodic side has to go down to the region of hydrogen evolution. Thus, the extent of the potential range that behaves as linear depends on the time scale.

It should be stated that the polarization curves in Figure 8-1 and 8-2 show laboratory data measured under conditions that do not necessarily correspond to the conditions in the repository. No attempt to estimate a polarization resistance from Figures 8-1 and 8-2 should be made. From the shape of the curves and the difference between one curve and the next, it is apparent that the data includes transient dynamic behavior of the electrode. Measurement of a polarization resistance demands static behavior, that is, currents that do not change with time.

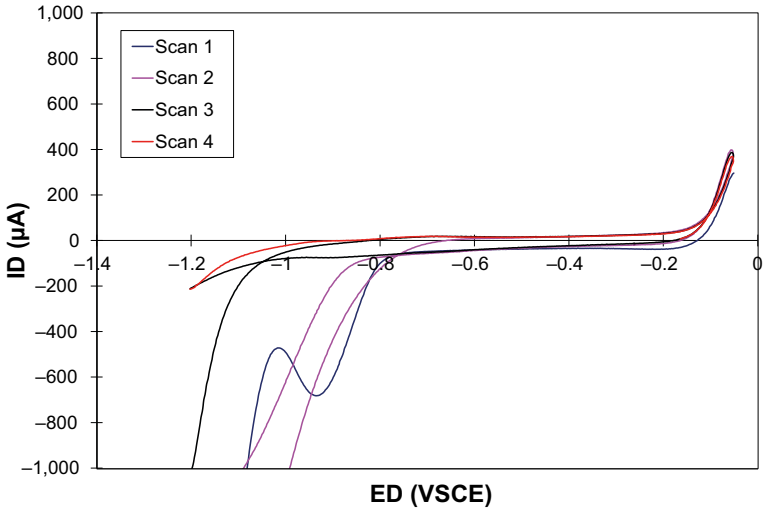

Figure 8-1. *Repetitive potential scans of a copper surface in chloride and sulfate containing solution. ID is the measured current from a copper electrode at the controlled potential ED relative the SCE (Saturated Calomel Electrode).*

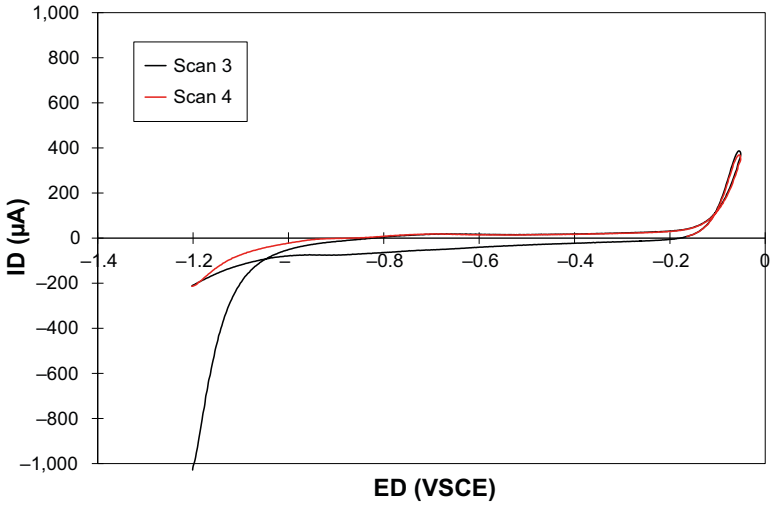

Figure 8-2. *The two last scans from Figure 8-1.*

Nevertheless, the polarization curves in Figure 8-2 indicate a larger span between the regions with exponential current increase than the 0.365 V that were used to determine the polarization resistance. No exponential increase in anodic current is seen at the potential of –0.3 V and no exponential increase in the cathodic current is seen at the potential of –0.8 V. With support from these observations, a value of 0.5 V for the extent of the linear region is applied in this study. This is relevant for conditions nominally free of molecular oxygen and where the cathodic surface is nominally free of corrosion products.

For short terms and/or in the presence of molecular oxygen, or other oxidants besides water and hydrogen ions, the polarization resistance may be much lower than the value used in this study. Corrosion would consume these oxidants so that the presence of an electrical field under these conditions would not cause more corrosion than mass transport and availability of the oxidants allows. The effect of an electrical field on the mass transport rate will be estimated in Section 8.4.2.

However, we apply the same value of the polarization resistance and the same linear range also to a later sulfide dominated stage of repository conditions. Clearly, when there is lots of sulfide around the copper surface, the polarization resistance should be relatively low, but that is not the chemical environment that the application of the linear polarization resistance attempts to describe. We use the

polarization resistance to estimate the effects of an electrical field on corrosion. Corrosion of copper during hydrogen evolution is possible because of the extreme stability of copper sulfide, the solid Cu_2S. The formation of this compound requires that copper meets sulfide, and the rate of formation cannot exceed the rate with which the two reactants meet.

Application of a low value of the polarization resistance, corresponding to sulfide rich conditions, to a situation where the rate of reaction is under mass transport control would clearly not give meaningful results. Application of a high value of the polarization resistance and a wide linear range, corresponding to sulfide free conditions, would underestimate the corrosion rate with the term that mass transport of sulfide to the copper surface allows.

When we here do apply the same value of the polarization resistance as for sulfide free conditions we get a measure of the effect of the external electrical field on the corrosion on top of the maximum sulfide corrosion rate. Recent assessments of the likely rate of supply of sulfide to the copper canister show that the rate of reaction most probably will be limited by the rate of sulfide diffusion and not by reaction kinetics (SKBdoc 1422182). Thus, the rates, in excess of mass transport limited sulfide corrosion, are limited by the same factors that define the polarization resistance before the sulfide dominated phase.

In conclusion, a limit for the linear range and limit for application of the measured value of the polarization resistance is set to 0.5 V. We get a measure of the corrosion rate in excess of the rate limited by mass transport for formation of Cu_2S. This approach will give meaningful results if estimates of the sulfide driven corrosion is based on mass transport for sulfide, which is the case in SR-Site (SKB 2011). If, however, estimates of the sulfide driven corrosion were to be based on slow kinetics of the electrochemical reaction between copper metal and sulfide, the application of a high value of the polarization resistance would underestimate the effect of the electrical field.

8.2 Pitting corrosion

Pitting corrosion occurs when most of the metal surface is protected by corrosion products that, at least partially, prevent corrosion. Local areas not protected by corrosion products can then suffer relatively high corrosion rates because of a moderately high corrosion current, as an average, can cause high corrosion rates when the current is localized to a small area.

The corrosion behavior of the canister is determined by the near-field environmental conditions, in particular the composition of the pore water in contact with the canister in the compacted bentonite surrounding the canister. Comparison of these environmental conditions with those found to promote passive behaviour suggests that the copper surface will dissolve actively at all times (King and Lilja 2013, 2014).

This study is based on literature data of the critical potential for localized corrosion, E_b, which is compared to predicted corrosion potentials, E_{corr}, of the canister. A passive $Cu_2O/Cu(OH)_2$ layer is a pre-requisite for pit initiation during the initial warm, aerobic phase. The near-neutral pH of the bentonite pore water and the predominance of Cl^- and SO_4^{2-} compared to HCO_3^- counteracts the formation of such a film.

The corrosion attack on the copper canister in the bentonite environment will thus be general corrosion in a form of surface roughening, which means all areas of the surface are corroded with slightly deeper penetrations in some locations, rather than discrete pitting. This type of roughened surfaces has been observed both in laboratory experiments with simulated repository environments and in long-term large scale tests in bentonite environment.

The environment in the repository will become reducing as the oxygen is consumed, and the sulfide will be the only corroding agent. The surface film of Cu_2S will be porous and non-protective, as a result of the low flux of sulfide to the canister surface (SKBdoc 1422182). To get a passive film, which is needed for a pitting process, a much higher sulfide flux is required.

Thus there is no process identified that could cause pitting under repository conditions, why only general corrosion is analysed in the assessment of the effects of stray currents.

8.3 Limits for application of the linear model

As noted in Section 8.1, the limit for linear behavior of the corrosion processes at the copper canister is set to 0.5 V across the canister for long term behavior. For short term behavior the linear region is smaller but as long as the cathodic reaction is reduction of molecular oxygen or reduction of previously formed corrosion products, an external electrical field does not cause more corrosion, but possibly relocates and collects the corrosion products to the anodic side of the canister.

8.4 General corrosion within the range of applicable voltages

8.4.1 Corrosion caused by currents through the linear resistance

The highest voltage difference that can be treated with the linear model is 0.5 V. This corresponds to a corrosion current that can be calculated as $I_{corr} = 0.5/(2\times R_c)$ which gives a current of about 70 μA. The volume of corroded copper per year can be calculated according to Faraday's law:

$$V_{Cu} = 3{,}600 \cdot 24 \cdot 365 \cdot \frac{I_{corr} \cdot Mw}{n \cdot F \cdot \rho} \qquad (8\text{-}1)$$

where n= 1, F = 96,485 As/mol, Mw =63.546 g/mol, and ρ = 8.92 g/cm^3.

The corrosion rate is given by dividing V_{Cu} with the area of the upper (or lower) canister end surface. The resulting corrosion rate is 0.19 ≈ 0.2 μm/year.

Thus the extent of the average corrosion caused by the electrical field is proportional to the voltage across the canister up to a level of 0.5 V, which corresponds to a corrosion rate of 0.2 μm/year.

The voltages found for the different cases, in Section 7, can be examined with this corrosion rate and the voltage limit as background.

8.4.2 Increased corrosion caused by electro-migration of charged species in an electrical field

The presence of an electrical field can accelerate the mass transport rate of charged reactants and products. For the case of copper in bentonite this could possibly apply to the transport of Cu^{2+} away from the copper surface and to the transport of HS^- towards the copper surface. These species may be considered as mutually exclusive. One of these species may be significant at the time but not both simultaneously. Electro-migration of Cu^{2+} away from the copper surface is predicted not to affect the corrosion rate and only the increased mass transport of HS^- towards the copper surface will be treated.

The mobility, u, of an ion is used to characterize the average velocity of the ion in an electrical field. The mobility is related to the diffusion coefficient by Equation 8-2.

$$D = \frac{u \cdot R \cdot T}{|z| \cdot F} \qquad (8\text{-}2)$$

where z is the charge number of the ion, and R (J/mol×K), T (K), and F (C/mol) are the gas constant, temperature, and Faraday constant, respectively. The use of Equation 8-2 for electro-migration in rock is discussed in (SKB 2010d). The cautionary words concerning its use in rock would seem to apply also to its use in bentonite. "There are … conceptual uncertainties associated with this analogy, and its applicability in the porous system of crystalline rock, as with the usage of Fickian diffusion theory. Perhaps one can say that there may be even more uncertainty associated with this analogy, as relatively few experiments and tracer tests have been carried out using electromigration as the migration mechanism." (SKB 2010d)

The average velocity or change in the average velocity is calculated as the mobility multiplied by the electrical field strength. The maximum voltage across the canister treated by the linear model was 0.5 V. The canister height is set to 5 m. Thus, for comparative purposes it seems appropriate to use 0.5 V/5 m=0.1 V/m for the field strength.

A pessimistic high value of $D = 1.2\times10^{-10}$ m^2/s for HS^- in bentonite was used (SKB 2010e). The corresponding value of the mobility of HS^- in bentonite from Equation 8-2 becomes

$u = 4.7\times10^{-9}$ m^2/V, s.

A concentration of HS^- of 1.2×10^{-4} moles/liter was used. This is the highest value used in the corrosion calculations in the safety assessment SR-Site (SKB 2010e), and is based on measured data.

The electro-migratory flux density, j, of HS^- to the canister surface can now be calculated:

$$j = c \cdot u \cdot \frac{\Delta V}{l} \text{ [mol HS}^-\text{/m}^2\text{, s]} \qquad (8\text{-}3)$$

c is the concentration, 1.2×10^{-4} moles/liter

u is the mobility, 4.7×10^{-9} m^2/V, s.

ΔV is the voltage, 0.5 V

l is the distance, 5 m

j is calculated to $5{,}6\times10^{-11}$ mol HS^-/m^2, s.

The relevant corrosion reaction for HS^- and copper is:

$HS^- + 2\ Cu(s) + H_2O \rightarrow Cu_2S(s) + H_2 + OH^-$

The corrosion rate caused by electro-migration is thus $2\times j$. Converting to an annual basis gives a corrosion rate of $2\times5.6\times10^{-11}\times3{,}600\times24\times365 = 3.5\times10^{-3}$ mol Cu/m^2, y, and recalculated to corrosion rate for comparison, 0.025 µm/year. Thus the increase in corrosion rate caused by electro-migration of HS^- at the concentration of 1.2×10^{-4} moles/liter, is about one tenth of the corrosion caused by the currents through the linear polarization resistance.

This value is arrived at by a series of approximations. One of the most coarse assumptions is that the concentration of HS^- remains at the high level of the groundwater through the bentonite and to the copper canister. For such low fluxes of sulfide, the corrosion is mass transport limited (SKBdoc 1422182). The consumption of HS^- by corrosion would have the effect of giving a concentration gradient so that the concentration and thereby also the migratory flux would decrease closer to the canister surface.

8.5 Corrosion for the case of a uniform electrical field of 50 V/km

600 m long tunnels

Table 7-1 shows a highest voltage of 0.20 V for resistivity function *f5* for a location of the deposition hole 5 m from the end of an edge tunnel when the bentonite has the same water content as at deposition. The form of corrosion would be general corrosion with a rate increased by the electrical field by 0.20/0.50×0.19 µm/year ≈ 0.08 µm/year. Table 7-2, for water saturated bentonite, shows lower voltages and give proportionally lower corrosion rates.

1,700 m long tunnels

Table 7-3 shows a highest voltage of 0.27 V for resistivity function *f5* for a location of the deposition hole 5 m from the end of a 100 m long tunnel when the bentonite has the same water content as at deposition. This gives correspondingly an increase of the corrosion rate with 0.27/0.50×0.19 µm/year ≈ 0.1 µm/year. Water saturated bentonite (Table 7-4) gives lower corrosion rates.

8.6 Corrosion for the case of a Forsmark power station as secondary electrode at 20 A

Table 7-5 shows a highest voltage of 0.08 V for the resistivity functions *f1* and *f6,* for a deposition hole located 5 m from the end of an edge tunnel, when the bentonite has the water content as when just deposited. The voltage of 0.08 V corresponds to a corrosion rate of 0.08/0.50×0.19 μm/year ≈ 0.03 μm/year, and is smaller than for the case with a uniform electrical field.

8.7 Corrosion effects of an HVDC electrode located directly on top of the repository

Table 7-7 shows voltages lower than 0.5 V for all the studied resistivity functions and locations. The highest voltage of 0.46 V is found for resistivity function *f5* and a deposition hole located 5 m from the end at position *G* in the model repository. The bentonite around the canisters is considered to be fully water saturated.

The voltage of 0.46 V corresponds to a corrosion rate of 0.46/0.50×0.19 μm/year ≈ 0.17 μm/year. Table 7-8 shows that the voltage over the canister decreases slightly for a repository at 700 m depth compared to 500 m, but the effects are rather small.

8.8 Corrosion effects of an HVDC electrode at variable distance from the repository

From Figures 7-3 and 7-4 it is evident that other positions of the electrode than directly on top of the shaft, as well as analyses of other parts of the tunnels give lower values of the voltage over the canister. The analysis of the corrosion effects of an electrode located directly on top of the shaft can thus be seen as a bounding case.

8.9 The influence situation of today

Bipolar, symmetric operation of Fenno-Skan would lead to negligible influence of the potentials because no current is transmitted through ground. However, monopolar operation is also possible and measurements performed during monopolar operation, before Fenno-Skan 2 was installed are used to evaluate the possible corrosion effects.

A local field strength of about 1.5 V/km has been observed close to Forsmark Power station, see Section 4.1. The cause of this field strength is most likely a case where Forsmark Power station acts as a secondary electrode (case 2 in this analysis). However, here we estimate the effects from the field strength observed and assume that the observed field strength is uniform and treat the situation as a variation of case 1. Table 7-3 shows the potentials that would arise along a canister if the field strength was 50 V/km for the case of as-deposited bentonite, for two 1,700 m tunnels. The highest value in Table 7.3 is 0.27 V. Linear scaling to a field strength of 1.5 V/km would give a highest value of 1.5/50×0.27 V = 0.008 V for the voltage along the height of the most exposed canisters, for the case when the bentonite has the same water content as at deposition. In terms of corrosion the rate is estimated to 0.008/0.5×0.19 μm/year ≈ 0.003 μm/year.

9 Discussion

In this study several factors influencing the effects of an HVDC electrode on the corrosion of a copper canister have been analyzed. The effects of most of these factors have been pessimistically bounded based on results from the sensitivity analysis. For two factors the task to represent the real features in the modeling is less simple to accomplish. These factors are the resistivity in the rock, and the timing and duration of the shoreline in the vicinity of the repository, and are discussed below.

The resistivity in the rock is represented in this study by 6 different resistivity functions, which cover the estimates of resistivity as described in Thunehed and Pitkänen (2007). In that study electromagnetic sounding from ground surface was the primary method for estimating the rock resistivity. Another method of estimating the rock resistivity is by geophysical logging in boreholes, where an alternating current is injected into the rock mass. Geophysical results from the Forsmark site investigation (e.g. Löfgren and Neretnieks 2005) indicate a somewhat higher in-situ rock resistivity in the upper 1,000 meters than given by resistivity function *f6* in Figure 4-14. Bounded by the maximum depth of the boreholes, no geophysical borehole logging has been performed below 1,000 m in Forsmark. The resistivity function *f5*, that in several of the analyzed cases gives the highest voltages over the canisters (and thus the highest corrosion rate), is even smaller and thus less representative compared to the geophysical logging results. Taking into account the different measurement methods, the resistivity function *f5* thus seems to well illustrate the effects of a pessimistic description of the rock resistivity.

The other factor with large uncertainties is the timing and duration of the location of the shoreline in the vicinity of the repository. A location of a future HVDC electrode 2 km from the shoreline has been used as an example in this study. The implication for the case where this location coincides with the site of the repository shafts is that the level of the sea has risen to about 2 m above the level where the shafts meet today's ground level. This will most probably not occur until after thousands of years when the bentonite is saturated, even if it cannot be excluded to occur during the saturation phase for some canisters. It is on the other hand likely that also a location 2 km from the shoreline would be too uneconomical to be realistic. Figure 4-20 shows the calculated potentials around an HVDC electrode with 1,250 A at 2.3 km distance from the shoreline. Comparing the potentials at short distances from the electrode with measured values for existing HVDC transmissions in Figure 4-3, it is apparent that the calculated potentials are much higher. The potentials at short distances from the electrode are of decisive importance for the power loss in the transmission. It is also a factor that is strongly affected by the distance from the shoreline as Figures 4-17 through 4-19 illustrate. Thus in order to be comparable in efficiency with today's transmissions a location of a future electrode 3 km from the shoreline is more reasonable than 2 km from the shoreline. Having the shafts of the repository 3 km from the shoreline instead of 2 km would require that the level of the sea rises yet another meter, which in turn shortens the possible duration for suitable conditions for an HVDC installation.

10 Conclusions

The type of corrosion that a canister can suffer by currents from HVDC transmissions and stray currents is partly determined by the voltages that arise along the height of a canister when it is surrounded by bentonite in a deposition hole. For the chemical environment expected in the repository, there is no process identified that could cause pitting, and thus only general corrosion is analyzed.

During the initial oxidizing conditions, where the cathodic reaction is reduction of oxygen gas or earlier formed corrosion products, corrosion would consume these oxidants so that the presence of an electrical field under these conditions would not cause more corrosion than availability of the oxidants allows. Possibly the stray current would move the already existing amount of corrosion products from one end of the canister to the other.

At reducing conditions with sulfide present in the repository, the corrosion due to sulfide is limited by mass transport of sulfide. The extent of the corrosion from the stray current can be estimated from the voltage across the canister and the polarization resistance in the interface between canister and bentonite. The dependence between the extent of corrosion and the voltage is linear up to a certain voltage, in this study estimated to 0.5 V. At this voltage over the canister the additional corrosion is estimated to 0.2 μm/year.

The water saturation of the bentonite that surrounds the canisters has a large influence on the resistance parallel to the canisters and thereby on the voltages that arise along the height of a canister. Two levels of saturation are considered here, corresponding to ‘as-deposited’ and ‘fully water saturated’, where the highest voltage (and corrosion rate) is obtained with the as-deposited bentonite. Values at intermediate water saturation can be estimated by linear interpolation.

With the electrical fields from the present Fenno-Skan installation, the voltages that arise along the height of a canister will be low also for conditions with ‘as-deposited’ bentonite. Estimated from the highest local field strength observed (1.5 V/km) the voltage may be about 0.008 V, corresponding to a corrosion rate of about 0.003 μm/year. These values are expected to decrease as the conductivity of the surrounding bentonite increases when its water content increases.

For future HVDC installations the largest effects are obtained if the electrode is placed close to the repository. For the most pessimistic combination of parameter values, and with the most unfavourable position of the electrode, the highest voltage obtained was 0.46 V for the most exposed canisters. This corresponds to a corrosion rate <0.2 μm/year. Increasing the depth of the repository from 500 m to 700 m would in most cases decrease the voltage over the canister, but the effect is rather small (up to 30% for the canisters obtaining the highest voltage drops). When assessing the additional corrosion from an HVDC installation also the lifetime of such an installation in monopolar operation must be taken into account.

It can thus be concluded that for the current situation of potential gradients over the canister at the Forsmark site, the estimates in the present report are in line with those estimated in the safety assessment SR-Site. The present study additionally addresses influences of possible future HVDC electrodes. The results show that, with pessimistic assumptions on future HVDC locations, the influences may be larger than today. However, also with the very pessimistic assumptions of a location directly on top of the shaft that connects the repository level and ground level, only moderate additional corrosion is predicted from an HVDC installation.

References

SKB's (Svensk Kärnbränslehantering AB) publications can be found at www.skb.se/publications. References to SKB's unpublished documents are listed separately at the end of the reference list. Unpublished documents will be submitted upon request to document@skb.se.

King F, Tang Y, 1998. The anodic dissolution of copper in chloride-sulphate groundwaters. Report 06819-REP-01200-0058 R00, Ontario Hydro, Nuclear Waste Management Division, Canada.

King F, Lilja C, 2013. Localised corrosion of copper canisters in bentonite pore water. SKB TR-13-27, Svensk Kärnbränslehantering AB.

King F, Lilja C, 2014. Localised corrosion of copper canisters. Corrosion Engineering, Science and Technology 49, 420–424.

Löfgren M, 2007. Formation factor logging in situ by electrical methods in KFM01D and KFM08C. Forsmark site investigation. SKB P-07-138, Svensk Kärnbränslehantering AB.

Löfgren M, Neretnieks I, 2005. Forsmark site investigation. Formation factor logging in-situ by electrical methods in KFM01A and KFM02A. Measurements and evaluation of methodology. SKB P-05-29, Svensk Kärnbränslehantering AB.

Magg T G, Mutschler H D, Nyberg S, Wasborg J, Thunehed H, Sandberg B, 2010. Caprivi Link HVDC Interconnector: site selection, geophysical investigations, interference impacts and design of the earth electrodes. CIGRE paper B4_302_2010.

Myers J R, Cohen A, 1984. Conditions contributing to underground copper corrosion. American Water Works Association Journal 76, 68–71.

NIOSH, 1998. Worker deaths by electrocution: a summary of NIOSH surveillance and investigative findings. Publication 98-131, U.S. Department Of Health And Human Services. Public Health Service, Centers for Disease Control and Prevention. National Institute for Occupational Safety and Health. Available at: http://www.cdc.gov/niosh/docs/98-131/pdfs/98-131.pdf. [26 June 2014].

Nyman A, Kuussaari M, Nielsen M, 1988. Calculation and measurements of the stray current effects of monopolar HVDC systems. CIGRE paper 36-03_1988.

Rothfuchs T, Miehe R, Moog H, Wieczurck K, 2004. Geoelectric investigation of bentonite barrier saturation. Gesellschaft fur Anlagen- und Reaktorsicherheit (GRS) mbH.

Rusck S, 1962. HVDC power transmission: problems related to earth return. Direct Current, Nov. 1962, 290–300.

Sandberg B, Ahlström J, Tidblad J, Sederholm B, 2010. Korrosion på stål i betong i kylvattenvägar. Delprojekt 3 – Korrosion på stål i vattenmättad betong [Corrosion of steel in concrete in cooling water systems]. Rapport 10:84, Elforsk. (In Swedish.)

SKB, 2009. Underground design Forsmark. Layout D2. SKB R-08-116, Svensk Kärnbränslehantering AB.

SKB, 2010a. Design, production and initial state of the backfill and plug in deposition tunnels. SKB TR-10-16, Svensk Kärnbränslehantering AB.

SKB, 2010b. Fuel and canister process report for the safety assessment SR-Site. SKB TR-10-46, Svensk Kärnbränslehantering AB.

SKB, 2010c. Climate and climate-related issues for the safety assessment SR-Site. SKB TR-10-49, Svensk Kärnbränslehantering AB.

SKB, 2010d. Data report for the safety assessment SR-Site. SKB TR-10-52, Svensk Kärnbränslehantering AB.

SKB, 2010e. Corrosion calculations report for the safety assessment SR-Site. SKB TR-10-66, Svensk Kärnbränslehantering AB.

SKB, 2011. Long-term safety for the final repository for spent nuclear fuel at Forsmark. Main report of the SR-Site project. SKB TR-11-01, Svensk Kärnbränslehantering AB.

SKB, 2014. Climate and climate-related issues for the safety assessment SR-PSU. SKB TR-13-05, Svensk Kärnbränslehantering AB.

SSM, 2012. Begäran om komplettering av ansökan om slutförvaring av använt kärnbränsle och kärnavfall – degraderingsprocesser för kapseln. Dnr SSM2011-2426-57, Strålsäkerhetsmyndigheten (Swedish Radiation Safety Authority). (In Swedish.)

Taxén C, 2011. Possible effects of external electrical fields on the corrosion of copper in bentonite. SKB P-11-43, Svensk Kärnbränslehantering AB.

Thunehed H, Pitkänen T, 2007. Forsmark site investigation. Transient electromagnetic soundings at Forsmark and the regional surroundings. Estimations of depth to saline groundwater. SKB P-07-165, Svensk Kärnbränslehantering AB.

Tykeson K, Nyman A, Carlsson H, 1996. Environmental and geographical aspects in HVdc electrode design. IEEE Transactions on Power Delivery 11. doi:10.1109/61.544281

von Baeckmann W, 1989. Handbuch des kathodischen Korrosionsschutzes: Theorie und Praxis der elektrochemischen Schutzfahren. 3rd ed. Weinheim: VCH. (In German.)

Unpublished documents

SKBdoc id, version	Title	Issuer, year
1422182 ver 2.0	Sulphide mass-transport limited corrosion.	SKB, 2014